Helsinki University of Technology Laboratory of Steel Structures Publications 19

Teknillisen korkeakoulun teräsrakennetekniikan laboratorion julkaisuja 19

Espoo 2000 TKK-TER-19

LOCAL AND DISTORTIONAL BUCKLING OF PERFORATED STEEL WALL STUDS

Jyrki Kesti

Dissertation for the degree of Doctor of Science in Technology to be presented with due permission for public examination and debate in Auditorium R1 at Helsinki University of Technology (Espoo, Finland) on the 8th of December, 2000, at 12 o'clock noon.

Helsinki University of Technology

Department of Civil and Environmental Engineering

Laboratory of Steel Structures

Teknillinen korkeakoulu

Rakennus- ja ympäristötekniikan osasto

Teräsrakennetekniikan laboratorio

Distribution:
Helsinki University of Technology
Laboratory of Steel Structures
P.O. Box 2100
FIN-02015 HUT
Tel. +358-9-451 3701
Fax. +358-9-451 3826
E-mail: sinikka.rahikainen@hut.fi

ISBN 951-22-5223-6
ISSN 1456-4327

Otamedia Oy
Espoo 2000

Kesti, J. 2000. Local and Distortional Buckling of Perforated Steel Wall Studs. Helsinki University of Technology Laboratory of Steel Structures Publications 19, TKK-TER-19, Espoo. 101 p. + app. 19 p. ISBN 951-22-5223-6, ISSN 1456-4327.

UDC: 624.014.2, 69.022.3, 693.97, 691.55, 691.71
Keywords: cold-formed steel, local buckling, distortional buckling, steel wall stud, perforation, gypsum board

ABSTRACT

The local and distortional buckling behaviour of flange and web-stiffened compression members was investigated. In particular, the behaviour of web-perforated sections was investigated both numerically and experimentally. Perforation reduces the perpendicular flexural stiffness of the web and thus particularly reduces the distortional buckling strength of the section. The main task of the research was to develop a design method for estimating the compression capacity of a perforated steel wall-stud under centric loading. The influence of the gypsum sheathing on the distortional buckling strength is also taken into account.

It was shown that the method given in Eurocode 3 is quite rough and sometimes gives inaccurate results for estimating the elastic distortional buckling stress of both C-sections and intermediate stiffened plates. In the case of C-sections, the method developed by Lau and Hancock and the method developed by Schafer and Peköz correlate better with the results defined numerically. The Finite Strip Method (FSM) and Generalized Beam Theory (GBT) provided particularly good tools with which to analyze local and distortional buckling modes. It was also shown that interaction between different distortional buckling modes should be taken into account when analysing sections having both web and flange stiffeners.

Distortional buckling stress of the web-perforated C-section with or without web stiffeners can be determined by replacing the perforated web part with an equivalent plain plate corresponding to the same perpendicular bending stiffness. Distortional buckling stress may be determined by some numerical method such as FSM or GBT. For the web-perforated C-section, an analytical method for the distortional buckling is also presented.

Gypsum sheathing connections give rotational restraint to the wall–stud, thus improving distortional buckling strength. Some practical guidelines are given for calculating the rotational restraint. Buckling analysis showed that relatively small restraint may double the distortional buckling stress of the web-perforated section. Buckling analysis and experimental research showed that screw pitch also has a considerable effect on the distortional buckling stress. Using restraint values given by the connection tests, the predicted values for the gypsum board braced columns are in good accordance with the test results. In practical design, utilizing the gypsum board in the determination of the distortional buckling stress requires that the sheathing retains its capacity and stiffness for the expected service life of the structure. Furthermore, the connection characteristics should be carefully examined.

Based on the results of the experimental and theoretical studies, design proposals were made for the design of compressed web-perforated steel wall studs. Some practical guidelines were also given for taking into account the gypsum sheathing. These design proposals are also valid for solid steel wall studs, especially for slender sections, which are sensitive to distortional buckling.

PREFACE

This work was carried out in the Laboratory of Steel Structures, Department of Civil and Environmental Engineering at Helsinki University of Technology during 1996-2000. One year period at the University of Manchester during 1998-99 was funded by the Academy of Finland. The additional financial support from The Foundation of Technology and Emil Aaltonen Foundation is gratefully acknowledged. Finnish companies Rautaruukki Oyj and Aulis Lundell Oy were also financed the project.

I would like to thank my supervisor, Professor Pentti Mäkeläinen, for his advice and support during this research. I would also like to thank Professor Mike Davies from the University of Manchester for providing working environment during my stay in UK. Professor Davies also gave me excellent aid and advice, especially concerning on generalized beam theory.

I wish to express my gratitude to my colleagues Mr. Jyri Outinen, Mr. Mikko Malaska, Mr. Olli Kaitila, Ms. Wei Lu and Dr. Ma Zhongcheng in Laboratory of Steel Structures providing enjoyable and encouraging working atmosphere. I am also very much obliged to the secretaries, Mrs. Sinikka Rahikainen and Mrs. Varpu Sassi. Special thanks are also given to Mr. Veli-Antti Hakala, Mr. Hannu Kaartinaho, Mr. Pekka Tynnilä and Mr. Esko Varis in the Testing Hall of the Department have made all my experimental tests.

Thanks are also given to Mr. Paavo Hassinen and Mr. Pekka Salmi for their comments and good discussion.

The preliminary examiners of this thesis, Professor Torsten Höglund from Royal Institute of Technology, Sweden and Professor Greg Hancock from University of Sydney, are also gratefully acknowledged.

Finally, I would like to dedicate this work to my family: Anni, Atte and Alma. I would like to thank them for the support, happiness and understanding during the project.

Jyrki Kesti
Espoo, October 2000

CONTENTS

NOTATIONS

A	cross-sectional area [mm^2]
${}^kB$	transverse bending stiffness applicable to mode k [N/mm^2]
${}^kC$	generalized warping constant applicable to mode k [mm^4]
C_D	rotational spring stiffness [Nmm/rad]
C_θ	rotational spring stiffness [Nmm/rad]
${}^kD$	generalized torsional constant applicable to mode k [mm^2]
D	plate flexural rigidity [Nmm]
E	modulus of elasticity [N/mm^2]
E_r	reduced modulus of elasticity [N/mm^2]
G	shear modulus [N/mm^2]
I	second moment of area [mm^4]
I_w	warping constant [mm^6]
K	spring stiffness [N/mm]
L	length [mm]
N_c	nominal compression member capacity [N]
N_{Test}	ultimate compression capacity of tested section [N]
N_P	predicted compression capacity [N]
R_d	distortional buckling stress reduction factor
${}^kV$	deformation resultant applicable to mode k [mm]
${}^kW$	stress resultant applicable to mode k [Nmm]

b	width of the element [mm]
c_{screw}	screw spacing [mm]
h	height of the element [mm]
f_{od}	distortional buckling stress [N/mm^2]
f_{cr}	critical buckling stress [N/mm^2]
f_u	ultimate tensile stress [N/mm^2]
f_y	yield stress [N/mm^2]
k	local buckling coefficient, mode symbol in GBT
k_ϕ	rotational stiffness [Nmm/rad]
k_x, k_y, k_z, k_A	spring stiffness [N/mm]
k_{red}	reduction factor
l_c	buckling length [mm]
m	number of half-wavelengths, unit bending moment [Nmm/mm]
${}^kq$	uniformly distributed load applicable to mode k [N/mm]
t	plate thickness [mm]
$t_r, t_{r,web}$	reduced plate thickness [mm]
u	unit load
w_{eff}	effective width [mm]

α_i	nondimensional variable
β_{cr}	critical length [mm]
δ	deflection [mm]
δ_i	nondimensional variable
γ_i	nondimensional variable
${}^{ijk}\kappa$	second order coefficient in GBT [1/mm]
λ	buckling half-wave length [mm], slenderness

λ_d	slenderness related to distortional buckling
σ_{cr}	critical buckling stress [N/mm^2]
$\sigma_{cr,perf.}$	elastic buckling stress of perforated plate [N/mm^2]
$\sigma_{cr,plain.}$	elastic buckling stress of plain plate [N/mm^2]
$\sigma_{cr,perf.-C}$	elastic local buckling stress of web-perforated C-section [N/mm^2]
$\sigma_{cr,plain.-C}$	elastic local buckling stress of plain C-section [N/mm^2]
σ_w	buckling stress of the web [N/mm^2]

Subscripts

w	web
f	flange
s	stiffener

1 INTRODUCTION

1.1 Background of Research

Cold-formed steel wall-studs are widely used in load-bearing walls, especially in housing. In the Nordic countries, the use of web-perforated steel wall-studs, as shown in Fig. 1.1, has increased. The slotted thermal stud offers a considerable improvement in thermal performance over the solid steel stud.

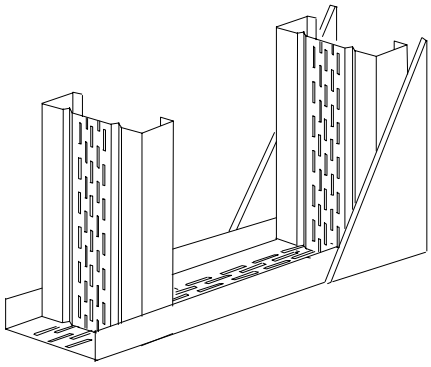

Fig.1.1: Wall structure including perforated steel wall-studs.

Unfortunately, the perforation also has an effect on the structural behaviour of the steel wall-stud, and it reduces, among other things, the compression capacity of the stud. The perforation reduces the elastic local buckling stress of the web as well as the bending stiffness of the web, which in turn results in decreased distortional buckling strength. There are no design guidelines available in the codes or standards for these kinds of sections. Research on this topic is therefore essential. The determination of elastic distortional buckling stress of even simple C-sections varies in the design codes and standards, and the situation is far less clear if there are intermediate web stiffeners. Especially the method given in Eurocode 3, Part 1.3 (1996) has been shown to be inaccurate. Therefore, the basis for studying distortional buckling is seen as necessary. Gypsum sheathing is usually considered only as a lateral support to the steel wall-stud. In the case of perforated steel wall studs, the gypsum sheathing screws also offer considerable resistance to distortional buckling, and therefore the influence of the sheathing on the distortional buckling stress of the stud is also examined.

1.2 Objectives of Research

The primary objective of this research is to gain an improved understanding of local and distortional buckling behaviour of the flange and web-stiffened compression members,

particularly when the web part is perforated, and thus having small transverse bending stiffness. The main task of the research is to create a design method for the compression capacity of the perforated steel wall-stud under centric compression loading. Considerable emphasis is placed on researching the distortional buckling of different kinds of stiffened and perforated sections. The influence of gypsum sheathing on the distortional buckling strength is also taken into account.

1.3 Scope of the Research

The scope of this research was limited to the compression members, thus the bending behaviour of the perforated steel wall-studs is beyond the scope of this research. Furthermore, the research concentrates on the local and distortional buckling, and thus the global buckling modes are ignored in this study. Two types of web-perforated sections were chosen for investigation. Web-stiffened and unstiffened C-sections were analyzed and former also tested. The thickness of the analyzed sections varied between 1 to 2mm. The wall thickness of the tested sections varied from 1.2mm to 1.5mm. Gypsum board was selected for the sheathing material, because it is commonly used in housing.

1.4 Outline of the Thesis

In order to obtain a basic knowledge, a brief summary of the literature study with respect to the analysis of compressed thin-walled members and the analysis and design of steel wall-studs is given in Section 1.5. Chapters 2-3 include the background for the analytical and numerical modelling of elastic distortional and local buckling, and the ultimate strength of the compressed web and flange-stiffened members, including the web-perforated sections. A comparison between the different methods is made. Modelling of the restraint provided by the gypsum sheathing is described in Chapter 4. Chapter 5 describes the compression tests and provides the test results for the web-perforated short columns and for the longer columns with gypsum sheathing attached to the flanges. Chapter 6 describes numerical analysis for the tested sections, including the buckling analysis and non-linear analysis. The influence of the gypsum sheathing on the distortional buckling stress is shown. Test results and analytical predictions are compared in chapter 7. The summaries and final conclusions are given in Chapter 8.

1.5 State of the Art

1.5.1 Analysis of compressed thin-walled members

The generic buckling modes of compressed thin-walled members are local, distortional or global buckling. Local buckling is particularly prevalent in cold-formed sections and it is characterized by relatively short wavelength buckling of individual plate elements. Global buckling modes are seen as flexural, torsional or flexural-torsional buckling. Global buckling modes are sometimes called rigid-body buckling because any given cross-section moves as a rigid body without cross-section distortion. The distortional mode repeats at wavelengths from short to long depending on the geometry, which generally involves the rotation and translation of multiple elements, but not the entire cross-section. Local and global buckling are quite well known and accounted for in current codes of practice, while distortional buckling is not yet so well documented, and has thus recently attracted the attention of a number of researchers.

Elastic local buckling stresses are typically treated by ignoring any interaction that exists between the elements (e.g., the flange and the web). Each element is treated independently and classic plate-buckling solutions based on isolated simply supported plates are generally employed. Elastic global buckling stresses for flexural, torsional or flexural-torsional buckling modes can easily be determined using analytical methods, which can be found in literature as well as in major design codes. Distortional buckling of the thin-walled section is a more complicated buckling mode than the local and global modes. Some manual calculation methods for predicting the elastic distortional buckling stress of simple sections such as C- and rack-sections have been presented, e.g. by Lau and Hancock (1987) and by Schafer and Peköz (1999). Manual calculation methods for distortional buckling are still relatively cumbersome.

Numerical methods, such as the finite element method (FEM), or finite strip method (FSM) may be used to determine the elastic buckling stresses of an entire member. The finite strip method has proved to be a useful approach, because it has a short solution time compared to the finite element method. The limitation of the finite strip method is that it assumes only simply supported end boundary conditions for the member. The Generalized Beam Theory (GBT) provides a particularly good tool with which to analyze different buckling modes in isolation and in combination with other modes.

The design of thin-walled members is conventionally based on the procedure where the elastic buckling stresses are determined first and the design values are then determined using the effective width approach for local buckling and column curves such as the Ayrton Perry formulas for global buckling. Distortional buckling is treated in different ways in various design codes.

Geometric and material non-linear finite element analysis has recently been successfully used to determine the load-bearing capacity of thin-walled members (e.g. Buhagiar et al. 1992, Teo 1998). The initial imperfections needed in the analysis are usually scaled from eigenvectors given by linear eigenvalue analysis. However, the characterization of geometric imperfections and residual stresses is largely unavailable. These fundamental quantities are necessary for reliable completion of advanced analysis and parametric studies of cold-formed steel members. Schafer and Peköz (1998) have suggested a simple set of guidelines to include geometric imperfections and residual stress patterns for the modelling. Based on the analysis of a simple flange lip, they noticed that distortional failure modes are more sensitive to initial imperfections than local failures, and that the final failure mechanism is consistent with the distortional mode even in cases where distortional buckling stress is higher than local buckling stress.

Davies and Jiang (1996b) have found that the patterns of linear buckling and non-linear buckling could be different, and they have developed a non-linear solution to the eigenvalue problem set up by using the finite element method. The analysis for the uniformly compressed columns is slightly more accurate for shorter wavelength local and distortional buckling modes than for the longer wavelength flexural-torsional buckling modes, probably as a result of geometric imperfections that would have a greater effect on the longer wavelength modes, and which were not accounted for in the eigenvalue analysis.

Key and Hancock (1993) have used finite strip method for the non-linear analysis of thin-walled and cold-formed steel sections. The analysis accounts for geometric non-linearity and material plasticity in the behaviour of sections subjected to axial compression. With the appropriate choice of displacement functions in the analysis, sections undergoing either inelastic local deformations or overall buckling deformations may be analyzed. Kwon and Hancock (1991b) have developed a non-linear elastic spline finite strip method to include the geometric non-linear analysis of prismatic thin-walled structures under arbitrary loading and non-simple boundary conditions. The method does not require an initial buckling analysis to determine the buckling mode and half-wavelength for further analysis in the post-buckling range. Lau and Hancock

(1989) and Lindner and Guo (1994) have also used the spline finite strip method for the analysis of inelastic buckling of thin-walled members.

Rasmussen and Young have widely described the overall bifurcation analysis of locally buckled columns (Rasmussen 1997, Young and Rasmussen 1997 and Young and Rasmussen 1999). The overall flexural and flexural-torsional bifurcation loads are calculated using the tangent rigidities of the locally buckled cross-sections. An elastic non-linear finite strip local buckling analysis is used to determine the tangent rigidities. The columns are assumed to be geometrically perfect in the overall mode but they may include imperfections in the local mode. The important result of their research was also that local buckling induces bending in a pin-ended column, but not in a fixed-ended singly symmetric column. Consequently, only fixed-ended singly symmetric columns exhibit bifurcation behaviour.

1.5.2 Research and Design of Steel Wall-Studs

The diaphragm bracing of steel wall-studs using gypsum wallboards and other materials was investigated by Simaan and Peköz (1976). They used an energy approach including the shear rigidity and rotational restraint of the diaphragm to develop a design procedure and an approximate solution for the buckling of diaphragm-braced wall-studs. The AISI (1986) Specification is based on Simaan's research. As far as the structural strength is concerned, the maximum load that can be carried by wall-studs is governed by either (1) column buckling between the fasteners in the wall plane, or (2) overall buckling of the studs taking into account the shear rigidity of the wallboards. Furthermore, the shear strain in the wallboard should not exceed the permissible value in order to prevent shear failure of the wallboard. Increased stud spacing increases the overall shear rigidity and results in increased strength predictions for both the overall diaphragm-braced buckling modes and for the shear failure of the sheathing itself.

Tests by Miller and Peköz (1994) on gypsum-sheathed wall-studs showed that the results contradict the shear diaphragm model. The strength of gypsum wallboard-braced studs was observed to be rather insensitive to stud spacing. Moreover, the deformations of gypsum wallboard panels (in tension) were observed to be localized at the fasteners, and not distributed throughout the panel as in a shear diaphragm. Due to this research, some limitations (e.g. maximum stud spacing) have been added to the AISI (1996) Specification. Miller and Peköz also investigated the effect of the web perforation on the local buckling and thus on the effective area of the section. The conclusion was that the effective area of the perforated web might be

determined by assuming the web to consist of two unstiffened elements, one on each side of the perforation.

Telue and Mahendran (1999) have reported results of 40 full-scale gypsum board lined wall frame tests and stub column tests. The tests included unlined, side–lined, and one-side-lined studs. The test results were compared with predictions from the Australian Standard AS 4600 (1996) and the American Specification AISI (1996). The investigated studs were made from unlipped C-sections. Almost all of the frames with plasterboard lining failed by buckling between the fasteners at the top of the stud, with the screws pulling through the plasterboard. The failure loads from the wall frame tests were generally close to the predicted ones according to the AS 4600, if the effective length factor of 0.75 for out-of-plane flexural buckling and the effective length factor of 0.1 corresponding to the fastener spacing for in-plane flexural buckling and for torsional buckling were used. Telue and Mahendran found that the shear diaphragm model assumed by AISI is not applicable to wall frames lined with plasterboard if the effective length factors given in the AISI specification were used. The experimental results were generally higher than those predicted by AISI and the failure mode was independent of the stud spacing.

One of the first studies on thermal wall studs with web perforation was reported by Ife (1975). The studied section is shown in Fig. 1.2. Two wall panels with thermal studs and one panel with solid web studs were tested. The wall elements consisted of two studs both with side lining. Plywood board was attached to one side of the studs and gypsum board to the other side. The elements were loaded with both an axial load and a lateral load. Ife found that the capacity of the element with the solid stud was only 10% higher than the element with the thermal stud.

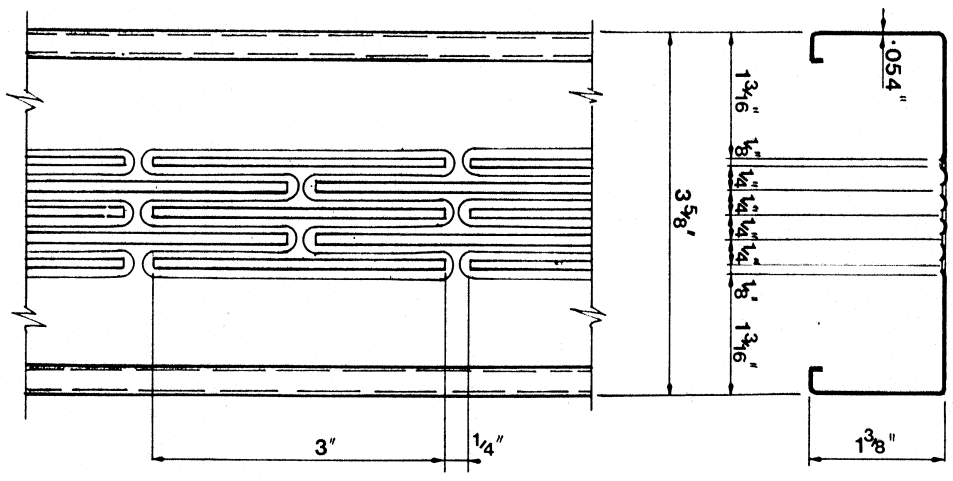

Fig. 1.2: Thermal Stud studied by Ife (1975).

In the Nordic countries, the first light-gauge steel-framing system based on thermal studs was designed by Engebretsen and Ramstad (1978) in Norway. In this system, both sides were lined with gypsum board. The compression and bending moment capacities were determined according to the 1968 AISI specification. The perforation was simply taken into account by multiplying the capacities with the reduction factor of 0.8.

Frederiksen and Spange (1992) performed quite a large test series for wall elements with web-perforated studs in Denmark. The section used in these tests is shown in Fig. 1.3. The test series included compression and bending tests as well as combined compression and bending tests. The failure was initiated in most cases by the stiffener buckling of the section.

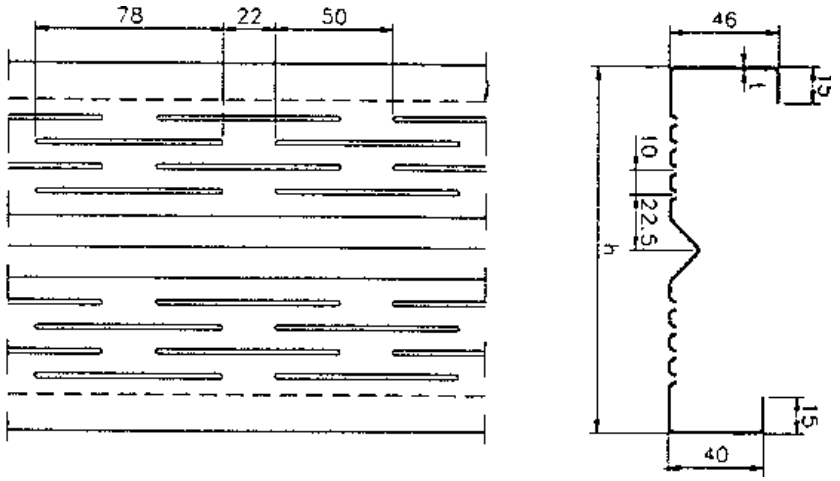

Fig. 1.3: Thermal Stud studied by Frederiksen and Spange (1992).

Höglund (Höglund 1998, Höglund and Burstrand 1998)has created a calculation method for slotted steel wall- studs. The calculation methods are mainly based in Swedish Code for Light-Gauge Metal Structures 79 (StBK-N5 1979). The calculation method has been verified with the test results of Frederiksen and Spange and with the test results obtained by the Royal Institute of Technology, Sweden (Borglund and Jonsson 1997, Marques da Costa 1999). Several types of failure modes are introduced depending on the loading and support conditions. In most cases, the resistance is affected by the shear deformation of the slotted web and by the reduced transverse bending stiffness of the web.

According to Höglund, the failure mode under concentric compressive loading may be 1) buckling in the plane of the web taking into account the shear deformations of the slotted web, or 2) lateral buckling of the flanges when the gypsum boards are assumed to act as elastic supports, or 3) buckling of the flange stiffeners in the span or at the support. Furthermore the local

buckling is taken into account using the effective area approach. When calculating the buckling of the flange stiffeners, the restraint given by the web is taken as negligible. The screws in the gypsum board mainly prevent buckling of the flange stiffener. The approximate effective buckling length given by the tests has been found to be $l_c = 0.72c_{screw}$, where c_{screw} is the spacing of the screws.

Under eccentric compressive loading or transverse loading, the stress distribution across the section is determined by taking into account the effect of the shear deformations of the slotted web. Höglund also presented a calculation method for the shear strength of the slotted web.

Salmi (1998) also performed a large test series for web-perforated steel wall-studs and wall elements. The test series included stub column tests, compression and bending tests, as well as combined compression and bending tests for wall elements. Salmi followed Eurocode 3, Part 1.3 (1996) in determining the effective cross-section area of the section. Local buckling is taken into account using effective widths, and stiffener buckling is taken into account using the effective thickness for the stiffener. The perforation is taken into account using reduced thickness for the perforated part of the section.

2 ELASTIC LOCAL AND DISTORTIONAL BUCKLING OF COMPRESSED THIN-WALLED MEMBERS

2.1 General

Elastic local buckling stresses of the thin-walled compressed member are typically treated independently by ignoring any interaction that exists between the elements. Classic plate-buckling solutions are generally employed. Distortional buckling of the thin-walled section is a more complicated buckling mode than the local and global modes. Distortional buckling of compression member such as C-sections usually involves rotation of each flange and lip around the flange-web junction. The whole section may translate in a direction normal to the web. The wavelength of distortional buckling is generally intermediate between that of local and distortional buckling. Typical distortional buckling mode of C-section is shown in Fig. 2.1.

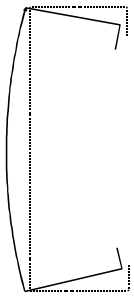

Fig. 2.1: Distortional buckling mode of C-section.

Some manual calculation methods for predicting the elastic distortional buckling stress of simple sections such as C- and rack-sections have been presented, e.g. by Lau and Hancock (1987) and Schafer and Peköz and Peköz (1999). Manual calculation methods for distortional buckling are still relatively cumbersome. Numerical methods, such as the finite element method (FEM), or the finite strip method (FSM) have been found to be efficient methods for determining elastic buckling stresses for both local and distortional buckling. The finite strip method has proved to be a useful approach because it has a short solution time compared to the finite element method. The finite strip method assumes simply supported end boundary conditions and it is applicable for longer sections where multiple half-waves occur along the section length. The Generalized Beam Theory (GBT) provides a particularly good tool with which to analyze distortional buckling in isolation and in combination with other modes. It also has a short solution time and the method is applicable for both pin-ended and fixed-ended members. The GBT is not so familiar as other methods and thus a short description of the method is presented here.

2.2 Generalized Beam Theory (GBT)

The Generalized Beam Theory has been presented in more detail by, e.g. Schardt (1989) and Davies and Leach (1994a, 1994b), and only a short description of the solution is given here. A unique feature is that GBT can separate and combine individual buckling modes and their associated load components. In GBT, each mode has an equation and, in second-order format, ignoring the shear deformation terms, the equation for mode 'k' is:

$$E\,{}^{k}C\,{}^{k}V'''' - G\,{}^{k}D\,{}^{k}V'' + {}^{k}B\,{}^{k}V + \sum_{i=1}^{n}\sum_{j=1}^{n} {}^{ijk}\kappa\,({}^{i}W\,{}^{j}V')' = {}^{k}q \quad for \quad k=1,2,...n \tag{2.1}$$

where the left superscript k denotes the mode k, ${}^{k}C$ is the generalized warping constant, ${}^{k}D$ is the generalized torsional constant and ${}^{k}B$ is the transverse bending stiffness. These are the generalized section properties that depend only on the cross-section geometry. In addition, ${}^{ijk}\kappa$ are the second-order section properties, which relate the cross-section deformations to the stress distributions, and E and G are the modulus of elasticity and shear modulus, respectively. ${}^{k}V$ and ${}^{k}W$ are the deformation resultant and stress resultant, ${}^{k}q$ is the uniformly distributed load and n is the number of modes in the analysis.

The section properties and the ${}^{ijk}\kappa$ values may be calculated manually, but in general, this task is best carried out by computer.

If the right-hand side terms ${}^{k}q$ of the equation (2.1) are zero, the solution gives the critical stress resultant ${}^{i}W$. In general, this requires the solution of an eigenvalue problem in which the analyst is free to choose which modes to include in the analysis.

When a constant stress resultant is applied along the member, which is assumed to buckle in a half sine wave of wavelength λ, GBT allows some particularly simple results to be obtained. Thus, the critical stress resultant for single-mode buckling is (Davies and Leach 1994b):

$${}^{i,k}W_{cr} = \frac{1}{{}^{ikk}\kappa}\left(\frac{\pi^2}{\lambda^2}E\,{}^{k}C + G\,{}^{k}D + \frac{\lambda^2}{\pi^2}\,{}^{k}B\right) \tag{2.2}$$

As the wavelength is varied, the minimum critical stress resultant is:

$$ {}^{i,k}W_{cr} = \frac{1}{ikk\kappa}\left(2\sqrt{E\,{}^{k}C\,{}^{k}B} + G\,{}^{k}D\right) \tag{2.3} $$

and the corresponding half-wavelength is

$$ {}^{k}\lambda = \pi\left(\frac{E\,{}^{k}C}{{}^{k}B}\right)^{0.25} \tag{2.4} $$

This approach allows some particularly simple solutions to be obtained for distortional buckling problems.

2.3 Analytical Methods for Determining Elastic Distortional Buckling Stress

2.3.1 General

Recently, a number of analytical methods have been developed for determining the elastic distortional stress of singly symmetric cross-sections. Some analytical methods have been presented, namely the Eurocode3 method (1996), which is based on flexural buckling of the stiffener, and the model developed by Lau and Hancock (1987) based on the flexural-torsional buckling of a simple flange including a stiffener. The latter method is used in the Australian and New Zealand Standard for Cold-Formed Steel Structures AS/NZS 4600 (1996). Schafer and Peköz (1999, 1999b) have also developed an analytical method to solve minimum distortional buckling stress of C-sections or longitudinally stiffened steel plates. Each method is briefly described and a numerical comparison between the different methods is carried out.

2.3.2 The Method in Eurocode 3: Part 1.3 (EC3)

In EC3, the design of compression elements with either edge or intermediate stiffeners is based on the assumption that the stiffener behaves as a compression member with continuous partial restraint. This restraint has a spring stiffness that depends on the boundary conditions and the flexural stiffness of the adjacent plane elements of the cross-section. The spring stiffness of the stiffener may be determined by applying a unit load per unit length to the cross-section at the location of the stiffener, as illustrated in Fig. 2.2. In Fig. 2.2, the rotational spring stiffness C_θ characterizes the bending stiffness of the web part of the section. The spring stiffness K per unit length may be determined from:

$$K = u / \delta \tag{2.5}$$

where δ is the deflection of the stiffener due to the unit load u.

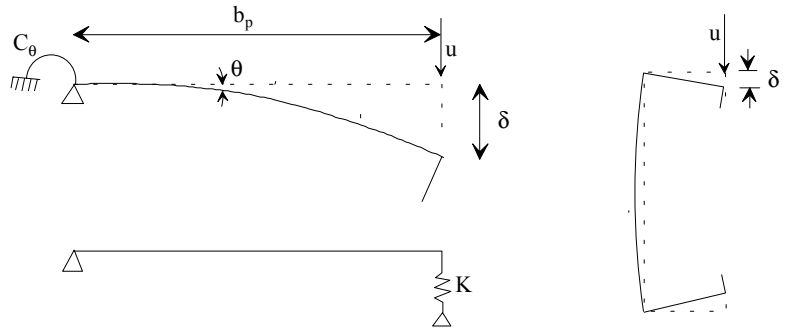

Fig. 2.2: Determination of the spring stiffness K according to Eurocode 3.

The elastic critical buckling stress for a long strut on an elastic foundation, in which the preferred wavelength is free to develop, is given by Timoshenko & Gere (1961):

$$\sigma_{cr} = \frac{\pi^2 E I_s}{A_s \lambda^2} + \frac{1}{A_s \pi^2} K \lambda^2 \tag{2.6}$$

where

A_s and I_s are the effective cross-sectional area and second moment of area of the stiffener according to EC3, as illustrated in Fig. 2.3 for an edge stiffener.

$\lambda = L / m$ is the half-wavelength

m is the number of half-wavelengths.

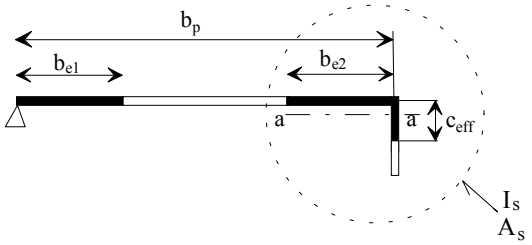

Fig. 2.3: Effective cross-sectional area of an edge stiffener.

The preferred half-wavelength of buckling for a long strut can be derived from Equation (2.6) by minimizing the critical stress:

$$\lambda_{cr} = \sqrt[4]{\frac{EI_s}{K}} \tag{2.7}$$

For an infinitely long strut, the critical buckling stress can be derived, after substitution, as:

$$\sigma_{cr} = \frac{2\sqrt{KEI_s}}{A_s} \tag{2.8}$$

Equation (2.8) is given in EC3; thus, the EC3 method does not consider the effect of column length but assumes that it is sufficiently long for integer half-waves to occur in the section length. In the case of intermediate stiffeners, the procedure is similar, but the rotational stiffness due to adjacent plane elements is ignored and the stiffened plane element is assumed as simply supported.

2.3.3 AS/NZS 4600 Method

Determination of the elastic distortional buckling stress is based on the flexural-torsional buckling of a simple flange, as shown in Fig. 2.4. The rotational spring, k_ϕ, represents the flexural restraint provided by the web, which is in pure compression, and the translational spring, k_x, represents the resistance to translational movement of the section in the buckling mode. The model includes a reduction in the flexural restraint provided by the web as a result of the compressive stress in the web.

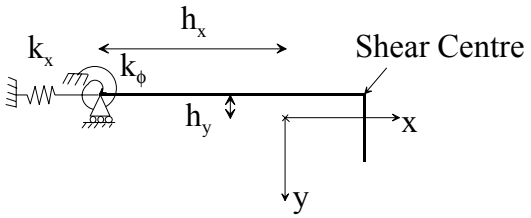

Fig. 2.4: Lau and Hancock's model for distortional buckling.

In Lau and Hancock's analysis (1987), it is shown that the translational spring stiffness k_x does not have much significance and it is assumed to be zero. The rotational spring stiffness can be expressed as:

$$k_\phi = \frac{Et^3}{5.46(b_w + 0.06\lambda)}\left[1 - \frac{1.1 f'_{od}}{Et^3}\left(\frac{b_w^2 \lambda}{b_w^2 + \lambda^2}\right)^2\right] \tag{2.9}$$

where f'_{od} is the compressive stress in the web at distortional buckling, computed by assuming k_ϕ as zero. b_w is the web depth, t is the thickness of the section, E is Young's modulus and λ is the half-wavelength in buckling and is expressed for simple C-section as:

$$\lambda = 4.80\left(\frac{E b_f^2 b_w}{t^3}\right)^{0.25} \tag{2.10}$$

where b_f is the flange width.

The elastic distortional buckling stress then has the form:

$$f_{od} = \frac{E}{2A}\left[(\alpha_1 + \alpha_2) - \sqrt{(\alpha_1 + \alpha_2)^2 - 4\alpha_3}\right] \tag{2.11}$$

where A is the cross-sectional area of the flange and stiffener and α_1, α_2 and α_3 are characteristic values of some complexity, which are given in Appendices D1 and D2 of AS/NZS 4600 and which are related to the k_ϕ, λ and the geometry and dimensions of the flange and the lip. The computation process is iterative due to the incorporation of f'_{od} in k_ϕ, but only one iteration is required.

This type of model proves to be sensitive to the value assumed for the rotational spring stiffness k_ϕ . Davies and Jiang (1998) proposed an improvement to the above method if the rotational spring stiffness k_ϕ is negative, i.e. the web buckles earlier than the flange. In this case, the buckling stress can be obtained with k_ϕ as zero, whereas the buckling stress of the web plate is (Timoshenko and Gere 1961):

$$\sigma_w = \frac{\pi^2 D}{t b_w^4}\left(\frac{b_w^2 + \lambda^2}{\lambda}\right)^2 \tag{2.12}$$

The final distortional buckling stress can be calculated approximately as the mean value of the buckling stresses of the web and flange:

$$\sigma_{cr} = \frac{2 f_{od} A_f + \sigma_w t b_w}{A} \tag{2.13}$$

where A_f is area of the flange and stiffener and A is area of the whole cross-section.

2.3.4 Schafer-Peköz Method

In the Schafer-Peköz method, the elastic distortional buckling stress of a compression member with one web and symmetric edge-stiffened flanges is also based upon an examination of the rotational restraint at the web/flange juncture. According to Schafer and Peköz, the rotational stiffness may be expressed as a summation of the elastic and stress-dependent geometric stiffness terms with contributions from both the flange and the web, and it can be expressed as:

$$k_\phi = \left(k_{\phi f} + k_{\phi w}\right)_e - \left(k_{\phi f} + k_{\phi w}\right)_g \tag{2.14}$$

where the subscript *f* refers to the flange and the subscript *w* refers to the web. Buckling ensues when the elastic stiffness at the web/flange juncture is eroded by the geometric stiffness, i.e.,

$$k_\phi = 0. \tag{2.15}$$

Using Equation (2.15) and writing the stress-dependent portion of the geometric stiffness explicitly, the following equation can be written:

$$k_\phi = k_{\phi fe} + k_{\phi we} - f_{od}\left(\tilde{k}_{\phi fg} + \tilde{k}_{\phi wg}\right) = 0. \tag{2.16}$$

Therefore, the buckling stress, $f_{od,}$ is

$$f_{od} = \frac{k_{\phi fe} + k_{\phi we}}{\tilde{k}_{\phi fg} + \tilde{k}_{\phi wg}}. \tag{2.17}$$

Analytical models are needed for determining the rotational stiffness contributions from the flange and the web. For the flange, cross-section distortion is not important. The flange is thus modelled as a column undergoing flexural-torsional buckling, as in Lau and Hancock's model shown in Fig. 2.4. For the web, cross-section distortion must be considered. The web is modelled as a single finite strip. Therefore, the transverse shape function is a cubic polynomial. The longitudinal shape of the functions of the flange and the web are matched by using a single half-wave for each. The final rotational stiffness terms for the flange and the web are presented in Appendix A. The critical length can also be found and it is function of the geometric terms. The solution for the critical length is also shown in Appendix A.

Schafer and Peköz (1996) have also presented a method to predict the distortional buckling stress of a stiffened element with single or multiple longitudinal stiffeners. Schafer and Peköz used a classical method for calculating the elastic buckling behaviour based on the use of the Fourier series for the deflected shape of the plate/stiffener assembly. The elastic buckling behaviour is described using energy methods. In the final solution, only one transverse sine term is taken into account, which provides an adequate description of the deflected shape for the overall buckling of the plate, as shown in Fig. 2.5.

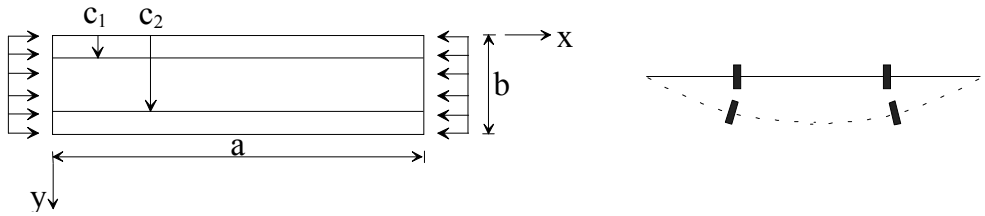

Fig. 2.5: Simply supported plate with two stiffeners in pure compression and its deflected shape.

The distortional buckling stress for a stiffened element with single or multiple stiffeners can be expressed as:

$$f_{cr} = k\frac{\pi^2 D}{b^2 t} \tag{2.18}$$

where D is the plate flexural rigidity and b is the width of the plate, as shown in Fig. 2.5. The minimum buckling factor k may be expressed as:

$$k = \frac{\left(1+\beta_{cr}^{2}\right)^{2} + 2\sum \gamma_i \sin^2(\pi\alpha_i)}{\beta_{cr}^{2}\left[1+2\sum \delta_i \sin^2(\pi\alpha_i)\right]} \tag{2.19}$$

where

$$\beta_{cr} = \left(2\sum \gamma_i \sin^2(\pi\alpha_i)+1\right)^{1/4} \qquad \gamma_i = \frac{E(I_s)_i}{bD} \qquad \delta_i = \frac{(A_s)_i}{bt} \qquad \alpha_i = \frac{c_i}{b}$$

where A_s is the cross-section area of the stiffener, and I_s is the second moment of area of the stiffener about the axis of the plate. Terms b and c_i are presented in Fig. 2.5.

2.3.5 Numerical Comparisons

2.3.5.1 C-Sections

Numerical calculations have been carried out for a variety of C-sections under concentric compression in order to compare the minimum elastic distortional buckling values determined using the different methods discussed above. The dimensions of the C-sections are given in Table 2.1 for web height h, flange width b, stiffener width c and thickness t. A value of E = 210 000 N/mm^2 was used in the analysis for the elasticity modulus. The results of the analytical methods were compared to the results given by GBT. GBT results were obtained using a computer program written by Davies and Jiang (1995). In the GBT analysis, the pin-ended conditions were used for distortional buckling. In all cases, the critical distortional buckling half-wavelength was assumed, thus leading to minimum distortional buckling stress. The iterative method was used in the EC3 method for calculating the effective stiffener properties.

The results are shown in Fig. 2.6 and in Table 2.1. The AS/NZS method gives, on average, 4% lower values of buckling stress than GBT for both t = 1.5 mm and t = 2.0 mm. All of the values are within 10% of the GBT values. The Schafer and Peköz method gives, on average, 2-3% lower values than GBT. Standard deviation is 0.09, which is higher than in the AS/NZS method. When compared with the GBT results, the EC3 method gives 9% higher values for t = 1.5 mm and 2% lower values for t = 2.0 mm. The variation in the EC3 method is, however, rather large.

If the web buckles earlier than the flange (marked by * in Table 2.1), the EC3 method seems to give very high values of buckling stress compared to GBT. This is because the EC3 model does not include a reduction in the flexural restraint provided by the buckled web. In the case of wide flanges or short stiffeners, the EC3 method gives rather low values. However, it should be noted that sections with b = 100 mm and t = 1.5 mm do not satisfy the b/t < 50 limit given in EC3 and the section with h = 100 mm, b = 100 mm and c = 15 mm does not satisfy the limit c/b > 0.2.

TABLE 2.1

COMPARISON OF ELASTIC DISTORTIONAL STRESSES FOR C-SECTION.

Section	**t=1.5mm**				**t=2.0mm**				**t=1.5mm**			**t=2.0mm**		
h-b-c	**AS**	**EC3**	**SCH**	**GBT**	**AS**	**EC3**	**SCH**	**GBT**	**AS/ GBT**	**EC3/ GBT**	**SCH/ GBT**	**AS/ GBT**	**EC3/ GBT**	**SCH/ GBT**
200-75-20	165	179	160	168	230	234	221	234	0.98	1.07	0.95	0.98	1.00	0.94
200-75-15	129	129	124	136	183	172	173	192	0.95	0.95	0.91	0.95	0.90	0.90
200-50-20	167*	331	171	179	214*	441	236	251	0.94	1.85	0.96	0.94	1.75	0.94
200-50-15	135*	251	132	149	136*	335	185	214	0.91	1.68	0.89	0.91	1.57	0.87
200-50-10	101*	163	90,1	113	74*	218	130	167	0.90	1.45	0.80	0.91	1.30	0.78
150-75-20	217	203	227	225	303	262	311	312	0.96	0.90	1.01	0.97	0.84	1.00
150-75-15	176	144	179	183	248	192	248	257	0.96	0.79	0.98	0.96	0.75	0.97
150-50-20	295	373	288	290	411	498	396	404	1.02	1.29	0.99	1.02	1.23	0.98
150-50-15	243	283	232	247	343	377	323	349	0.98	1.15	0.94	0.98	1.08	0.92
150-50-10	173	184	164	189	253	246	235	276	0.91	0.97	0.87	0.92	0.89	0.85
100-100-30	234	209	297	258	325	289	402	351	0.91	0.81	1.15	0.93	0.82	1.14
100-100-20	182	151	217	193	254	188	296	265	0.94	0.78	1.12	0.96	0.71	1.12
100-100-15	146	103	168	152	205	131	232	210	0.96	0.68	1.11	0.98	0.62	1.10
100-50-20	420	438	460	441	584	583	630	609	0.95	0.99	1.04	0.96	0.96	1.03
100-50-15	372	332	386	383	523	443	535	535	0.97	0.87	1.01	0.98	0.83	1.00
100-50-10	287	216	285	296	411	288	404	423	0.97	0.73	0.96	0.97	0.68	0.95
100-30-15	503	725	494	493	707	967	689	699	1.02	1.47	1.00	1.01	1.38	0.99
100-30-10	401	501	380	417	583	668	541	607	0.96	1.20	0.91	0.96	1.10	0.89
							Mean		**0.96**	**1.09**	**0.98**	**0.96**	**1.02**	**0.97**
							St.dev.		**0.04**	**0.34**	**0.09**	**0.03**	**0.32**	**0.09**
							Max		1.02	1.85	1.15	1.02	1.75	1.14
							Min		0.90	0.73	0.80	0.91	0.68	0.78

*Values have been calculated according to proposed method by Davies and Jiang (1998) when k_ϕ is negative.

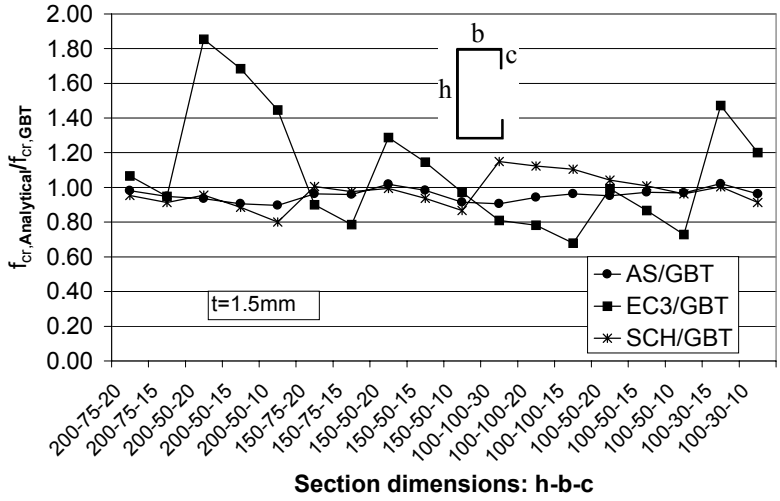

Fig. 2.5: Comparison of elastic distortional stresses for C-section.

2.3.5.2 Simply Supported Plate with Stiffeners

In cold-formed steel design, a member is idealized as a summation of elements. For instance, the flange and the web are treated independently as simply supported plates and examined accordingly. Elements supported along both longitudinal edges are defined as stiffened elements. The flange and the web are therefore defined as stiffened elements if they are supported by other adjacent plane elements such as a web, a flange or a stiffener. The following cases illustrate the differences between the various methods for determining the minimum distortional buckling stress of simply supported plates with one or two stiffeners. In these cases, the plate with stiffener could be, for instance, the web part of a C-section or the flange part of a hat-section. Two analytical methods have been used, namely the EC3 method and the Schafer-Peköz method. The numerical results have been determined using the Finite Strip Method (FSM). The THIN-WALL program (1996) was used in this case.

Simply Supported Plate with One Stiffener

The stiffened plate with a width of 200 mm and plate thickness of t = 1 mm and t = 2 mm was studied. The V-shaped stiffener is positioned in the middle of the plate and its height varies from 2 mm to 14 mm. Figure 2.7 presents the buckling analysis results for the plate thickness of 1 mm and Fig. 2.8 for the plate thickness of 2 mm. Figures 2.7 and 2.8 present the minimum distortional buckling stress versus stiffener height. The analytically determined local buckling stress values of the sub-elements are also included in the figures. As Fig. 2.7 shows, the distortional buckling mode is dominant if the stiffener height is less than 10 mm in the case of

the plate thickness of 1 mm. For the plate thickness of 2 mm, the distortional buckling is more dominant in the whole studied interval of stiffener height. Figure 2.7 shows that both analytical methods give reasonable results for the slender plate (h/t=200) compared to the values given by the finite strip method. For the stockier plate (h/t=100, Fig. 2.8), the EC3 overestimates the distortional buckling stress, especially in the case of high stiffener heights. The Schafer-Peköz method provides a good correlation with the FSM results in this case as well.

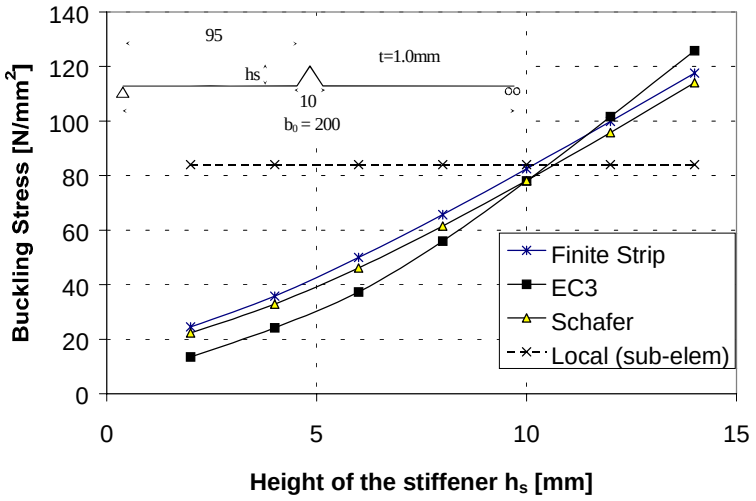

Fig. 2.7: Minimum distortional and local buckling stresses for simply supported plate with single stiffener by varying stiffener height. Plate thickness is 1 mm.

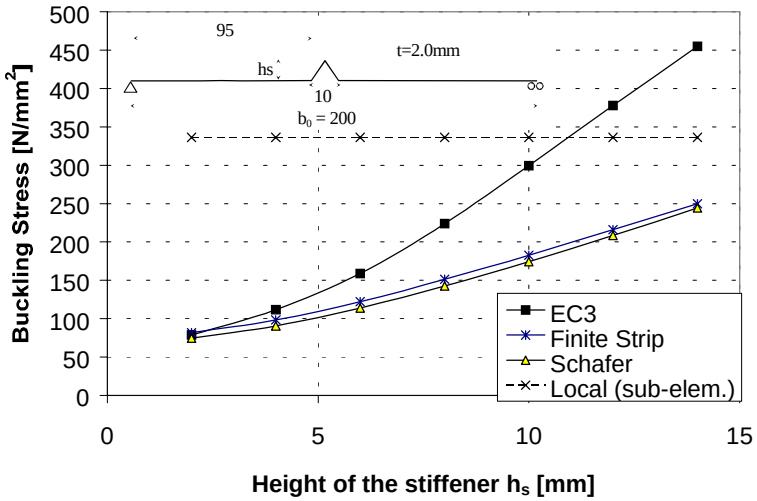

Fig. 2.8: Minimum distortional and local buckling stresses for simply supported plate with single stiffener by varying stiffener height. Plate thickness is 2 mm.

Simply Supported Plate with Two Stiffeners

In this case, the plate width is the same as previously, but two symmetrically located stiffeners are used. The stiffener size is presented in Figs 2.9 and 2.10. Figures 2.9 and 2.10 present the minimum distortional buckling stresses versus stiffener location for plate thicknesses of 1 mm and 2 mm, respectively. As Figs. 2.9 and 2.10 show, the EC3 method very firmly overestimates the distortional buckling stress if the stiffeners are positioned near the edges. In the EC3 method, the distortional buckling stress increases when the location of the stiffener moves towards the edge of the plate. This behaviour is opposite to the results of the FSM or Schafer and Peköz method. In EC3, the buckling of the stiffener is based on the assumption that the stiffener behaves as a compression member with continuous partial restraint. This restraint, which is described as spring stiffness, is higher near the support due to the fact that under point loading, the deflection of the beam is smaller there. EC3 results are reasonable when the stiffener location is near one-third of plate width, but the results clearly show that some limitations on stiffener location should be made. The Schafer and Peköz method predicts the distortional buckling stress with adequate accuracy for both the studied plate thicknesses. The results are slightly conservative compared to the FSM results.

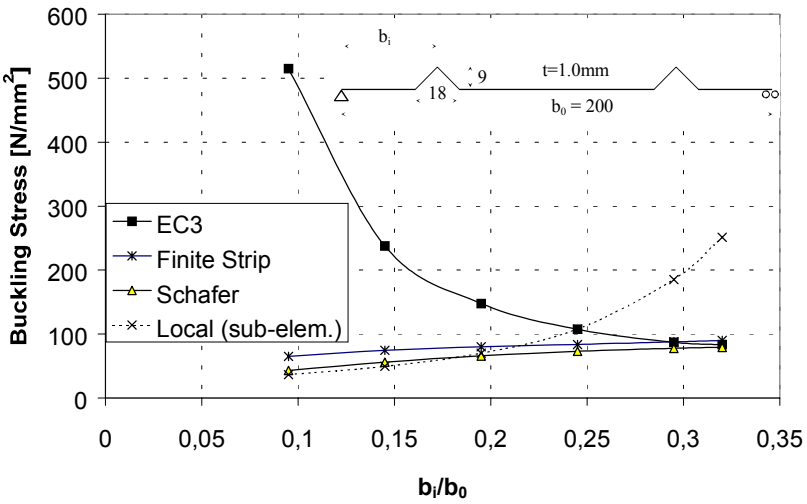

Fig. 2.9: Minimum distortional and local buckling stresses for a simply supported plate with two stiffeners having different stiffener locations. Plate thickness is 1 mm.

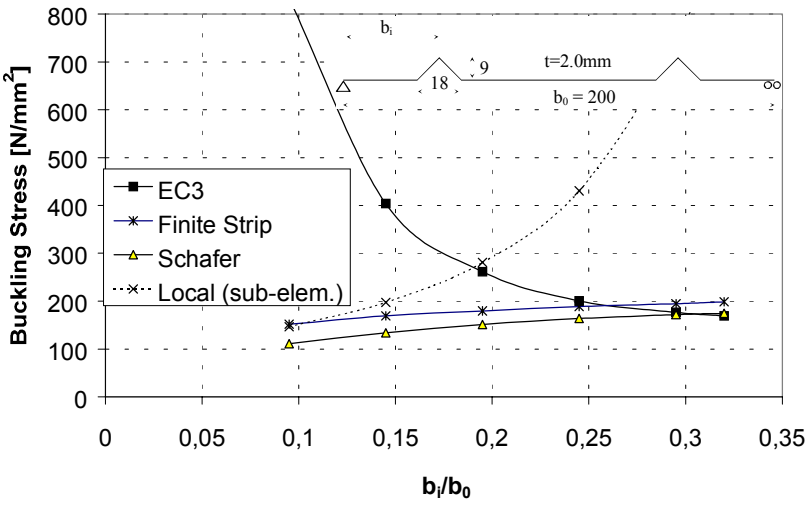

Fig. 2.10: Minimum distortional and local buckling stresses for a simply supported plate with two stiffeners having different stiffener locations. Plate thickness is 2 mm.

Due to above mentioned inaccuracies, the EC3 method is proposed to replace with the more simple and accurate Schafer-Peköz method in Eurocode 3.

2.4 Influence of End Boundary Conditions on Distortional Buckling Stress

It should be noted that all the manual calculation methods mentioned above assume pin-ended conditions for distortional buckling. In practice, this means that the column should be long enough so that several distortional buckling half-waves may occur along the column length. Of course, from the design point of view of, it is not critical if the column is short and the end boundary conditions have an effect on the distortional buckling stress, but this should be considered, e.g. if test results of the short columns are compared to the predictions from the design codes. Figure 2.11 illustrates the effect of the end boundary conditions on the distortional buckling stress for a typical C-section. The graph has been determined by GBT. The higher curve gives the distortional buckling stress for the fixed-ended column and the lower curve for the pin-ended column. It can be seen that the influence of the end boundary conditions is considerable and the distortional buckling stress of the fixed-ended column reaches that of the pin-ended column only with multiple distortional buckling half-waves. The distortional buckling, like local buckling, is usually taken into account using the effective cross-section area. If the effective area is determined using conventional stub column tests, the influence of the end boundary conditions should be considered.

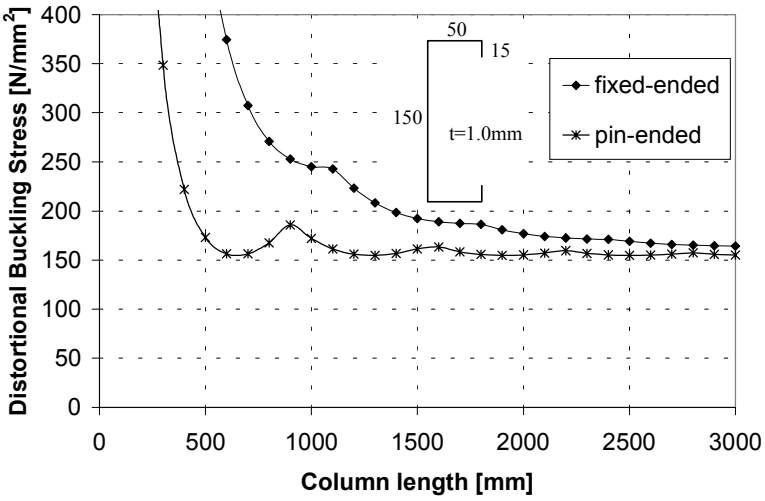

Fig. 2.11: Influence of the end boundary conditions on distortional buckling stress.

2.5 Local and Distortional Buckling of C- and Web-Stiffened C-Sections

The additional stiffeners in the web of the compressed C-section increase the local buckling stress of the section. Nevertheless, due to the stiffeners, more distortional buckling modes occur in the section. Depending on the section dimensions, each distortional buckling mode may reach the minimum value independently, or the minimum value may be the result of interaction of the different modes. In the design, the web is usually treated independently and considered as simply supported. The purpose of this chapter is to study buckling behaviour of the C- and web-stiffened C-section as a whole section.

There may be significant interaction between the local and distortional buckling modes for slender C-sections without the web stiffener. Figure 2.12 and 2.13 show examples of the buckling analysis for a pin-ended C-section with dimensions shown in corresponding figure. Local and distortional buckling stresses were calculated separately for each buckling half-sine wavelength using GBT. Local and distortional buckling modes were allowed to buckle interactively in a single half-sine wave when the critical stress resultant is (Davies et al 1998):

$$ {}^{i,jk}W_{cr} = {}^{i,j}W\frac{\beta}{2}(1+\omega)\left[1-\sqrt{1-\frac{4\omega}{\beta(1+\omega)^2}}\right] = \gamma\ {}^{i,j}W \qquad (2.20) $$

where

$$\beta = \frac{1}{1 - \frac{{}^{ijk}\kappa \; {}^{ikj}\kappa}{{}^{ijj}\kappa \; {}^{ikk}\kappa}}$$

and

$$\omega = \frac{{}^{i,k}W_{cr}}{{}^{i,j}W_{cr}} \geq 1$$

The index j corresponds to the buckling mode that gives the lowest critical stress in each half-wavelength. As Fig. 2.13 shows, there is significant mode interaction between the local and distortional buckling for the C-section with a height of 200 mm, if they were allowed to buckle interactively in a single half-sine wave. The interaction curve has no clear minimum point for distortional buckling contrary to such as shown in Fig. 2.12 for the C-section with a height of 100 mm. Thus, using a method, such as FSM, where only the lowest buckling stress (i.e. the interaction curve based on sine half waves) is determined, the minimum distortional buckling stress may be impossible to be determined in some cases. However, in actual structures the local buckling of the studied cross-section occurs first at a lower stress level than distortional buckling, forming multiple buckling half-waves, as can be seen in Fig. 2.14 where a free buckling mode is assumed in GBT analysis. Distortional buckling occurs at a higher stress level, and interaction with local buckling at the same buckling half-wavelengths is not obvious. It can be seen from Fig. 2.14 that the interaction mode follows the local buckling mode. In design, it is reasonable to use minimum local buckling stress for the design of the web and the minimum distortional buckling stress for the design of the flange and the edge stiffeners.

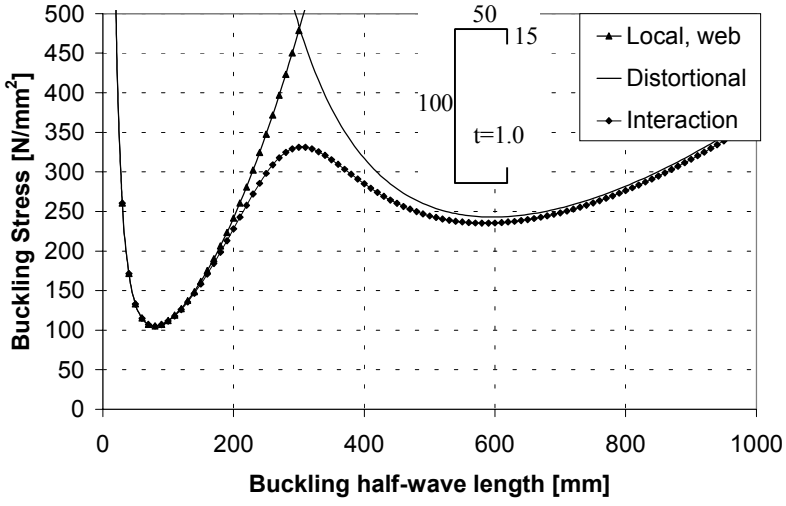

Fig. 2.12: Local and distortional buckling of a C-section with height of 100 mm assuming sine half wavelength.

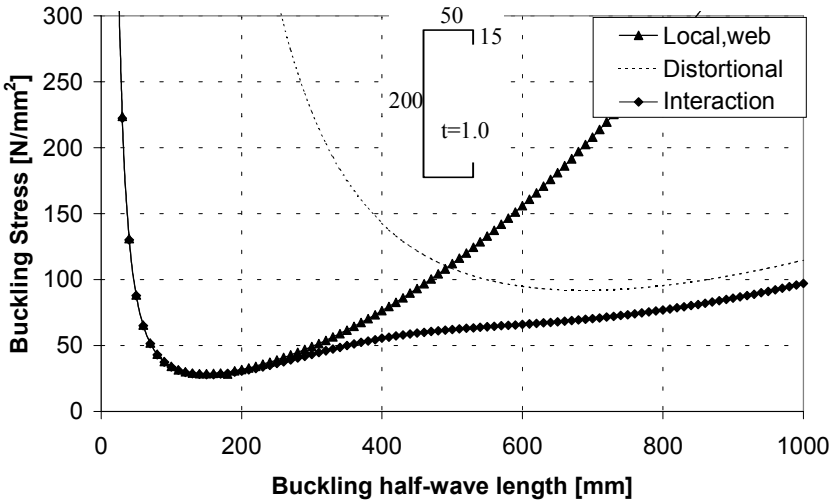

Fig. 2.13: Local and distortional buckling of a C-section with height of 200 mm assuming sine half wavelength.

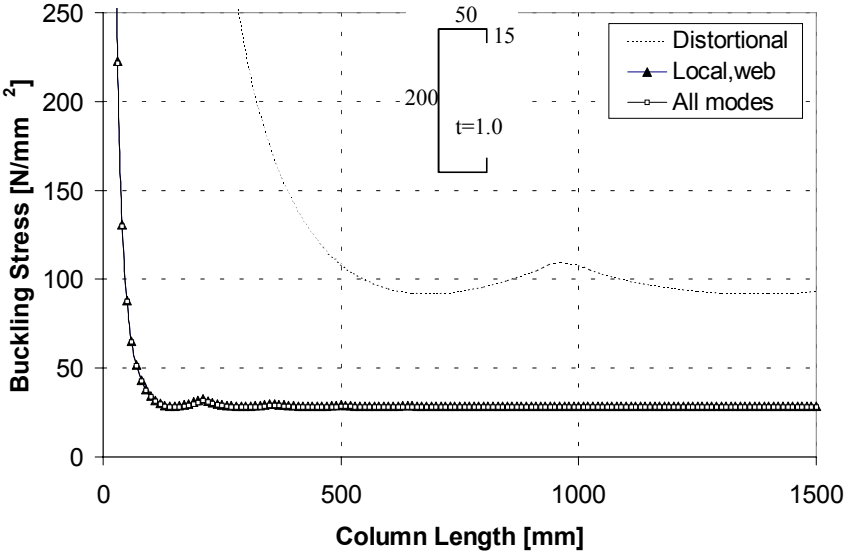

Fig. 2.14: Local and distortional buckling of a C-section with height of 200 mm assuming free buckling mode.

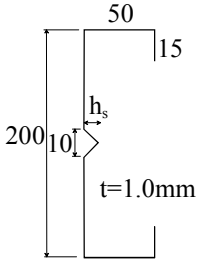

Fig. 2.15: Studied web-stiffened C-section

Local buckling of the web may be increased using web stiffeners such as shown in Fig. 2.15. Figures 2.16 and 2.17 show the GBT analysis results for the section described in Fig. 2.15, when the height of the web stiffener is 3 mm or 6 mm. Each figure shows the individual distortional buckling mode for the edge stiffener (Flange) and for the web stiffener (Web) and the interaction mode, which includes all the distortional buckling modes. In these analyses, the buckling mode is free to develop and there can be several buckling half-waves along the column length. In order to see the contribution of the flanges to the distortional buckling stresses of the web, each figure shows also buckling analysis for an isolated, simply supported web without flanges. Figure 2.17 shows two minimums for that graph. The first minimum corresponds to the local buckling of the sub-elements and the second minimum corresponds to the distortional buckling mode of the web. These graphs are based on FSM and they show the lowest buckling stress at each buckling sine half-wavelength. It should be noted that the curves for whole sections are based on GBT analysis, where the buckling mode is free to develop and there can be several buckling half-waves along the column length.

Figures 2.16 clearly shows that the interaction between different buckling modes is weak for sections with small web stiffener. In that case the interaction mode mainly consists of web buckling. On the other hand, Fig. 2.17 shows quite a significant interaction between web and flange-mode distortional buckling for a section with a web stiffener height of 6 mm. The combined distortional buckling mode gives a minimum buckling stress value over 20% lower than the lowest individual mode.

Figs 2.16 and 2.17 also show that the web-buckling stresses are conservative if they have been determined assuming the web as simply supported and ignoring the contribution of the flanges.

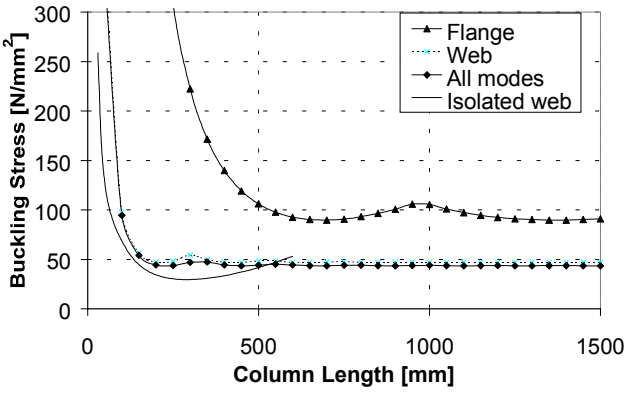

Fig. 2.16: Buckling stresses for C-section web stiffener height of h_s=3 mm.

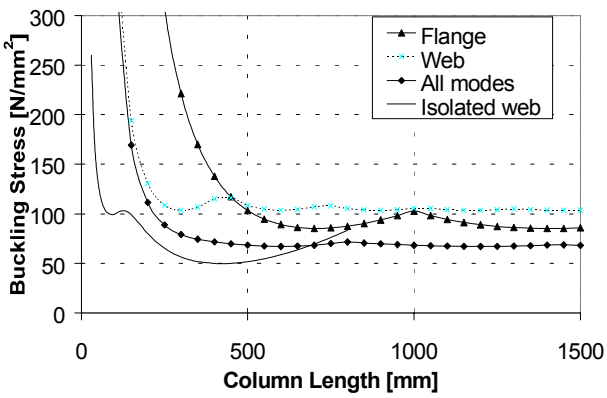

Fig. 2.17: Buckling stresses for C-section with web stiffener height of h_s=6 mm.

Furthermore, finite strip analysis was performed to study the elastic buckling behaviour of a C-section with a lower web height of 100 mm, flange width of 50 mm and thickness of 1 mm. The width of the intermediate stiffener of the web was 10 mm while its height varied between 0-12 mm. The width of the edge stiffener was either 10 mm or 20 mm. Figures 2.18 and 2.19 show the results for the buckling analysis. In both figures, the first graphical minimum for the section without web stiffener (h_s=0) represents the local buckling mode of the web. When the height of the stiffener is 3 mm, the first minimum is the buckling mode where the web stiffener deflects with the web plate. This buckling mode should be considered now as the distortional buckling mode, though the buckling mode and critical half-wave length does not differ considerably from the local buckling mode.

When the web stiffener height is 6 mm, the buckling behaviour is different depending on the edge stiffener height. In the case of the smaller edge stiffener, the first minimum represents the local buckling mode of the sub–element, while the second minimum corresponds to the distortional buckling, which is the interaction mode of the edge and web stiffener buckling. In this case there is, however, quite a small interaction between different distortional modes. In the case of wider edge stiffeners, three graphical minimums can be seen in Fig. 2.19. The second minimum mainly corresponds to the web stiffener buckling and the third minimum mainly corresponds to the edge stiffener buckling. Figure 2.20 more clearly shows the distortional buckling behaviour for this particular section as a result of using GBT. It should be noted that only the distortional buckling modes have been considered in Fig. 2.20, where buckling modes for the edge and web stiffener are displayed separately and the interaction mode of all the distortional buckling modes is displayed as a single curve.

Figures 2.18 and 2.19 show that for other web stiffener heights there are only two graphical minimums. The first one corresponds to the local buckling of the sub-element and the other one corresponds to the combined distortional buckling mode. Figure 2.19 shows that the interaction of the distortional buckling modes is more important for sections with wider edge stiffeners. The graphs show that the distortional buckling stress decreases although the web stiffener height increases.

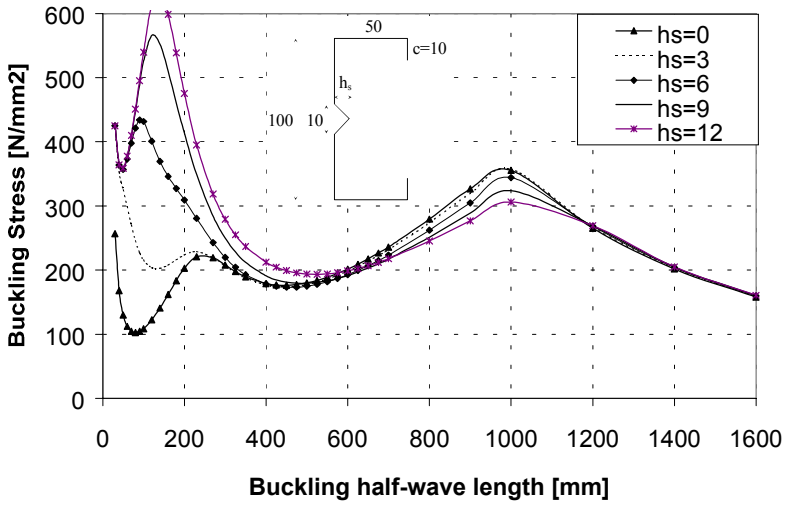

Fig. 2.18: Elastic buckling stress for web-stiffened C-section. Lip width is 10 mm.

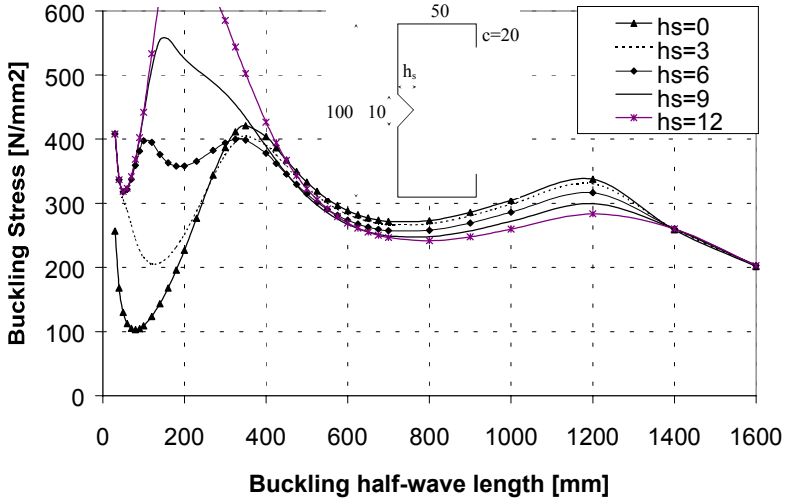

Fig. 2.19: Elastic buckling stress for web-stiffened C-section. Lip width is 20 mm.

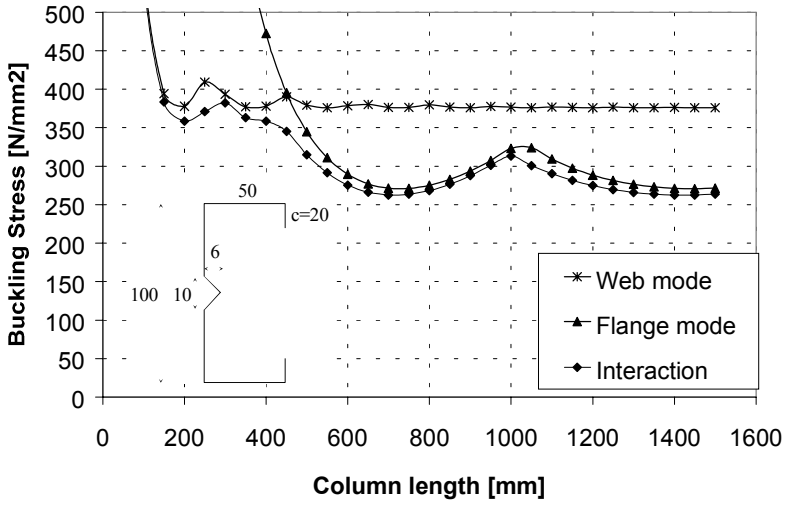

Fig. 2.20: GBT analysis for C-section with web stiffener height of 6 mm.

The previous examples showed that some interaction might occur between different distortional buckling modes. The interaction is usually more considerable if the distortional buckling stress of the web mode is much higher than that of the flange mode.

Each buckling mode can be separately analyzed using GBT. However, Fig. 2.17 showed that the interaction of different distortional buckling modes can be considerable and give lower values than independent buckling modes. For web-stiffened sections, it may be difficult to decide when the design should be conducted independently for the web and the flange and when the interaction of different distortional buckling modes should be considered. Usually, when the distortional buckling of the web is lower than the flange distortional buckling mode, or it has clear minimum point, the web and flange may be designed independently. The web may be considered as a simply supported (stiffened) plate without contribution of the flanges or the web distortional buckling stress may be determined taking into account the whole section.

2.6 Comparison of different web-stiffening systems

The web stiffeners are usually V-shaped grooves, as shown in Fig. 2.21. One possibility for the web stiffening is to form the section into a sigma-shape. In general, the sigma-section has higher distortional buckling stress than the groove-stiffened C-section. On the other hand, the distortional buckling of the sigma-section is more complicated and there is often an interaction between the different distortional buckling modes and between the distortional and global buckling modes as well.

Figure 2.21 shows an example of a C-section with a relatively slender web with height of 200 mm and thickness of 1 mm. Figure 2.21 also shows sigma-shaped and V-grooved sections as modifications of the plain C-section. Both stiffening methods considerably increase the local buckling stress by dividing the whole web into the three sub-elements. Figure 2.22 shows the elastic distortional buckling stresses for all three sections given by GBT. As the graphs show, the sigma-section has much higher critical stress than the plain and the groove-stiffened C-section. In Fig. 2.22, the distortional buckling stresses have been determined including all the distortional buckling modes but not the global buckling modes. This means that the distortional buckling modes of the edge and web stiffeners may interact in the case of the web-stiffened sections. Figure 2.23 shows elastic buckling stresses when all modes are considered. By comparing the stresses in Fig. 2.22 and Fig. 2.23, the interaction between the distortional buckling mode and

global buckling mode for the sigma-section can clearly be seen. In a practical application such as wall structures, the global buckling is often prevented such that this interaction is not important.

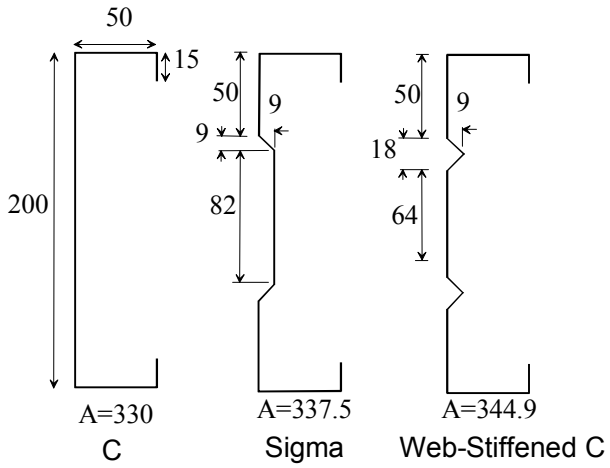

Fig. 2.21: Stiffening of C-section.

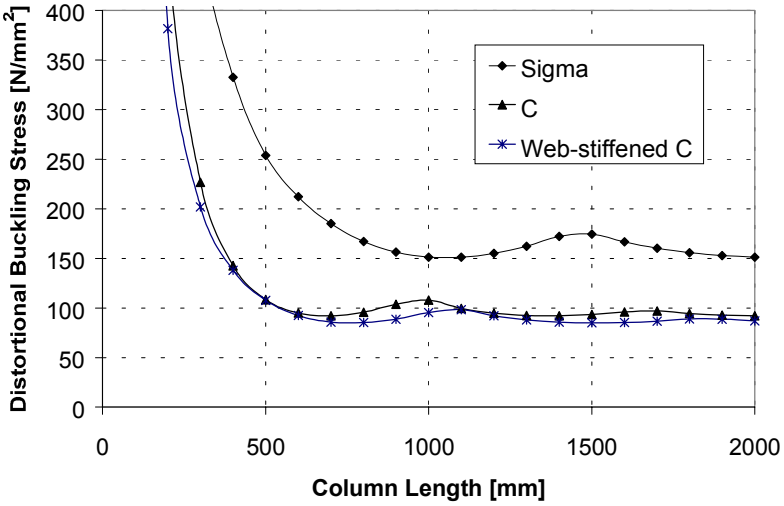

Fig. 2.22: Distortional buckling stress for C-, Sigma- and Web-stiffened C-section.

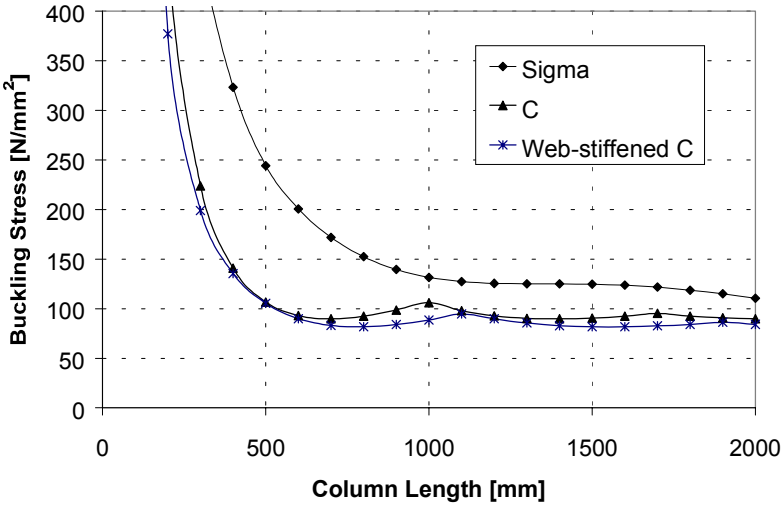

Fig. 2.23: Buckling stress for C-, Sigma- and Web-stiffened C-section.

2.7 Treatment of perforations

2.7.1 Properties of the perforated web part

The web perforation has a considerable effect on the compression behaviour of the section. Mainly, the perforation reduces the local and distortional buckling stress of the section. The perforation changes the web part into very anisotropic material. The axial stiffness in the longitudinal direction is quite high and it is reduced in proportion to the perforated area. On the other hand, the axial stiffness of the perforated web is very low in the perpendicular direction. The bending stiffness of the perforated web is also dependent on the direction. The geometry of the studied perforation-type is illustrated in Fig. 2.24. The reduced stiffness values were achieved by linear FE analysis. Table 2.2 shows the reduction for axial and bending stiffness for the perforated plate in longitudinal and perpendicular direction. The reduction factor indicates the ratio between the stiffness of the perforated part of the web and that of the plain plate with the same dimensions.

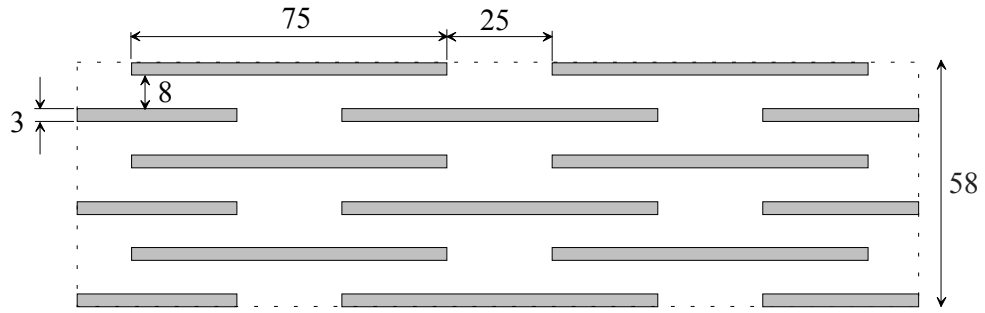

Fig. 2.24: Perforation dimensions.

TABLE 2.2
REDUCTION FACTORS FOR STIFFNESS DUE TO PERFORATION

	Reduction
Axial stiffness =	0.77
Axial stiffness ⊥	0.002
Bending stiffness =	0.77
Bending Stiffness ⊥	0.06

For analysis purposes, it is convenient to replace the perforated part of the web by the plain plate, which has the same stiffness properties as the perforated web part.

The buckling behaviour of different buckling modes, such as local and distortional buckling modes, is dependent on the different properties of the section. For example, the local buckling of

the web-perforated C-section is mainly dependent on the longitudinal axial stiffness of the plates and the longitudinal and perpendicular bending stiffness of the plates. The distortional buckling of the perforated sections is mainly dependent on the perpendicular bending stiffness of the web. These facts lead to the situation where only one equivalent plate thickness is not necessarily adequate for the different buckling analyses. FE analyses were carried out to study the local and distortional buckling behaviour of the perforated sections.

2.7.2 Analysis of the Web-Perforated C-Sections

2.7.2.1 Local Buckling

Local buckling is the most dominant buckling mode for the web-perforated C-sections such as those shown in Fig. 2.25. Local buckling of the perforated sections was studied using the elastic buckling analysis in the NISA finite element application (1996). The analyses were carried out for the isolated web part, which was assumed simply supported, and for the whole section including edge-stiffened flanges. The width of the flanges was 50 mm, and the width of the stiffeners was 15 mm. The plates and sections with a length of 800 mm were modelled including perforations. The length was chosen in order that minimum local buckling stress could be achieved. Parabolic, 8-node shell elements were used in the analysis. The maximum aspect ratio of the element was eight. The buckling analyses were carried out for the plates and sections whose width varied between 150 mm –and 225 mm, and plate thicknesses of 1 mm and 2 mm were included in the analysis.

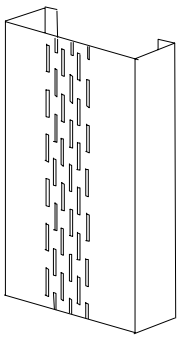

Fig. 2.25: Web perforated C-section.

Local Buckling Analysis of Simply Supported Plate

The results of the buckling analysis for the uniformly compressed and simply supported perforated plates are shown in Table 2.3. Perforation dimensions were same as shown in Fig. 2.24. Table 2.3 also includes analytically determined local buckling stresses for the plates with

the same dimensions but without the perforations. The reduction factor for thickness, as presented by Salmi (1998), is shown in the last column of Table 2.3. The reduction factor is determined from the following equation:

$$k_{red} = \sqrt{\frac{\sigma_{cr.perf.}}{\sigma_{cr.plain}}} \tag{2.21}$$

where $\sigma_{cr.perf.}$ is the elastic buckling stress of the perforated plate, and $\sigma_{cr.plain}$ is the elastic buckling stress of the plain plate. The elastic buckling stress of the equivalent plate with reduced thickness $t_{r.web} = k_{red}\, t$, is thus the same as that of the plate with a perforated part. The $\sigma_{cr.perf}$ has been determined by dividing the buckling load by the gross cross-section area ignoring perforations. This assumption gives a lower bound value for the buckling stress. Figure 2.26 shows the buckling mode of the perforated plate with a thickness of 2 mm and a width of 150 mm.

TABLE 2.3

DETERMINATION OF FACTOR k_{red}

Plate thickness [mm]	Plate width [mm]	$\sigma_{cr.plain}$ [N/mm^2]	$\sigma_{cr.perf}$ [N/mm^2]	k_{red}
1	150	33.7	17.3	0.72
	175	24.8	13.4	0.74
	200	19.0	10.7	0.75
	225	15.0	8.6	0.76
2	150	135.0	67.3	0.71
	175	99.2	52.3	0.73
	200	75.9	41.9	0.74
	225	60.0	33.5	0.75

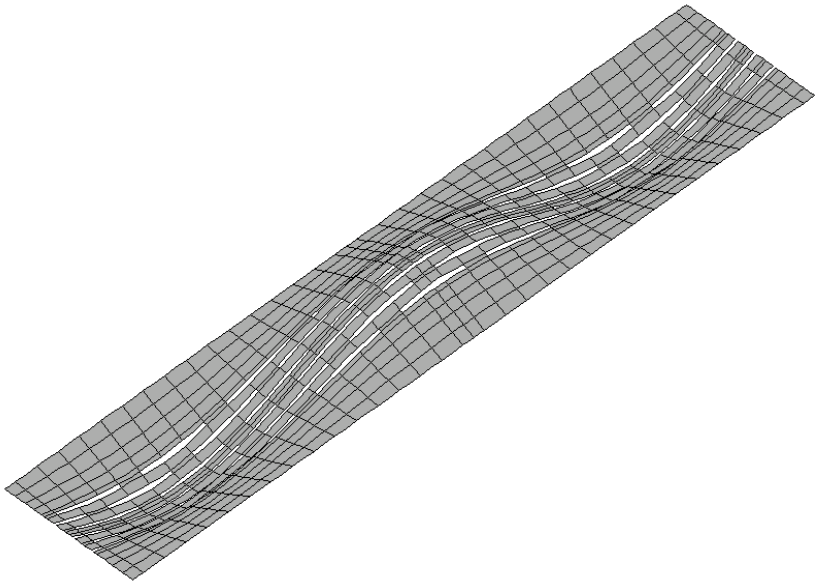

Fig. 2.26: Local buckling mode for the perforated plate.

Local Buckling Analysis of Whole Section

In the design, the local buckling of the web of the C-section is usually analyzed separately assuming simple support along the edges. For slender webs with relatively stocky flanges, this assumption may be conservative. FE analyses were also carried out for whole sections to study this behaviour. Figure 2.27 shows the buckling mode for the plain and perforated section with a web width of 150 mm and a thickness of 2 mm. It can be seen that the buckling half-wave length is shorter in this case than when assuming the web as a simply supported plate in Fig. 2.26. Table 2.4 shows the buckling analysis results ($\sigma_{cr.plain\text{-}C}$) for the plain section including edge-stiffened flanges and Table 2.5 for similar but perforated sections ($\sigma_{cr.perf\text{-}C}$). To obtain the minimum value, the results of the plain sections were verified by calculating several buckling half-wave lengths using the finite strip method. Tables 2.4 and 2.5 also show the difference between the local buckling stress of the simply supported plate (such as shown in Table 2.3) and that of the whole section. The results show that the local buckling stresses of the whole section are over 40% higher than that of the simply supported plate for plain sections. Due to the slender web, the difference is about 75% for the perforated sections. This observation indicates that the restraint given by the flanges is rather more rigid than the simply supported and local buckling coefficient value k = 6.97 that could be used for the web. It should be noted that some of the ratios $\sigma_{cr.perf\text{-}C}$ /$\sigma_{cr.perf}$ in Table 2.5 are greater than theoretical value 1.7425 (6.97/4). This is because the buckling stresses were determined from buckling loads using gross cross-section.

In general, it is evident that local buckling analysis for the whole sections with numerical methods such as FEM, FSM or GBT lead to more economical design than with the use of analytical methods for isolated simply supported elements.

TABLE 2.4
LOCAL BUCKLING STRESS FOR PLAIN C-SECTION

Plate thickness [mm]	Plate width [mm]	$\sigma_{cr.plain\text{-}C}$ [N/mm^2]	$\sigma_{cr.plain\text{-}C}$ / $\sigma_{cr.plain}$
1	150	48.2	1.43
	175	35.7	1.44
	200	27.7	1.46
	225	22.0	1.47
2	150	187.2	1.39
	175	141.0	1.42
	200	108.9	1.43
	225	86.5	1.44

TABLE 2.5
LOCAL BUCKLING STRESS FOR PERFORATED C-SECTION

Plate thickness [mm]	Plate width [mm]	$\sigma_{cr.perf\text{-}C}$ [N/mm^2]	$\sigma_{cr.perf\text{-}C}$ / $\sigma_{cr.perf}$
1	150	28.5	1.65
	175	23.5	1.75
	200	19.2	1.79
	225	15.8	1.84
2	150	110.9	1.65
	175	91.1	1.74
	200	73.9	1.76
	225	60.0	1.79

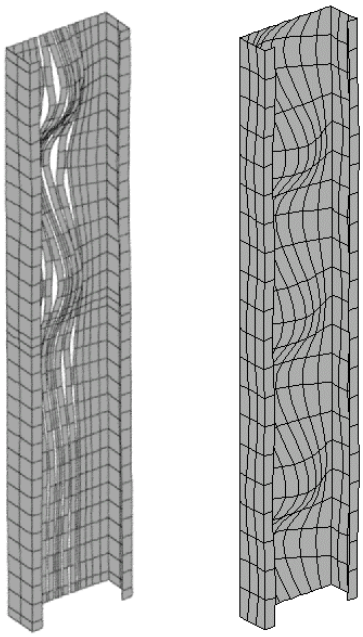

Fig. 2.27: Local buckling modes for perforated and plain C-section.

Conclusions of Local Buckling Analysis

Using the manual calculation method, the local buckling of the web-perforated C-section can be determined by replacing the whole web with a plate of equivalent thickness of 0.72t for studied section dimensions. The local buckling coefficient value of k = 6.97 can be used, which corresponds to the rigid support along the longitudinal edges. A conservative value of k = 4.00 for the local buckling coefficient may be used if the section dimensions significantly differ from the studied sections.

If some numerical analysis such as FEM, FSM or GBT is used, it is reasonable to analyze the whole section. The following study will compare different ways of modelling the perforated web in numerical analysis. In the first method, the whole web was replaced with the plate of equivalent thickness as described earlier. On the other method, only the perforated part of the web was replaced with the plain plate with reduced thickness corresponding to the same perpendicular bending stiffness of the perforated web part. The perpendicular bending stiffness of the perforated web part is 6% of that of the plain plate, i.e. the reduced thickness can be expressed as follows:

$$t_r = \sqrt[3]{0.06}\, t = 0.39t\,. \tag{2.22}$$

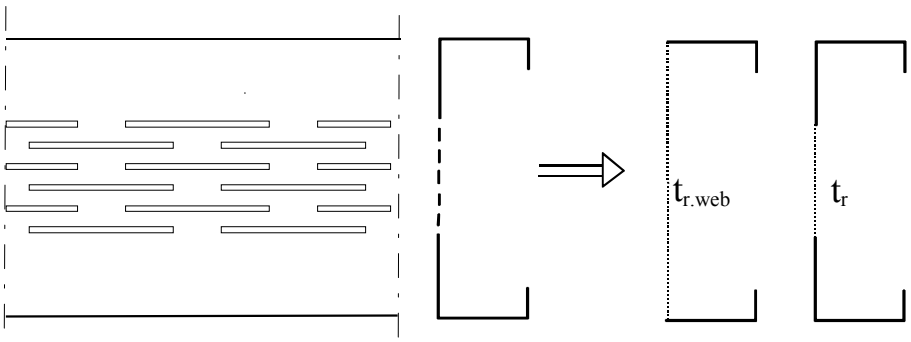

Fig. 2.28: Two ways to model the perforated web.

The local buckling stresses were determined again by FEM for the sections with the same dimensions as above. Table 2.6 shows the comparison of the local buckling stress of the C-section with equivalent thickness ($t_{r,web}$ or t_r) and local buckling stress of a C-section modeled including perforations. Table 2.6 shows that the first method, where the whole web is replaced, is quite conservative while the latter method only slightly overestimates the local buckling stresses.

TABLE 2.6
COMPARISON OF LOCAL BUCKLING STRESSES OF C-SECTION WITH EQUIVALENT THICKNESS AND C-SECTION MODELLED INCLUDING PERFORATIONS

Plate thickness [mm]	Plate width [mm]	$\sigma_{cr}(t_{r.web})/\sigma_{cr.perf\text{-}C.}$	$\sigma_{cr}(t_r)/\sigma_{cr.perf\text{-}C.}$
1	150	0.85	1.17
	175	0.78	1.09
	200	0.75	1.04
	225	0.73	1.02
2	150	0.82	1.12
	175	0.77	1.07
	200	0.74	1.06
	225	0.74	1.05

2.7.2.2 Distortional Buckling

As the analytical expressions for distortional buckling showed, the distortional buckling of the C-section is mainly affected by the rotational restraint at the web/flange juncture. Another factor, which is omitted, e.g. in Eurocode 3, is the compression stress in the web, which reduces the flexural restraint. Schafer and Peköz (1999) take into account the latter factor by using a so-called geometric stiffness term that is stress-dependent. Because the perforated part of the web has low perpendicular bending stiffness, the rotational restraint is considerably reduced compared to the plain section. The distortional buckling behaviour of the perforated section is best described by replacing the perforated part of the web with an equivalent plain plate corresponding to the same perpendicular bending stiffness.

An analytical model for distortional buckling of the web-perforated C-section was developed by the author by modifying the expressions for a plain section given by Schafer and Peköz. In the modified model, the elastic rotational stiffness, $k_{\phi we}$, is modified taking into account the reduced bending stiffness of the perforated part of the section. The web of the C-section in compression is treated as a simply supported beam in flexure, as shown in Fig. 2.29. The reduced rotational stiffness at the end of the beam with thicknesses t and t_r subjected to equal and opposite end moments may be expressed as:

$$k_{\phi we} = \frac{1}{\frac{6(1-\upsilon^2)}{E t^3}\left(b_w + \frac{2b_w^2}{h_w} + \frac{b_w b_r}{h_w}\right) + \frac{12(1-\upsilon^2)}{E t_r^3}\left(\frac{b_r^2}{2h_w} + \frac{b_w b_r}{h_w}\right)} \tag{2.23}$$

where h_w is the height of the whole web and b_w and b_r as shown in the Fig. 2.29.

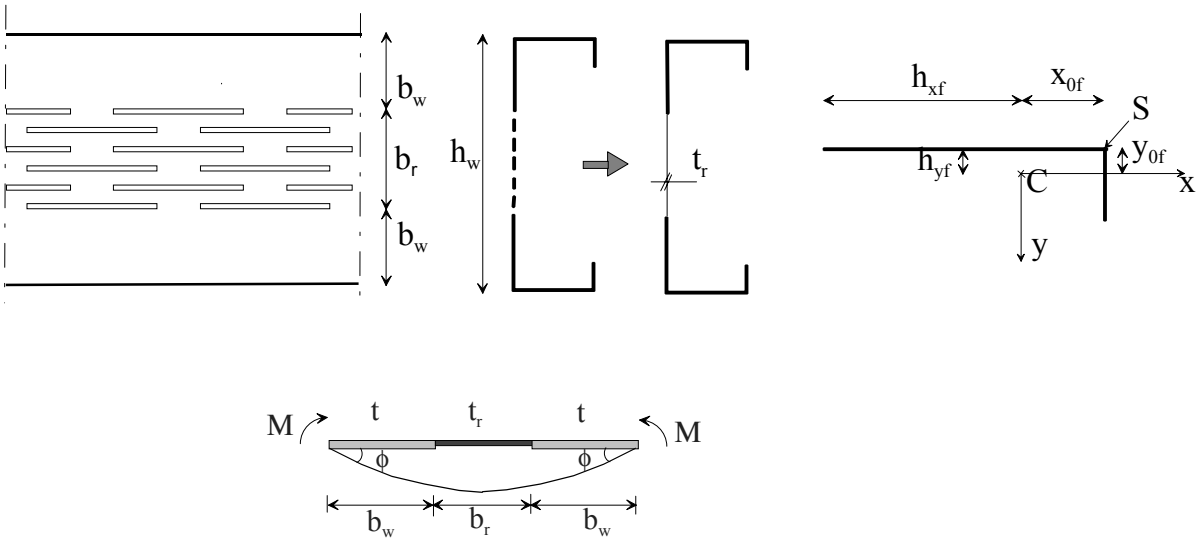

Fig. 2.29: Notations for perforated C-section.

The critical half-wave length in distortional buckling may be expressed now as:

$$L_{cr} = \pi \left[\frac{E}{k_{\phi we}} \left[I_{xf} \left(x_{0f} - h_{xf} \right)^2 + I_{\omega f} - \frac{I_{xyf}^2}{I_{yf}} \left(x_{0f} - h_{xf} \right)^2 \right] \right]^{0.25} \tag{2.24}$$

where the terms in inner brackets are the cross-sectional values of the flange part, and are shown in Fig. 2.29 and Appendix A. The elastic and geometric stiffness terms of the flange are the same as those in the original Schafer and Peköz method, which is shown in Appendix A.

The geometric stiffness $\tilde{k}_{\phi wg}$ of the web is determined using full plate thickness. This approximation gives results that are on the "safe side."

Comparison of Analytical Predictions and GBT Solution

The analytical expressions were verified by comparing analytically determined elastic distortional buckling stresses to the results given by GBT. The comparison was performed for the series of C-sections whose height varied between 150 mm and 225 mm with thicknesses varying between 1 mm and 2 mm. The flange width was again 50 mm and the width of stiffener was 15 mm. The reduced thickness value of 0.39t for the perforated web part with a height of 58 mm was used in both the analytical method and GBT analysis. Figure 2.30 shows the difference of the critical buckling length determined using the above-mentioned methods. As Fig. 2.30

shows, the analytical method gives similar values for critical length as GBT. Fig. 2.31 shows that analytical method also predicts distortional buckling stress with adequate accuracy for all of the sections studied despite quite a rough estimation for the geometric stiffness of the web. Figure 2.31 also shows that the ratio between the analytical and GBT values decreases with the wall thickness and increases with height of the section. These factors indicate the effect of the web slenderness on local buckling and thus on the geometric stiffness terms.

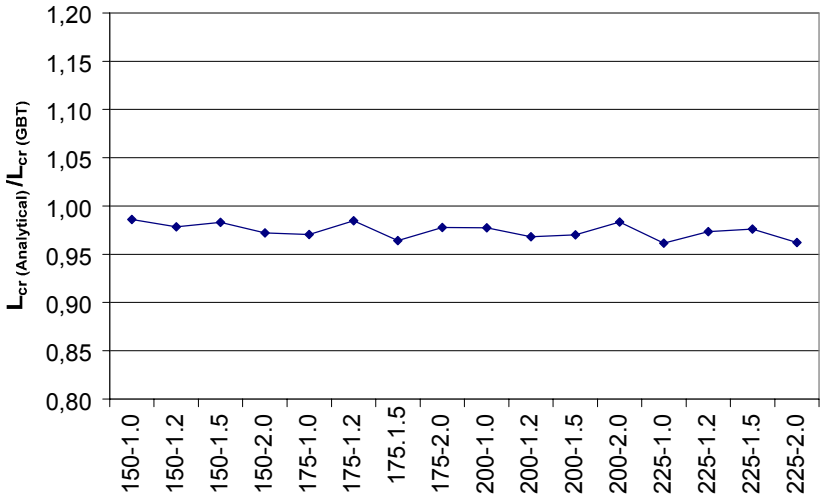

Fig. 2.30: Comparison of critical buckling length in distortional buckling given by analytical expression and GBT.

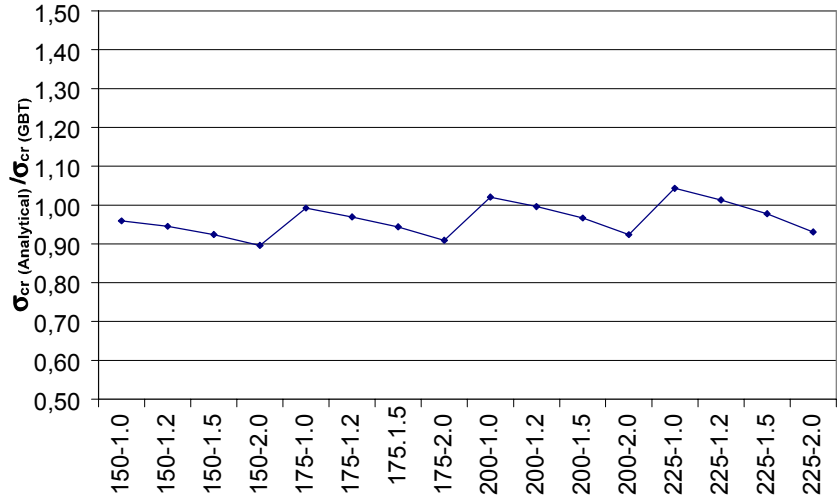

Fig. 2.31: Comparison of elastic distortional stresses given by analytical expression and GBT.

2.7.6 Distortional Buckling of Perforated, Web-Stiffened C- Sections

Distortional buckling stress for the web-stiffened perforated C-section, as shown in Fig. 2.32, should be determined in a similar way as for the plain web-stiffened C-section, but using the reduced thickness for the perforated web part. The analysis is best carried out by a numerical method such as GBT, FSM or FEM. The buckling stress, which corresponds to the interaction of all the distortional buckling modes, is again the safest solution for the elastic distortional buckling stress. Nevertheless, if the distortional buckling stress of the web is much lower than that of the flange and the interaction between different distortional buckling modes is weak, it may be reasonable to use a different distortional buckling stress for the web and the flange.

The main purpose of the web stiffeners is to divide local buckling to the separate fields. Because the plain part of the web, *d*, between the web stiffener and the perforation is quite short, the influence of the middle web part on the whole effective area is quite small. Thus, it may be assumed as an outstanding element with an unsupported edge towards the perforation.

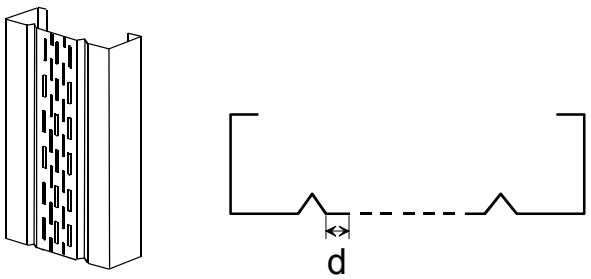

Fig. 2.32: Web-stiffened, web-perforated C-section.

3 LOCAL AND DISTORTIONAL BUCKLING OF COMPRESSED THIN-WALLED MEMBERS IN DESIGN CODES

The current approach for the capacity of the member in the cold-formed steel structure codes and specifications, such as in Eurocode 3: Part 1.3, the American AISI Specification or the Standard of Australia and New Zealand AS/NZS 4600, involve determining an effective width of plane elements to account for local buckling. The reduction is based on an empirical correction to the work of von Kármán et al. (1932) completed by Winter (1947). In design, local buckling is generally treated by ignoring any interaction that exists between the elements. Each element is treated independently and classic plate-buckling solutions based on isolated simply supported plates are generally employed.

In the AISI Specification and AS/NZS4600, the inability of an edge stiffener to prevent distortional buckling is taken into account by reducing the local buckling coefficient for the plate element supported by the stiffener to a value below the basic value of 4.0. If the stiffness of the stiffener is adequate to prevent its deformation in a plane normal to the plane of the element, the adjacent element is assumed as stiffened. This design method does not account for the restraint to distortional buckling provided by the web.

The design against the pure distortional mode of buckling is provided in AS/NZS4600, which includes separate design curves for distortional buckling. These design curves are based on research including testing for rack and C-sections by Lau and Hancock (1988), and by Kwon and Hancock (1991). Nominal member capacity of the section subject to distortional buckling may be expressed as:

$$\begin{aligned} N_c &= A f_y \left(1 - \frac{f_y}{4 f_{od}} \right) \quad when \ f_{od} > \frac{f_y}{2} \\ N_c &= A f_y \left[0.055 \left(\sqrt{\frac{f_y}{f_{od}}} - 3.6 \right)^2 + 0.237 \right] \quad when \ \frac{f_y}{13} \le f_{od} \le \frac{f_y}{2} \end{aligned} \tag{3.1}$$

where A is the area of the full cross-section and f_{od} is the elastic distortional buckling stress and f_y is the yield stress. These formulas allow some post-buckling reserve when the elastic distortional buckling stress is less than half of the yield stress.

In EC3, the distortional buckling is taken into account by reducing the thickness of the stiffener. Thus, the distortional buckling is involved in the effective area approach and the interaction of local and distortional buckling modes with global buckling modes may be accounted for. The cross-section of the stiffener should be taken as comprising the effective portions of the stiffener itself plus the adjacent effective portion of the plane element. The reduction factor for the stiffener thickness is based on the "column curve" a_0 with α = 0.13. Since the thickness reduction is only applied to the stiffeners, not to the whole cross-section, this method also allows post-buckling reserve.

Schafer and Peköz (1999) proposed a new method for determining the effective cross-section area. They found that if distortional buckling is considered, then the critical buckling stress of an element (flange, web or stiffener) is no longer solely dependent on local buckling. In order to properly integrate distortional buckling, reduced post-buckling capacity in the distortional mode and the ability of the distortional mode to control the failure mechanism even when at a higher buckling stress than the local buckling mode must be incorporated. They proposed the method where the critical buckling stress is defined for each plane element as:

$$f_{cr} = min\left[f_{cr,local}, R_d f_{cr,dist.}\right] \tag{3.2}$$

where R_d is the distortional buckling stress reduction factor to account for reduced post-buckling capacity in this mode. Further, the method also allows distortional mode control even when the distortional buckling stress is greater than the local buckling stress. The selected form for R_d based on numerical analysis by Schafer and Peköz and the experimental results of Hancock et al. (1994) is:

$$R_d = min\left(1, \frac{1.17}{\lambda_d + 1} + 0.3\right) \tag{3.3}$$

where

$$\lambda_d = \sqrt{f_y / f_{cr,dist.}} \tag{3.4}$$

The reduction factor for effective cross-section area is finally defined using Winter's approach:

$$\rho = \frac{1}{\lambda}\left(1 - \frac{0.22}{\lambda}\right) \tag{3.5}$$

where

$$\lambda = \sqrt{f_y / f_{cr}} \tag{3.6}$$

If local and distortional buckling stress is determined by manual calculation methods, the local buckling may be derived by treating each element independently, or using local buckling solutions to account for the interaction between the two elements, as given by Schafer and Peköz (1999).

The above method has been examined for the strength capacity of laterally braced flexural members using the experimental data of 190 experiments of several researchers. The same approach may be possibly used for compressed members. If the local and distortional buckling stress is determined numerically, e.g. using the finite strip method or generalized beam theory, the design formulas could be used for the entire member instead of for an element-by-element approach.

Each of the above-mentioned methods has advantages and disadvantages. In the current AISI Specification, the distortional buckling is included in the effective area approach, then the interaction with local, distortional and global buckling modes is possible. Nevertheless, AISI does not explicitly cover the distortional mode and thus it may be unconservative for members subject to distortional buckling. The Australian Standard is broadly similar to AISI, but it provides design formulas for pure distortional buckling of compression or flexural members. This method requires that the capacity of the members, which may fail in the distortional buckling mode, should be checked for pure distortional buckling and furthermore for interaction of local, distortional and global buckling using a similar expression as in AISI. The sections that are sensitive to distortional buckling usually buckle in pure distortional buckling mode in intermediate column lengths. In these cases the distortional buckling approach usually gives better predictions than the AISI method. The weak link of the Australian Standard is short columns, where distortional buckling can interact with local buckling, or long columns where interaction of all these three buckling modes can occur. On the other hand, the tests have shown (Kwon and Hancock 1991) that the pure distortional buckling approach is applicable for the mixed local and distortional modes, including the case where local buckling occurs before distortional buckling, when sections mainly fail in the distortional buckling mode.

In EC3, the effective area approach accounts for both local and distortional buckling. Local buckling is taken into account by using effective widths for plane elements, and distortional

buckling is taken into account using the effective thickness for stiffeners. The cross-section area reduction is thus carried out independently for these buckling modes, which allows interaction between local and distortional buckling. The effective area approach for local and distortional buckling also allows interaction with global buckling modes. Kesti and Davies (1999a) compared available test results of short columns with different cross-sections with the predictions of EC3, and they showed that the EC3 method gives reasonable results if the elastic distortional buckling stress is determined taking into account the actual column length and end boundary conditions by using, e.g. the generalized beam theory. The original EC3 calculation method for the elastic distortional buckling stress was not appropriate for comparison, because it assumes free buckling of the stiffener giving minimum distortional buckling stress, and it is thus appropriate for longer columns where several distortional buckling half-waves may occur. Table 2.1 in Section 2.3.5.1 showed, however, that the EC3 method for calculating minimum elastic distortional buckling stress is not accurate in all cases. Thus, it is suggested that the elastic distortional buckling stress should be determined using a more accurate method such as presented in AS/NZS4600, or that proposed by Schafer and Peköz, or by using some numerical method. The original EC3 method and the modified method, where the distortional buckling stress was determined using GBT, were used in the study by Kesti and Davies (1999b). The comparison of predicted and test results for short to long columns of different cross-sections showed that both methods are slightly conservative for long columns when global buckling is dominant. This indicates that column curve b used in the analysis may be too conservative, or that the interaction between distortional and global buckling does not occur in practice.

Local buckling and distortional buckling are treated as competitive buckling modes in the method proposed by Schafer and Peköz. Either one of them is chosen to represent the buckling mode for each plane element. Since local and distortional buckling are taken into account by the effective width approach, their interaction with global buckling modes is also considered. The proposal, that the local or distortional buckling mode is chosen as the critical buckling mode for the entire section instead of sub element when using, e.g. finite strip method, may be conservative in some cases. For example, the web of C-sections with a very slender web and stocky flanges buckles considerably earlier than the flange, and the reduction of the whole section due to the web buckling seems to be conservative.

4 PERFORATED STEEL WALL-STUD RESTRAINED BY GYPSUM SHEATHING

Gypsum sheathing has an important role on the compression capacity of the perforated steel wall-stud. The perforation reduces the flexural stiffness of the web and thus the section is very sensitive to distortional buckling. The gypsum sheathing connections give rotational stiffness to the section, thus improving the distortional buckling strength. Another important function of the sheathing is to give lateral support to the stud and thus eliminate or improve flexural buckling of the stud in the plane of the wall.

The lateral and rotational restraint given by the sheathing may be modelled as a lateral spring k_y and rotational spring C_D acting at the corner of the flange and the web, as shown in Fig. 4.1. The rotational restraint mainly consists of the flexural stiffness of the sheathing and rotational stiffness of the connection between the sheathing and the stud. The restraint is slightly different for opposite distortional buckling modes such as illustrated in Fig. 4.1. In the case when the lips buckle inwards, the screw tends to penetrate the sheathing. The lateral spring stiffness k_y represents the shear stiffness of the shear fasteners. The value of the stiffness may be derived using wallboard fastener connection tests, as described, e.g. by Miller and Peköz (1994).

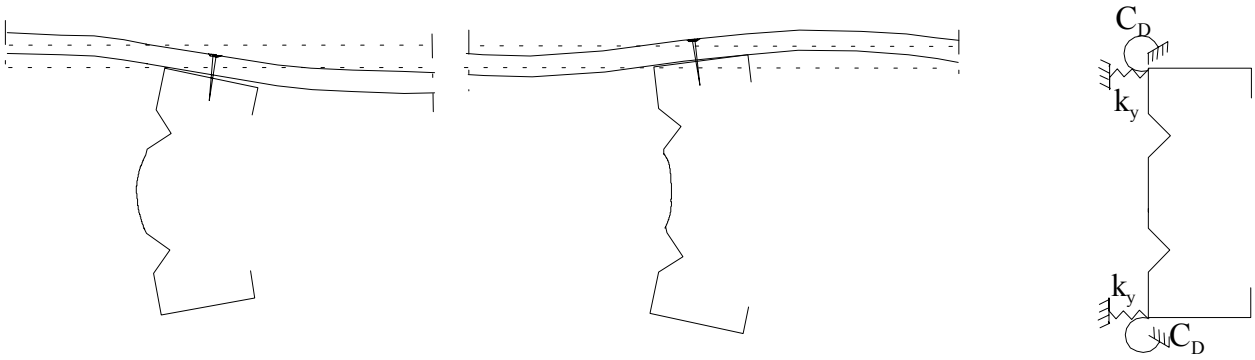

Fig. 4.1: Rotational and lateral restraint given by the sheathing.

The rotational stiffness C_D can be determined as:

$$C_D = \frac{1}{1/C_{D.C} + 1/C_{D.A}} \tag{4.1}$$

where

$C_{D,C}$ is the rotational stiffness corresponding to the flexural stiffness of the sheathing;

$C_{D,A}$ is the rotational stiffness of the connection between the sheathing and the stud.

The value of the $C_{D,C}$ may be taken as the minimum value obtained from a calculation model of the type shown in Fig. 4.2, taking account of the rotations of the adjacent studs and the degree of continuity of the sheathing, using the following formulas:

$$C_{D,C} = m / \theta \tag{4.2}$$

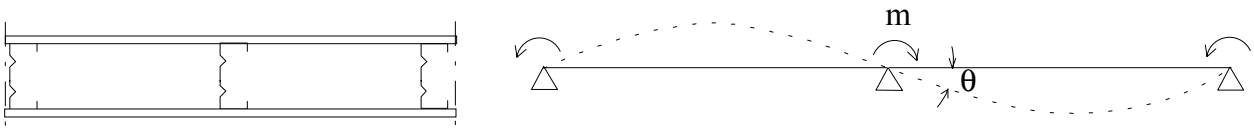

Fig. 4.2: Model for calculating $C_{D,C}$.

When calculating the flexural stiffness of the sheathing, the effective width of the sheathing should be considered. If the screw pitch is under 300 mm, the whole width may be used. If the screw pitch is longer, the effective width should be determined, e.g. by testing.

The value of $C_{D,A}$ is mainly determined by the spring stiffness k_A between the gypsum board and the screw, and it is affected by the penetration of the screw into the gypsum board. The value of k_A may be determined by the penetration test where the screw is pulled through the sheathing. Using the model shown in Fig. 4.3, the value of the $C_{D,A}$ may be then obtained from:

$$C_{D,A} = k_A (b/2)^2 \tag{4.3}$$

where b is the width of the flange and k_A is determined per unit length and the screw is assumed to locate in the middle of the flange.

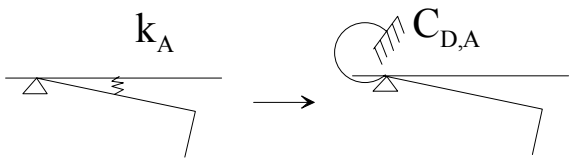

Fig. 4.3: Model for calculation $C_{D,A}$.

The elastic distortional buckling stress of the stud may be then determined using the above-mentioned additional rotational stiffness C_D in the intersection of the web and the flange. However, the connection between the stud and the gypsum board is not uniformly continuous in

reality. Thus, e.g. the FE model should be created by using linear springs k_z and k_y, as shown in Fig. 4.4. The springs should be located in the same locations as the screws and correspond to the lateral and perpendicular stiffness of the screw connection. The k_z is now a linear spring corresponding to the flexural stiffness of the sheathing and rotational stiffness of the connection between the sheathing and the stud. Where the screw is located in the middle of the flange, the k_z can be determined as:

$$k_z = \frac{1}{\frac{1}{k_A} + \frac{(b/2)^2}{C_{D,C}\, w_{eff}}} \tag{4.4}$$

where k_A is the spring stiffness of one connection, $C_{D,C}$ is the rotational stiffness corresponding to the flexural stiffness of the sheathing, and w_{eff} is the effective width of sheathing between screws.

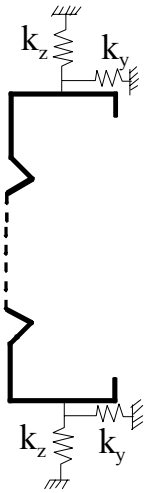

Fig. 4.4: Calculation model for the gypsum sheathed stud in FE analysis.

In practical situation, the influence of the penetration stiffness of the screw and the bending stiffness of the gypsum board are in the same magnitude when determining the value k_z.

5 EXPERIMENTAL RESEARCH

5.1 Short Column Tests

5.1.1 Test Specimens

The tests were performed on sigma-sections and web-stiffened C-sections, whose webs were perforated. Two test series were performed for each section-type. In the first series, the section was tested as a whole, and in the other test series the perforated area was cut away. The latter arrangement was used to investigate the influence of the perforated web on the compression resistance of the section. The sections were labelled as CC-1.2-# and CC-1.5-# for web-stiffened C-sections with a thickness of 1.2 mm and 1.5 mm, respectively. For the code, #, W was used for whole sections and F for sections with only flange parts. The ordinal 1 or 2 was also added if there were two identical tests. The dimensions of the specimens using the nomenclature defined in Fig. 5.1 are shown in Tables 5.1. The mid-line dimensions are the averages of the measured values at both ends. The dimensions and position of the perforations are described in Fig. 5.2. The measured core thickness for the C-sections was 1.15 mm and 1.47 mm, respectively.

TABLE 5.1
MEASURED SPECIMEN DIMENSIONS FOR WEB-STIFFENED C-SECTIONS

	h [mm]	b_1/b_2 [mm]	c_1/c_2 [mm]	e_1/e_2 [mm]	a_1/a_2 [mm]	f_1/f_2 [mm]	d_1/d_2 [mm]	Area A [mm^2]
CC-1.2-W-1	173.7	49.8/48.9	16.2/16.4	22.8/24.8	9.3/9.2	22.4/22.4	13.1/10.7	301.3
CC-1.2-W-2	173.7	49.7/49.8	16.2/16.1	22.8/24.7	9.3/9.3	22.4/22.4	13.1/10.7	300.8
CC-1.2-F	173.6	49.7/49.4	16.3/16.0	23.0/23.1	9.3/8.5	22.8/22.4	11.7/12.6	299.3
CC-1.5-W-1	174.1	49.9/50.2	16.2/16.8	23.6/22.9	8.8/8.3	23.3/22.5	10.0/10.9	377.2
CC-1.5-W-2	174.2	49.5/49.8	16.3/16.7	23.0/23.1	8.9/7.9	22.6/22.5	11.3/10.6	377.1
CC-1.5-F	173.5	49.9/49.6	16.6/14.6	22.3/22.2	8.4/8.2	22.6/22.8	10.0/12.5	373.2

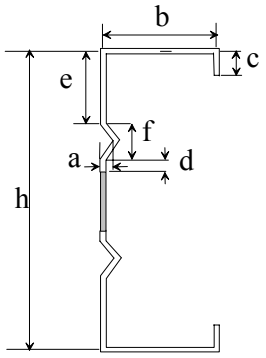

Fig. 5.1: Definition of symbols for web-stiffened C-sections.

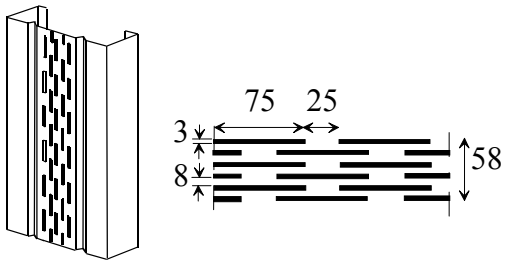

Fig. 5.2: The perforation of web-stiffened C-section.

5.1.2 Material Properties

The material of the test specimens was S350GD+Z250 (EN 10147) with a nominal yield strength of 350N/mm^2. The material properties of each series were determined by tensile coupon tests. Four longitudinal coupons were tested for each series. The coupons were cut out from the centre of the flange plates of the finished specimens. The coupons were prepared and tested according to the EN-10002-1 standard. The mean values of the test results are shown in Table 5.2.

TABLE 5.2

MEASURED MATERIAL PROPERTIES

	Core Thickness [mm]	Yield stress f_y [N/mm^2]	Tensile strength f_u [N/mm^2]	Modulus of elasticity E [N/mm^2]	A_g^* [%]	A^* [%]
CC-1.2	1.15	386	490	200455	15.1	23.4
CC-1.5	1.47	380	492	204167	14.3	23.1

A_g^*: Percentage total elongation at maximum force minus elastic elongation

A^* : Percentage total elongation at fracture minus elastic elongation

The stress-strain curves obtained from the coupon test are shown in Figs. 5.3 and 5.4 for CC-1.2 series, and in Figs. 5.5 and 5.6 for CC-1.5 series. The left Figs. 5.3 and 5.5 show the initial part of the curves including determination of yield stress. The right Figs. 5.4 and 5.6 show the complete stress-strain curve.

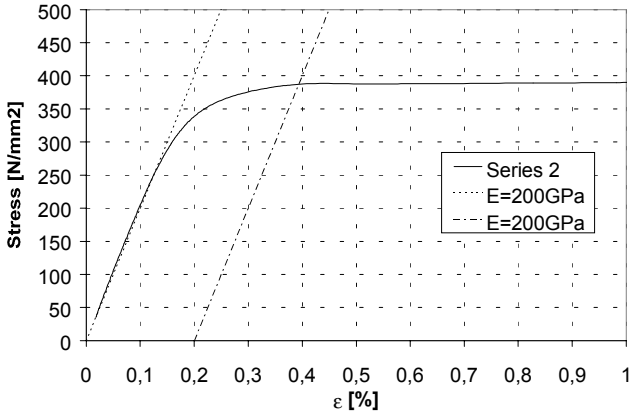

Fig. 5.3: Initial Stress-Strain Curve for Series CC-1.2.

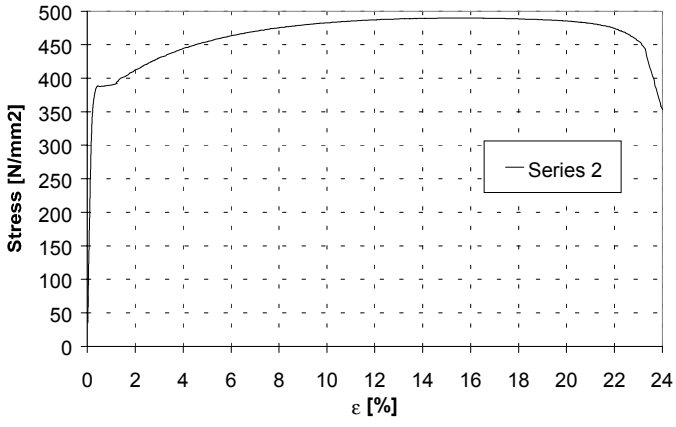

Fig. 5.4: Complete Stress-Strain Curve for Series CC-1.2.

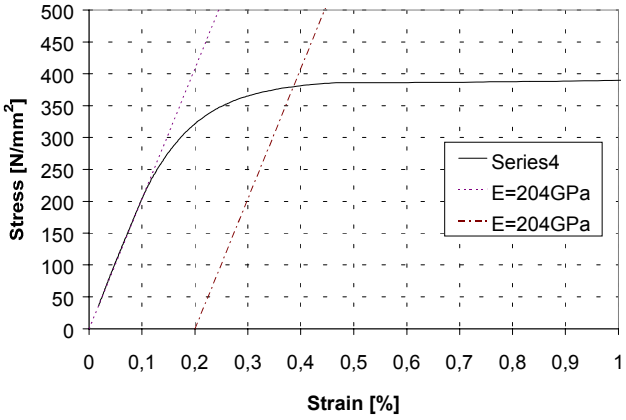

Fig. 5.5: Initial Stress-Strain Curve for Series CC-1.5.

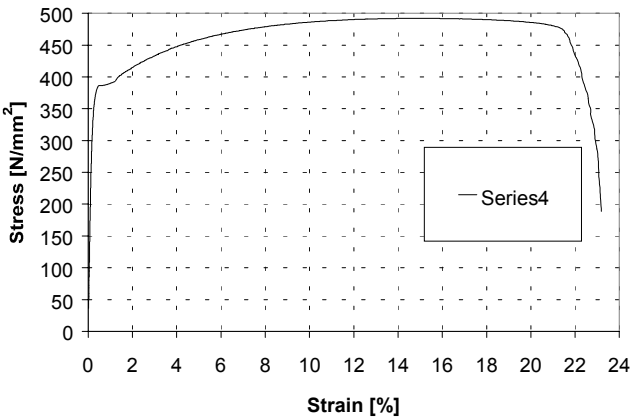

Fig. 5.6: Complete Stress-Strain Curve for Series CC-1.5.

5.1.3 Test Arrangement

All the test specimens were tested in a fixed-end condition. The fixed-end conditions were arranged by casting each end of the specimen in concrete. This kind of arrangement was used to ensure explicit end conditions for the sections. If the section is placed between end plates without fixing, warping is not necessarily completely prevented and comparison to analytical results is difficult. Warping is problematic especially for perforated sections, whose web areas have low bending and shear stiffness. For the plain C-section, the end plates without fixing may give sufficient restraint against warping if the flanges and stiffeners are wide enough. On the other hand, the pin-ended conditions for distortional buckling mode are impossible to arrange for short test specimens. The free length of each specimen between the concrete blocks was 800 mm when minor axis flexural buckling was not critical. The columns with concrete blocks were centred in a 500kN hydraulic testing machine equipped with a lockable plate at one end. The lockable plate allowed the ends of the specimen and the loading plates to bed-in, thus ensuring full contact between the end bearing and test specimen. The loading rate used was 4 kN/min, corresponding to about 10.5 – 13.5N/mm^2 stress increase per minute. The set-up for the column tests is shown in Fig. 5.7. The displacements of the specimens were measured using linear displacement transducers around the sections, as shown in Fig. 5.8. One displacement transducer measured the axial shortening of the specimen.

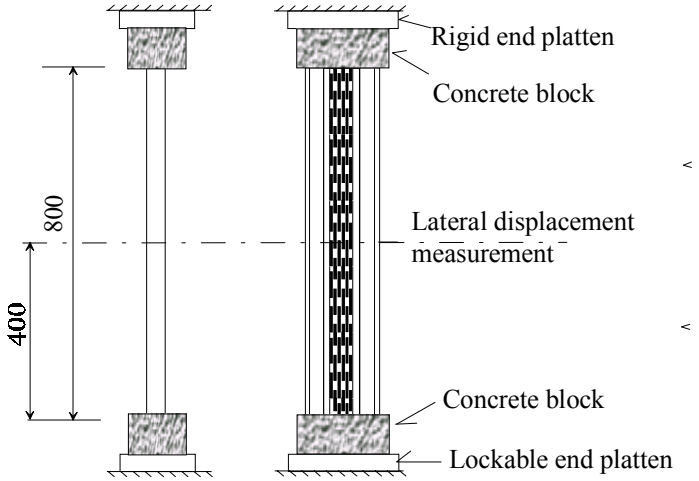

Fig. 5.7: Test set-up for column tests

The initial geometric imperfections along the test specimens were measured before testing. The imperfections were measured in the tip of the flange and in the groove of the web (marked as dz5 and dy3 in Fig. 5.8). The measurements were made at five different locations (at x=0, L/4, L/2, 3L/4, L) along the specimens. The magnitudes of the imperfections were found to be about 0.0-0.6 mm. The imperfection magnitudes at the locations x=L/4, L/2 and 3L/4 and each end of the cross-section (a and b) are presented in Table 5.3. The values shown in Table 5.3 indicate divergences from the straight line between the specimen ends. Positive values indicate imperfections outwards, as shown in Fig. 5.8.

TABLE 5.3

MEASURED INITIAL IMPERFECTION MAGNITUDES ALONG THE SPECIMEN

	Tip of the flange			Web stiffener		
	x=0.25L	x=0.50L	x=0.75L	x=0.25L	x=0.50L	x=0.75L
CC-1.2-W-1a	-0.3	0.6	0.3	0.2	0.0	0.2
CC-1.2-W-1b	-0.0	0.1	0.1	0.3	0.2	0.8
CC-1.2-W-2a	-0.2	-0.2	-0.1	0.4	0.2	-0.2
CC-1.2-W-2b	0.1	0.1	-0.0	0.5	0.4	-0.0
CC-1.5-W-1a	-0.3	0.6	0.3	0.2	0.2	0.2
CC-1.5-W-1b	0.0	0.1	0.1	0.3	0.2	0.8
CC-1.5-W-2a	0.2	0.3	0.2	0.1	0.1	0.2
CC-1.5-W-2b	-0.1	-0.0	-0.0	0.2	0.3	0.2
CC-1.2-Fa	-0.1	-0.2	-0.3	0.2	0.3	0.2
CC-1.2-Fb	-0.2	-0.1	0.1	0.4	0.4	0.2
CC-1.5-Fa	-0.2	-0.3	-0.3	0.3	0.4	0.4
CC-1.5-Fb	-0.2	-0.3	-0.4	0.3	0.3	0.3

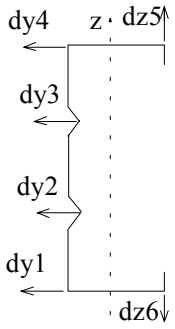

Fig. 5.8: Locations of transducers around section.

5.1.4 Test Results

Both flange parts of the test specimens, whose perforated parts were removed, independently failed in the flexural-torsional buckling mode. The failure loads of these specimens are shown in Table 5.4. The failure loads for whole specimens are shown in Table 5.5. These sections failed in the distortional buckling mode, which was naturally almost similar to the buckling mode failure of the specimens whose perforated parts were removed. In both test series, CC-1.2-W and CC-1.5-W, one specimen failed such that the lips buckled inwards and the other identical specimen such that the lips buckled outwards, as can be seen in Appendix C. In the latter case, the capacity was considerably lower. The restraint of the perforated web with respect to distortional buckling mode was found to have some importance. The failure loads of the whole sections were approximately 10% higher than those of the sections without the web part, when the lips of the whole section failing outwards, and 27% when the lips failing inwards. The load-displacement curves are shown in Appendix B and figures for failed specimens are shown in Appendix C for all tests.

TABLE 5.4
TEST RESULTS FOR "FLANGE PART" SECTIONS

Test specimen	Failure load [kN]	Lips failure mode direction
CC-1.2-F	58.0	inw.+outw.
CC-1.5-F	76.2	inward

TABLE 5.5
TEST RESULTS FOR WHOLE SECTIONS

Test specimen	Failure load [kN]	Lips failure mode direction
CC-1.2-W-1	64.4	outward
CC-1.2-W-2	73.5	inward
CC-1.5-W-1	96.2	inward
CC-1.5-W-2	83.1	outward

5.2 Gypsum Board Braced Column Tests

5.2.1 General

The aim of the gypsum board braced column tests was to define the influence of the gypsum board screw connection on the distortional buckling strength of the section. In this test series, the pitch of the screws connecting the flanges to the boards was varied from 200 mm to 600 mm. The length of the specimen was chosen to be as high as 1800 mm to reduce the effect of the end boundary conditions. Reference tests without gypsum boards were also performed.

5.2.2 Test Specimens

The tests were performed on web-stiffened perforated C-sections, similar to those used in the short column compression tests. The sections were labelled CB-1.2-# and CB-1.5-# with section wall thicknesses of 1.2 mm and 1.5 mm. For the code, #, defines the gypsum board screw pitch used in the tests. CC-1.2-1800 and CC-1.5-1800 specimens are without gypsum boards. The dimensions of the specimens using the nomenclature defined in Fig. 5.9 are shown in Table 5.6. The mid-line dimensions are the averages of the measured values at both ends. The tested sections were taken from same production batch as the short columns, except for specimen CC-1.2-1800. Therefore, the material data shown in Table 5.3 is valid for other specimens. The measured core thicknesses of the sections were 1.15 mm and 1.47 mm. The measured column lengths were within 10 mm of 1800 mm.

TABLE 5.6

MEASURED SPECIMEN DIMENSIONS FOR WEB-STIFFENED C-SECTIONS

	h [mm]	b_1/b_2 [mm]	c_1/c_2 [mm]	e_1/e_2 [mm]	a_1/a_2 [mm]	f_1/f_2 [mm]	d_1/d_2 [mm]	Area A [mm^2]
CB-1.2-200	173.4	49.8/50.4	14.2/16.1	22.7/23.6	9.6/9.7	22.5/22.6	13.8/10.6	299.6
CB-1.2-300	173.6	49.8/50.2	15.0/16.7	22.8/23.9	9.6/9.5	22.5/22.5	13.7/10.4	300.5
CB-1.2-450	173.2	49.6/50.5	13.9/16.5	22.5/23.8	9.7/9.4	22.7/22.6	13.9/10.0	298.8
CB-1.2-600	173.5	49.7/50.3	15.4/16.4	23.0/24.4	9.6/9.5	22.7/22.6	12.8/10.2	300.6
CC-1.2-1800*	173.4	44.4/46.0	13.1/16.6	31.3/25.3	5.8/5.9	18.1/18.2	10.7/13.0	279.9
CB-1.5-200	173.4	49.5/49.4	16.0/15.8	22.5/22.3	9.6/9.9	22.6/22.6	11.5/11.3	379.0
CB-1.5-300	173.7	49.7/50.1	14.8/16.8	22.1/23.0	9.6/9.6	23.0/22.4	11.7/10.3	379.0
CB-1.5-450	173.4	49.6/49.9	15.0/16.3	22.3/22.4	9.7/9.8	22.5/22.6	12.6/10.3	379.1
CB-1.5-600	173.6	49.6/49.6	15.2/16.4	22.5/22.0	9.7/9.8	22.8/23.2	11.7/10.5	378.8
CC-1.5-1800	173.5	49.5/50.0	14.8/16.4	22.7/22.6	9.5/9.5	22.5/22.3	11.7/10.7	378.0

*specimen from different production lot (t_c=1.13 mm, f_y=390N/mm^2 and E=196000N/mm^2).

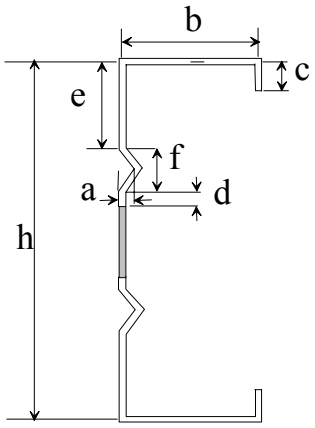

Fig. 5.9: Definition of symbols for web-stiffened C-sections.

The test specimen with gypsum boards is illustrated in Fig. 5.10. Each end of the specimen was cast in concrete to ensure the fixed-end condition. Gypsum boards (Gyproc GN13) with a thickness of 13 mm were screwed to the flanges of the section. Self-drilling gypsum board screws of 25x3.5 mm were used. Four different screw pitches were used: 200 mm, 300 mm, 450 mm and 600 mm. A 600-mm screw pitch was used only in the middle, and the distance to the next screw was 300 mm. In the tests, the board width was 1200 mm and the board was supported at the edges by three wooden struts. Thus, the flexural stiffness of the board was quite the same as that in real structures, with a stud spacing of 600 mm.

The initial geometric imperfections along the test specimens were measured before testing. The imperfections were measured only in the tip of the flange (dz5 or dz6 in Fig. 5.8). The magnitude of the imperfections was found to be about 0.0-1.0 mm except in the case of specimens CB-1.2-600 and CC-1.2-1800, where the maximum initial imperfection was 1.5 mm (=L/1200) and 1.3 mm, respectively.

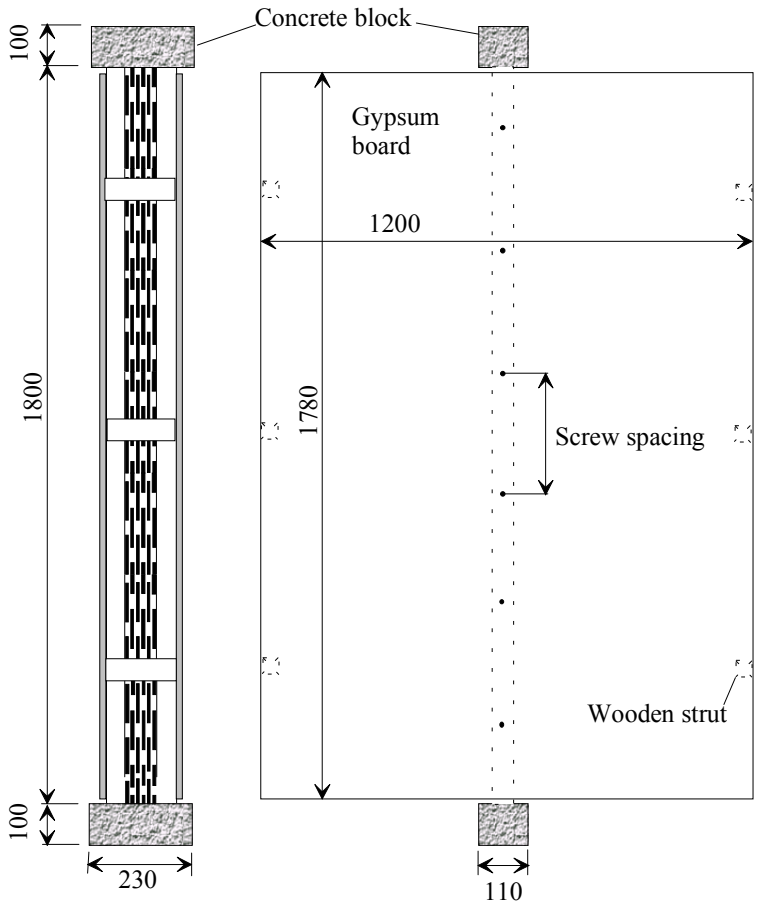

Fig 5.10: Test specimen in gypsum board braced column tests.

5.2.3 Test Arrangement

The columns with concrete blocks were centred in a 500kN hydraulic testing machine equipped with a lockable plate at each end. The upper and lower head are presented in Figs. 5.11 and 5.12. The lockable plates allowed the ends of the specimen and the loading plates to bed-in, thus ensuring full contact between the end bearing and test specimen. The loading rate used was 4kN/min, corresponding to about 10.5 – 13.5 N/mm^2 stress increase per minute. The specimen was loaded until failure. The displacements of the specimens were measured using linear displacement transducers around the sections, as shown in Fig. 5.8. The temperature was around 23 °C, and the relative air humidity was 33% during the test.

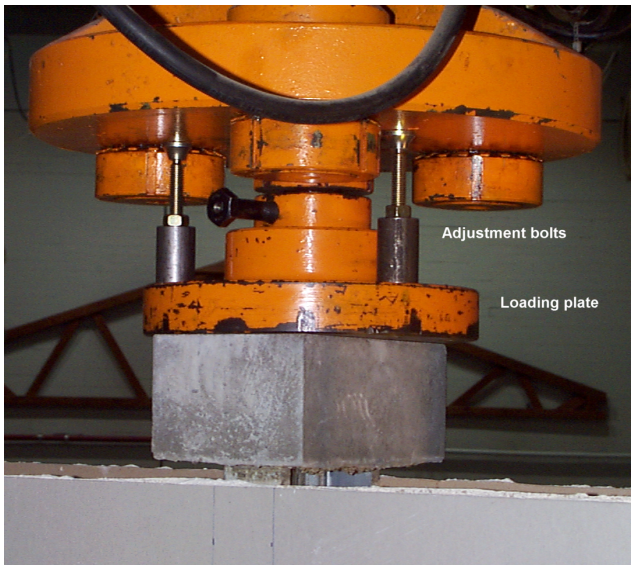

Fig 5.11: Upper loading head.

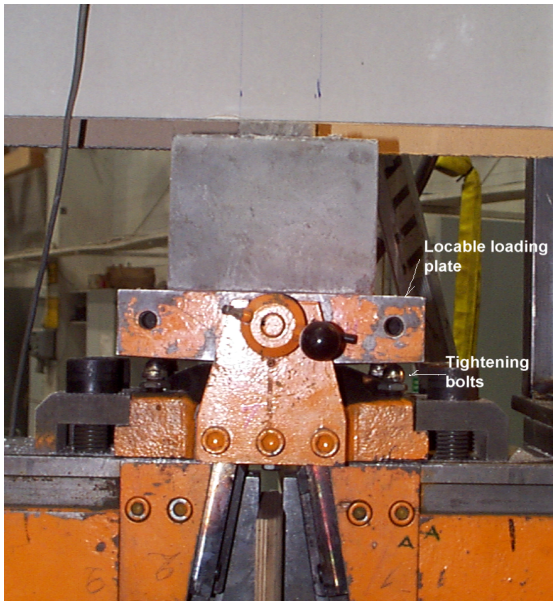

Fig. 5.12: Lower loading head.

5.2.4 Test Results

All the specimens with gypsum board failed in distortional buckling mode. At the final stage, the screws pulled through the gypsum board where the stiffeners buckled inwards, as can be seen in Fig. 5.13. Three buckling half-waves were observed along the specimen. Buckling half-waves did not form between the screws, but the buckling mode was quite similar for each specimen and the buckling mode was independent of screw pitch. However, two opposite buckling modes were observed in the tests. The buckle in the middle formed inwards and the buckles at the ends formed outwards or opposite. The CC-1.2-1800 specimen without gypsum board also failed in a distortional buckling mode forming one buckling half-wave along the section. During the test, two buckling half-waves were observed along the CC-1.5-1800 section. All the failed specimens are shown in Appendix C.

Fig. 5.13: Failure of specimen SB-1.5-600.

The failure loads and the direction of the buckling mode in the middle of the column are summarized in Table 5.7. It can be seen that the screw pitch influences the failure load. Using a screw pitch of 200 mm, the failure load is about 20% higher (t=1.2 mm) and 12% higher (1.5 mm) than using a screw pitch of 600 mm. The test results are in accordance with the observations in the wall panel tests (Kesti & Mäkeläinen 1998), which showed that the thinner the wall thickness of the section, the bigger is the influence of the gypsum board on the failure load of the wall-stud. For a section thickness of 1.5 mm, the failure load of the section with the densest screw pitch (cc200) was 33% higher than that of the section without gypsum board. The difference in the case of 1.2 mm is over 50%, but it should be noted that the cross-section of the CC-1.2-1800 specimen differs from other specimens to some degree.

TABLE 5.7
TEST RESULTS FOR GYPSUM BOARD BRACED COLUMNS

Test specimen	Failure load [kN]	Buckling mode direction in the middle of the specimen
CB-1.2-200	74.6	outw.
CB-1.2-300	69.3	inw.
CB-1.2-450	65.4	outw.
CB-1.2-600	62.2	inw.
CC-1.2-1800	48.7	inw.
CB-1.5-200	95.3	outw.
CB-1.5-300	92.5	inw.
CB-1.5-450	90.5	inw.
CB-1.5-600	85.4	outw.
CC-1.5-1800	71.6	outw.

The load-lateral displacement curves for all the specimens are given in Appendix B. One example of the curves is shown in Fig. 5.14 for the SB-1.2-600 specimen. As Fig. 5.14 shows, the behaviour of this specimen is quite near to the behaviour of a perfect column. There is no lateral displacement until the load reaches the critical value of about 52kN. In the bifurcation point, the lateral displacements increase and the initial post-buckling curves are of a parabolic form. Figure 5.14 clearly shows the post-buckling reserve of the column after distortional buckling has occurred. The load-displacement curves in Fig. 5.14 also show that the buckling of the edge stiffener and the web stiffener occur simultaneously and the displacements are of about the same order. The lateral displacements of the section in the intersection of the flange and the web (dy1 and dy4) can also be seen clearly. The maximum value of these displacements is about 7 mm at the stage of the failure. When the screw pitch is denser, the lateral displacement is usually 1-2 mm, as can be seen in Figs. B12 - B20 in Appendix B.

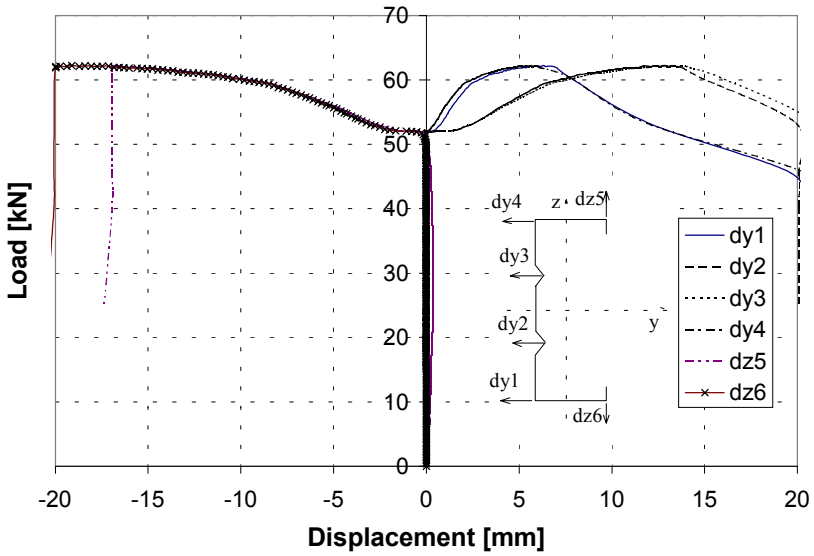

Fig. 5.14: Load-displacement curves for specimen SB-1.2-600.

The influence of the gypsum sheathing on the lateral displacement (dz5) of the flange stiffener of the sections with a wall thickness of 1.5 mm can be seen in Fig. 5.15. Figure 5.15 clearly shows that the gypsum sheathing efficiently prevents the lateral displacement. At the stage of failure, the lateral displacement of the gypsum-sheathed studs is usually under 5 mm, while the lateral displacement of the unsupported stud is over 10 mm. The behaviour is quite similar for sections with a wall thickness of 1.2 mm.

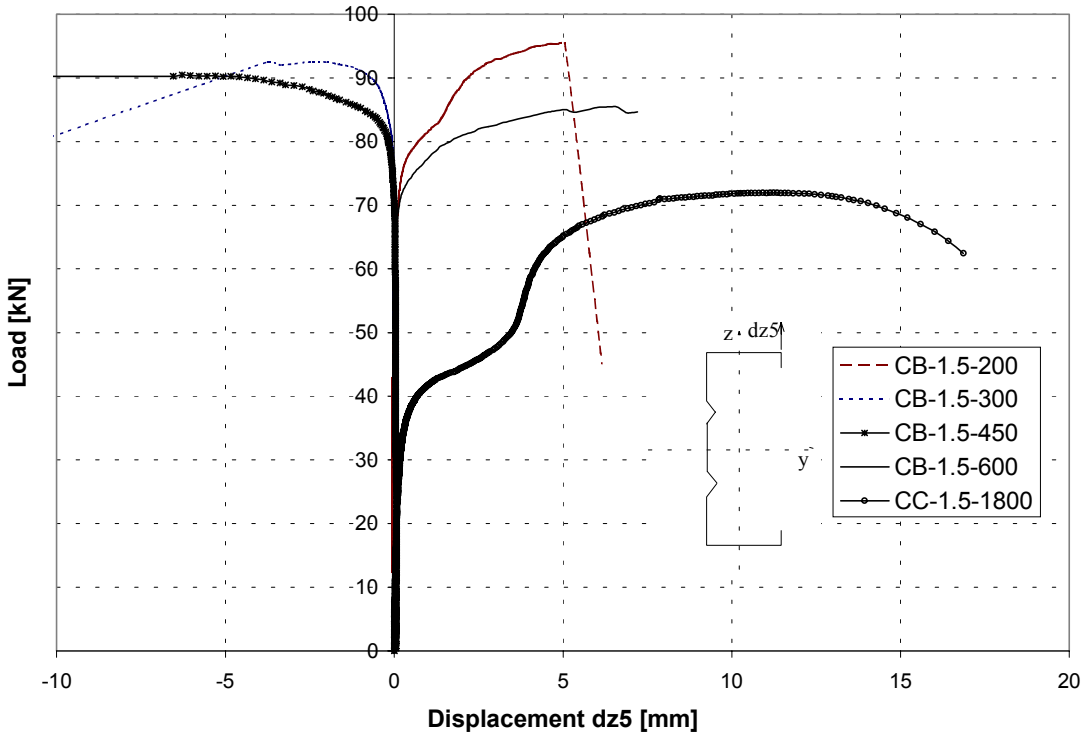

Fig. 5.15: Lateral displacements dz5 for sections with a thickness of 1.5 mm.

5.3 Gypsum Board Connection Tests

Gypsum board connection tests were performed in order to get a stiffness value of the connection which is needed when calculating the restraint stiffness given by the gypsum board. The test set-up is shown in Fig. 5.16. The rectangular piece of gypsum board (100 mm x 100 mm) where fixed between two steel plates having a hole of 45 mm diameter. The steel plates were then anchored to the underframe. The gypsum board screw was drilled through the board into the wooden tension bar. The tension bar was then attached to the testing machine and the tension force and the displacement of the screw-head were registered. The temperature was around 21 °C and the relative air humidity was 45% during the test.

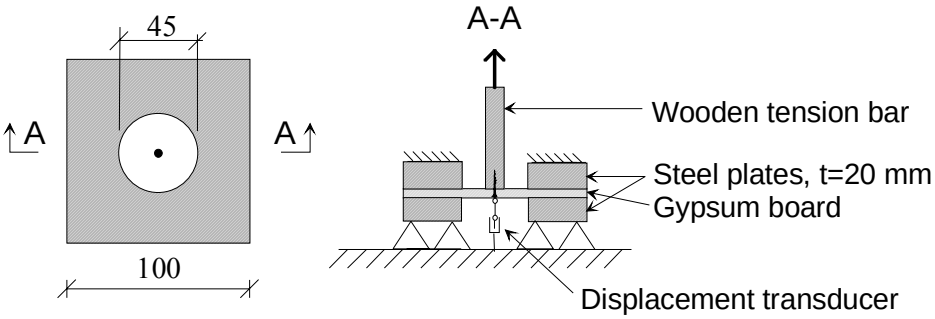

Fig. 5.16: Gypsum board penetration test set-up.

Test results are shown in Table 5.8 and Fig. 5.17. The mean value of the failure load was 0.57 kN. The fastener secant stiffness value was determined at 0.8 times the failure load to provide a more consistent measure of this non-linear quantity. Mean value of the secant stiffness value was 3120 N/mm.

TABLE 5.8

TEST RESULTS FOR GYPSUM BOARD PENETRATION TESTS

	Failure load [kN]	Secant stiffness [N/mm]
Specimen 1	0.55	3017
Specimen 2	0.61	2754
Specimen 3	0.55	3590
Mean	**0.57**	**3120**
St.dev.	**0.03**	**427**

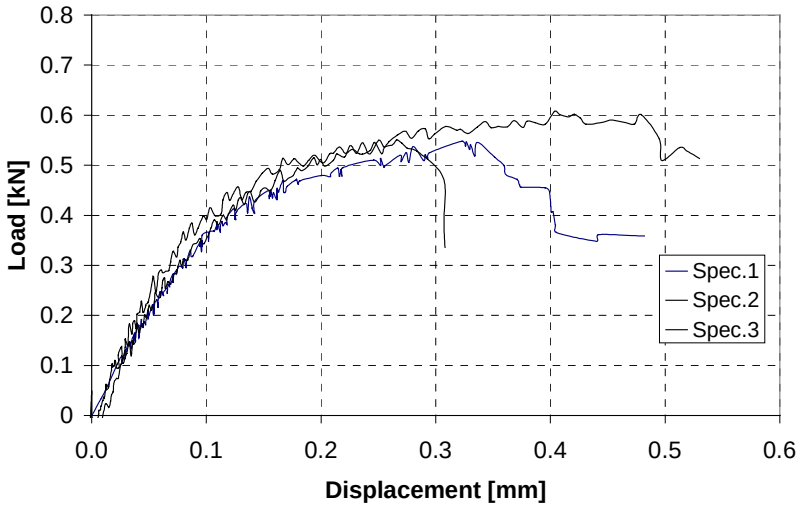

Fig. 5.17: Load-displacement curves for gypsum board penetration tests.

6 NUMERICAL ANALYSIS FOR TESTED SECTIONS

6.1 Elastic Buckling Analysis

6.1.1 GBT Analysis

The generalized beam theory was used to determine the elastic buckling stresses for the tested sections. All buckling modes apart from local buckling were included in the analysis. Each section was analyzed as pin-ended and as fixed-ended for column lengths of 100…2500 mm. The mid-line dimensions of the specimens using the nomenclature defined in Fig. 6.1 are shown in Table 6.1. The width of the perforated web was 58 mm for web-stiffened C-sections. A Young's modulus value of E=200 000 N/mm^2 was used in the analysis for the sections with thickness of 1.2 mm and a value of E=204 000 N/mm^2 for the sections with thickness of 1.5 mm.

TABLE 6.1

SPECIMEN DIMENSIONS FOR WEB-STIFFENED C-SECTIONS

	h [mm]	b [mm]	c [mm]	e [mm]	a [mm]	f [mm]	d [mm]	Area A [mm^2]
CC-1.2	173.6	49.3	16.2	23.4	9.1	22.4	12.0	301.0
CC-1.5	173.6	49.3	16.2	23.4	9.1	22.4	12.0	381.4
CC-1.5-Flange	173.5	49.8	15.6	22.2	8.3	22.6	11.3	373.2

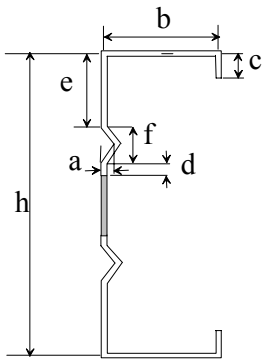

Fig. 6.1: Definition of symbols for sigma-sections and web-stiffened C-sections.

Figures 6.2 and 6.3 show the analysis results for section type CC-1.2, and Figs. 6.4 and 6.5 for section-type CC-1.5, respectively. Each figure contains three curves. The "t-red."-curve is for the section whose perforated web part was modelled as a plain plate with a reduced thickness corresponding to the same bending stiffness of the perforated web. The "Flange"-curve is for the pure flange part without a perforated web part, and the "Full Section"-curve is for comparison of the entire section without perforation. The bending stiffness of the perforated part is 6% for the stiffness of the plain plate. These values were determined by linear FE analysis.

The buckling mode for the pure flange is torsional. For the full and t-reduced section, the buckling mode is mainly distortional buckling in the studied column lengths. However, the critical buckling mode for the pin-ended full sections is flexural in long column lengths, as can be seen from the slopes in the buckling graphs.

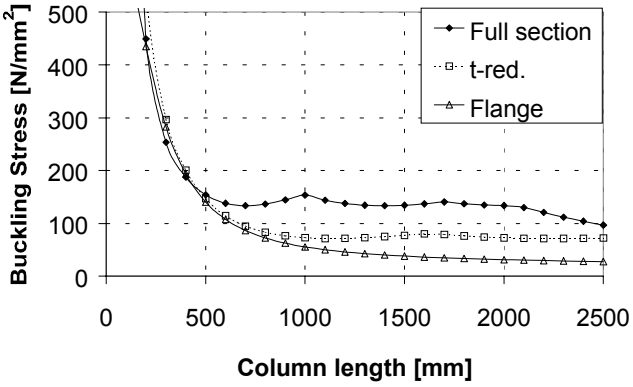

Fig. 6.2: Elastic buckling stress for section CC-1.2, pin-ended conditions.

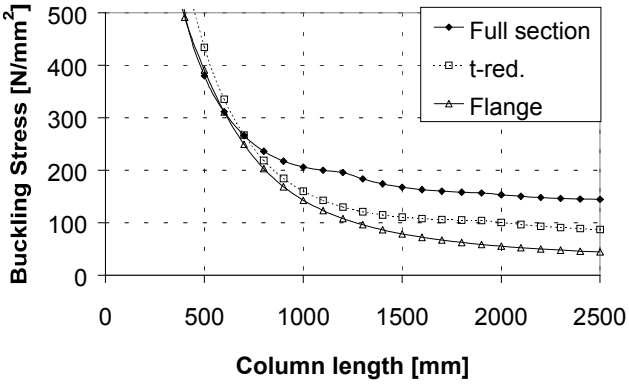

Fig. 6.3: Elastic buckling stress for section CC-1.2, fix-ended conditions.

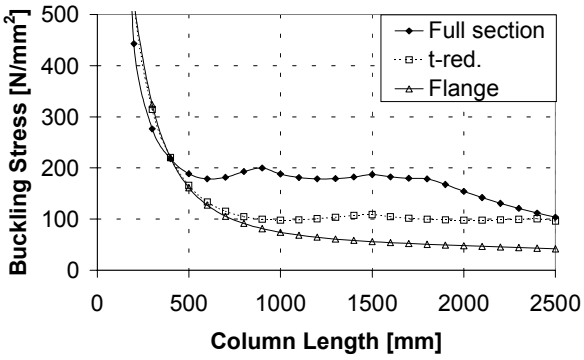

Fig. 6.4: Elastic buckling stress for section CC-1.5, pin-ended conditions.

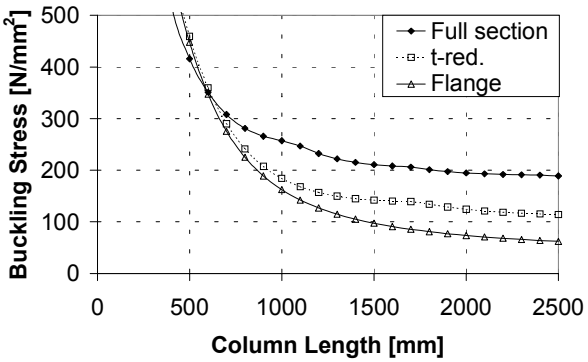

Fig. 6.5: Elastic buckling stress for section CC-1.5, fix-ended conditions.

Figures 6.2-6.5 clearly show the influence of the end boundary conditions on the buckling stresses. The flange sections simply follow the rule that the buckling length of the fixed-end column is half that of the pin-ended column. The distortional buckling does not indicate so clear a relationship, but the distortional buckling of the fixed-end column reaches that of the pin-ended column only with multiple distortional buckling half-waves.

The length of the fixed-ended test specimens was 800 mm. Figures 6.3 and 6.5 show that the difference between the elastic buckling stress of the flange part and the t-reduced section is quite small for the web-stiffened section-types at that column length.

6.1.2 FE Analysis for Short Columns

Elastic FE analyses were carried out for the CC-1.2 sections with a length of 800 mm to compare the elastic buckling stresses with those given by GBT. The buckling loads were determined using the buckling analysis in the NISA application. Four cases were modelled: 1° The section was modelled perfectly including perforations; 2° The perforated area was modelled using a plain element with reduced thickness or Young's modulus; 3° Only the flange part was modelled; 4° The entire section was modelled without perforations. Figure 6.6 shows the FE models for these cases. Eight node parabolic shell elements were used for modelling the sections. A typical element mesh is shown in Fig. 6.6. An attempt was made to limit the number of element aspect ratios to less than eight. The perfectly modelled sections had higher aspect ratios in the perforation region.

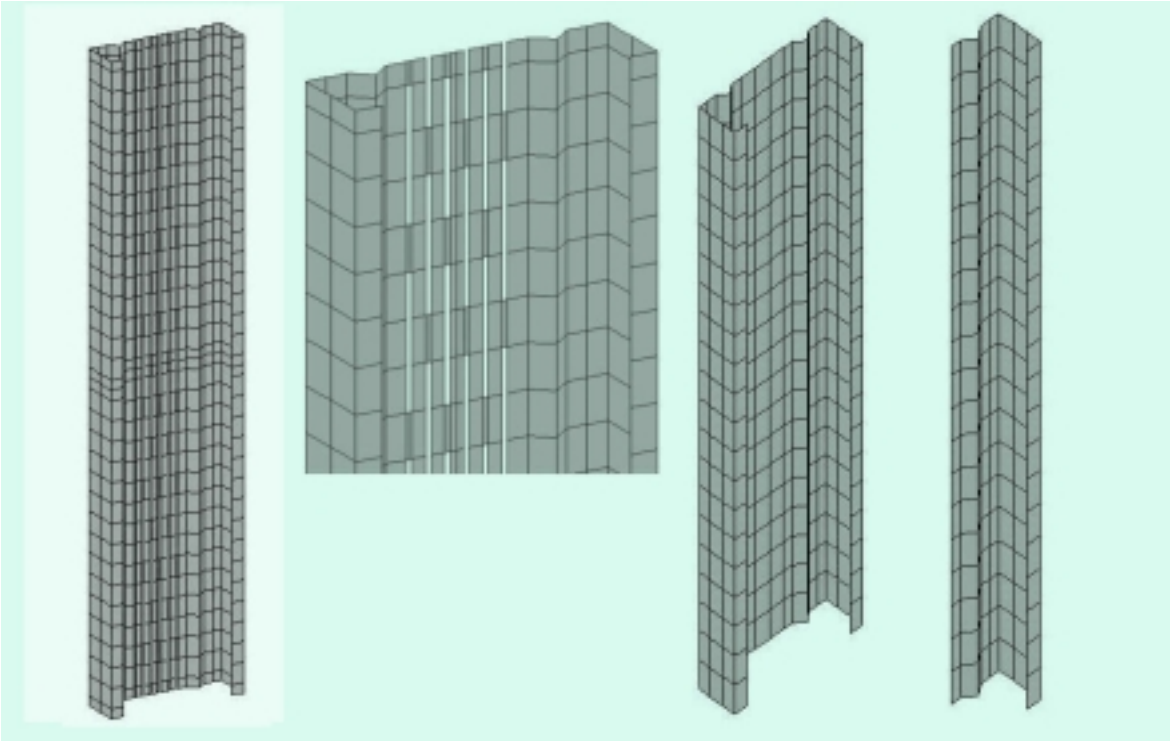

Fig. 6.6: FE models for CC-1.2-section; Perforated model (with zooming), entire section and flange-model.

One end of the section was fixed-end and the other end was fixed but the longitudinal displacement was free in the FE model. Loading was placed for one node and longitudinal displacements of other nodes in the end of the section were coupled to the loaded node. Conventional sub-space acceleration was used in the eigenvalue extraction.

The elastic buckling stresses given by FEM and GBT are shown in Table 6.2. GBT gives slightly (4-6%) higher values than FEM for entire and t-reduced models. The difference may be explained by the interaction with local and distortional buckling, which was allowed in the FE model. Both methods give the same result for the flange model. The lowest eigenmodes of the model, which included perforations, had many variations of different local buckling modes in the perforated area. Some of them also included buckling of the edge stiffeners, but the actual distortional buckling stress level was impossible to determine. The t-reduced model also had some eigenmodes characterized by local buckling, but the lowest distortional buckling mode was quite clear. To avoid these local buckling modes of the web, the perforated web was also modelled using the reduced Young's modulus instead of reduced thickness. In this case the axial stiffness of the equivalent plate is lower than in the t-reduced case, thus leading to lower acted stress under compression force compared to the plain part of the section. For this reason, the E-reduced equivalent plate buckles locally at higher load levels than the t-reduced equivalent plate. The elastic (distortional) buckling stress of the E-reduced model is 14% higher than that of the t-reduced model.

TABLE 6.2
ELASTIC BUCKLING STRESSES FOR CC-1.2 SECTION

	FEM [N/mm^2]	GBT [N/mm^2]
Entire section	222	236
Flange section	203	203
t-reduced model	210	219
E-reduced model	239	-

6.1.3 FE Analysis for Gypsum-Sheathed Columns

A support given by the gypsum sheathings was modelled using lateral and perpendicular linear springs at the point of the gypsum board screw, as described in Chapter 4 and shown in Fig. 6.7. A comparative analysis was carried out for the sections with a thickness of 1.2 mm and with a length of 1800 mm. The spring stiffness values and screw pitch were varied in order to examine their influence on elastic distortional buckling stress. The t-reduced model was used in the buckling analysis.

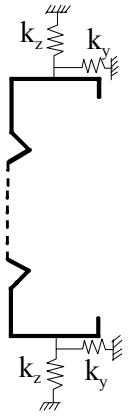

Fig. 6.7: Model for taking into account the support given by the gypsum boards.

Figure 6.8 shows the lowest distortional buckling modes for the CB-1.2-300 section when the perpendicular spring stiffness is variable. A spring stiffness value of k_y = 350 N/mm was used for the lateral springs corresponding to the typical shear stiffness of the gypsum board connection. The stiffness values for the perpendicular springs were varied so that k_z = 100, 1000 and 3000 N/mm. Figure 6.8 shows that, using a relatively low value of k_z = 100 N/mm, there are two buckling half-waves along the section. Three buckling half-waves may be observed in the case of higher values of k_z. It should be noted that even in the case of k_z = 3000 N/mm, the screw position does not form the nodal point for the buckling half-wave.

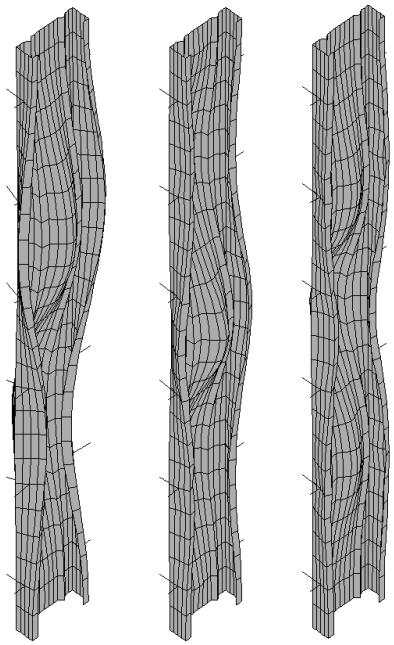

Fig. 6.8: The lowest distortional buckling mode for section CB-1.2-300 using spring stiffness values k_y = 350 N/mm and k_z = 100, 1000 and 3000 N/mm.

In the following study, the screw pitch was varied and constant spring stiffness values of k_y = 350 N/mm and k_z = 1000 N/mm were used in the analysis. As Fig. 6.9 shows, the buckling mode does not considerably differ although the screw pitch is different. In one case, the middlemost buckling mode is inwards and in an other case it is outwards.

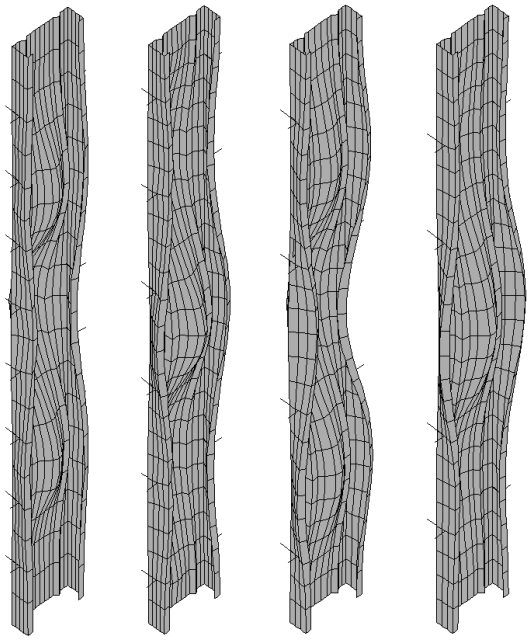

Fig. 6.9: The lowest distortional buckling mode for section CB-1.2 using spring stiffness values k_y = 350 N/mm and k_z = 1000 N/mm and varying screw pitches from 200 mm to 600 mm.

Figure 6.10 presents the influence of the spring stiffness value on the distortional buckling stress of section CB-1.2-300. In Fig. 6.10, the axis of abscissas indicates the stiffness value k_z of the perpendicular spring. Three different cases were determined where the value of k_y was 0 N/mm, 350 N/mm and 1.0e+09 N/mm. Figure 6.10 clearly shows that the value of k_z has a considerable effect on the distortional buckling stress. If the value of k_z increases from the value of 0 N/mm to 500 N/mm, the distortional buckling stress doubles. Above that value, the influence is not so considerable. Figure 6.10 also shows that the distortional buckling stress does not considerably increase if the lateral spring stiffness value increases from k_y = 0 N/mm to k_y = 350 N/mm. If the stud is assumed as fully laterally braced, the distortional buckling stress is slightly higher.

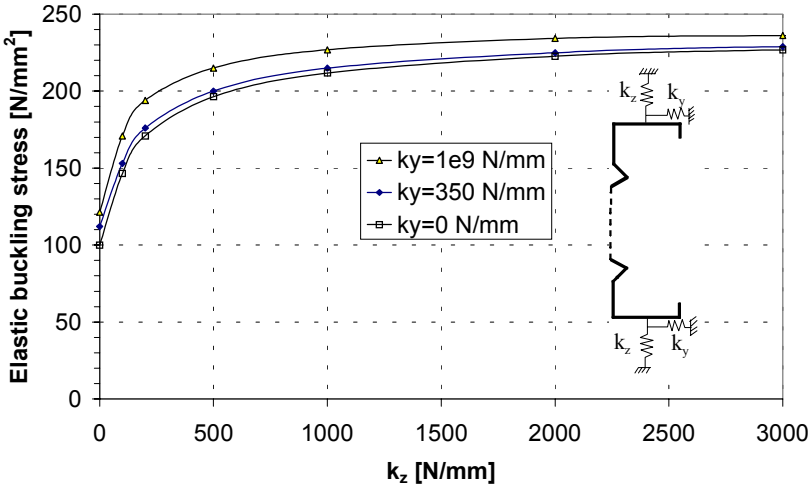

Fig. 6.10: Elastic buckling stress for section CB-1.2-300 (screw pitch 300 mm) using different spring stiffness values.

The influence of the screw pitch on the distortional buckling stress is shown in Fig. 6.11. Three different curves are presented by varying the perpendicular stiffness value k_z. A constant spring stiffness value of k_y = 350 N/mm was used in this analysis. Figure 6.11 shows that, by making the screw pitch dense from 600 mm to 200 mm, the distortional buckling stress increases about 50%.

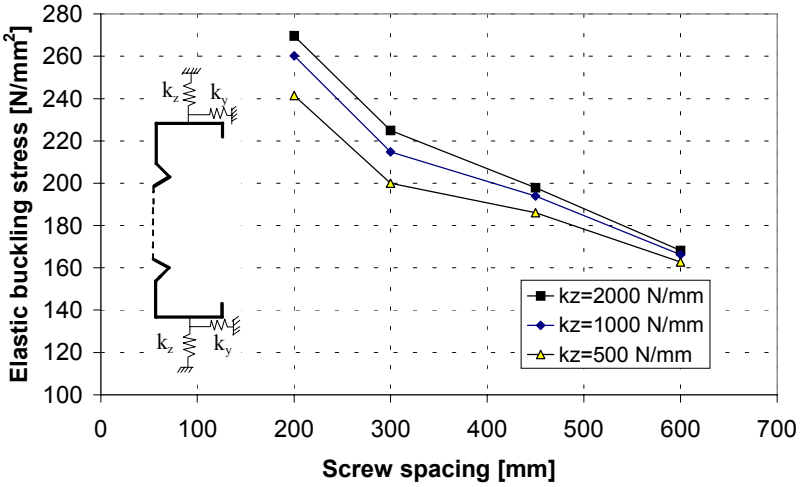

Fig. 6.11: Influence of the screw pitch on the elastic buckling stress of section CB-1.2 using value of k_y= 350 N/mm.

6.2 Non-linear Analysis

6.2.1 General

Non-linear analyses were performed to simulate the short column compression tests to get a better understanding of the different failure modes and importance of the initial imperfection on the failure load. Material and geometric non-linear finite element analyses were carried out using the NISA (1996) application. Similar models and element meshes were used as in the elastic buckling analysis. The E-reduced model was chosen for the non-linear analysis instead of the t-reduced model to avoid local buckling behaviour of the web part. It should be noted here that this method is not better, but the E-reduced model was found to be more stable and easier for the non-linear analysis than the t-reduced model.

Lagrangian formulations were used in the analysis and arch length stepping was used to follow the structural response beyond the critical point. Displacement controlled loading was used in some cases where a small initial imperfection was used. The material model was defined using an elastic, piecewise linear hardening model for the stress-strain curve. Geometric imperfections of different magnitude (0.1t - 1.0t) were included in the analysis. In the first step, small lateral loads were applied to the tip of the edge stiffeners in the middle of the section length. The deformed shape of the section was then used as the imperfection pattern for the model. Both directions for load (inwards, outwards) were used in order to ensure that the lowest capacity of the section would be achieved. Schafer & Peköz (1998) used eigenmode shapes to create an imperfection pattern. In this case, the eigenmode shapes were used only in some cases, because the eigenmode shape of the full-perforated model included many local bucklings within the perforated area.

6.2.2 Material Models

A Young's modulus value of E=200 000 N/mm^2 was used in the analysis. In the E-reduced models, Young's modulus values of E_r= 12600 N/mm^2 were used for the equivalent plain plate in the perforated web area of the web-stiffened C-section. The elastic, piecewise linear hardening model for the stress-strain curve corresponding to the material test results was used in the analysis. The stress-strain relationships of different materials are given in Table 6.3.

TABLE 6.3
MATERIAL MODELS FOR STUDIED SECTIONS

CC-1.2		CC-1.5	
Strain [%]	Stress [N/mm^2]	Strain [%]	Stress [N/mm^2]
0.13	260	0.1225	250
0.2	340	0.2	325
0.35	383	0.4	381
1	390	2	415
10	485	10	487
16	485	16	487

6.2.3 Influence of Initial Imperfection Magnitude

A number of simulations were carried out to determine the influence of the initial imperfection magnitude on the failure load level and on the lateral displacement of the edge stiffener. The results are shown in Fig. 6.12, where different imperfection magnitudes were used for the E-reduced model and for the flange model. The horizontal axis indicates the lateral displacement of the edge stiffener in the middle of the section length. As Fig. 6.12 and Table 6.4 shows, the magnitude of the initial imperfection has little importance for the ultimate load of these sections.

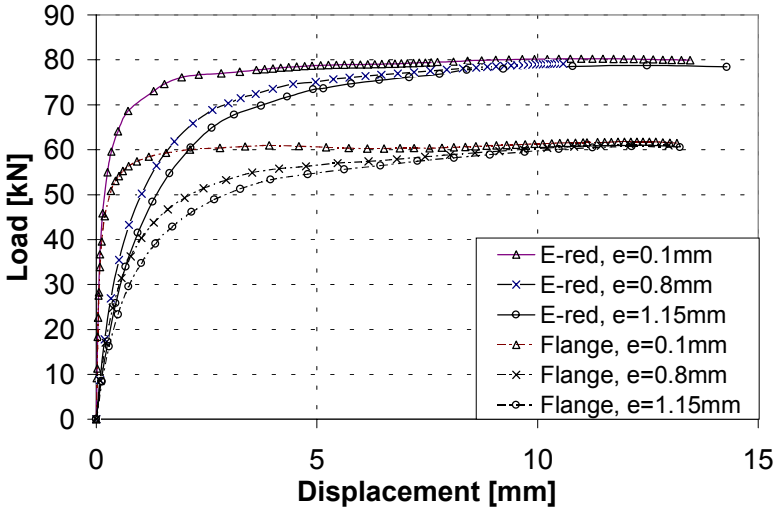

Fig. 6.12: Failure load versus lateral displacement for section CC-1.2 using different magnitudes of initial imperfection.

TABLE 6.4
FAILURE LOADS USING DIFFERENT INITIAL IMPERFECTION MAGNITUDES FOR SECTION CC-1.2

	Flange [kN]	E-red. model [kN]
e = 0.1	61.8	80.3
e = 0.8	61.1	79.2
e = 1.15	60.7	78.8

6.2.4 Influence of Direction of Initial Imperfection

The failure load level and failure mode were found to be sensitive to the given initial imperfection direction. The failure loads were usually considerably lower if the imperfection was given outwards. The failure loads of the flange models were independent of imperfection direction, thus leading to the same ultimate load with a similar (but opposite) path for stiffener lateral displacement. Figure 6.13 shows the analysis results for the E-reduced model and also for the perforated model for section CC-1.2. Two different imperfection magnitudes were used in the perforated model. It is interesting to note that, by using a small imperfection magnitude of 0.1mm outwards, the failure mode is still inwards, although the outwards imperfection gives a lower failure load than the inwards imperfection using an initial imperfection magnitude of 0.8 mm.

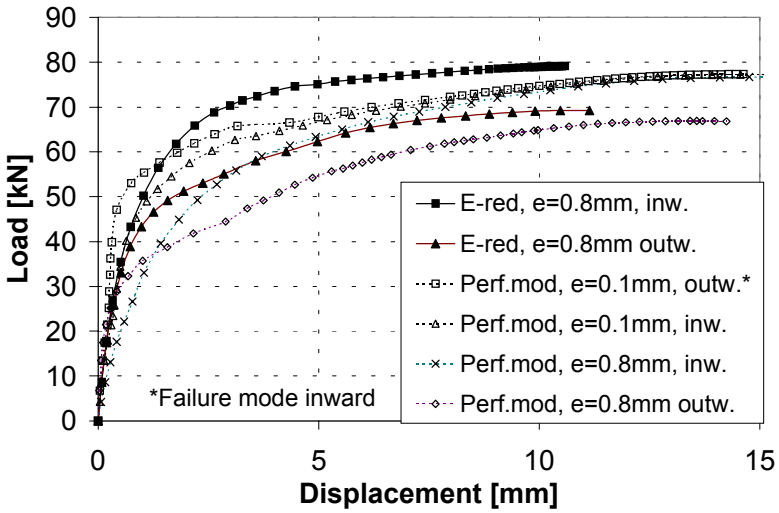

Fig. 6.13: Influence of initial imperfection direction for section CC-1.2.

6.2.5 Comparison Between Different Models and Comparison to Entire Sections

Figure 6.14 shows the difference between different models and a comparison of the perforated section and entire, non-perforated sections. Figure 6.14 shows that the difference between the entire and the perforated section is not very high, if the same initial imperfection magnitude is used. Figure 6.14 also shows that the ultimate load of the E-reduced model is almost the same as that of the perforated model; thus the path is slightly different.

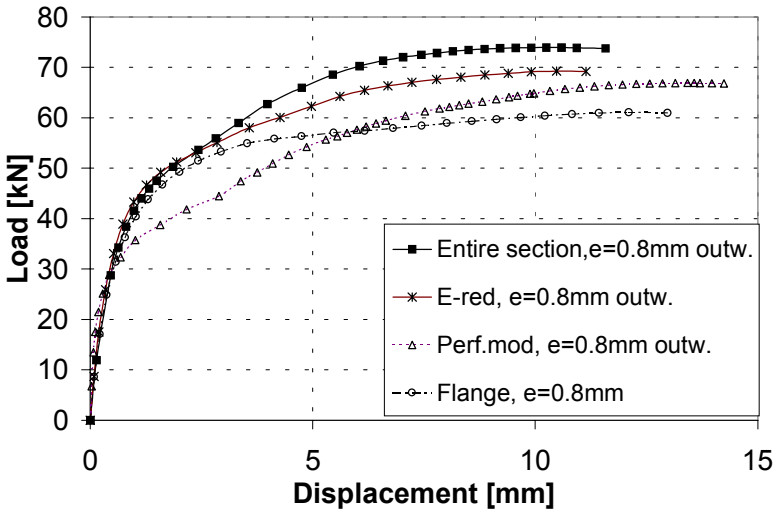

Fig. 6.14: The load-deformation curves for section CC-1.2 using different models and comparison to entire, non-perforated section.

Figure 6.14 clearly shows the difference between the entire section, the E-reduced section and the flange section. The initial part of the load-deformation curve is almost similar. The differences are mainly in the post-buckling area. The change of the stiffness of the perforated model at the load level of 32 kN is due to local buckling of the perforated area. Figure 6.15 shows the deformed shape of the section at this stage, and Fig. 6.16 shows the deformed shape at the ultimate load level. The maximum load is quite the same using the perforated or E-reduced model.

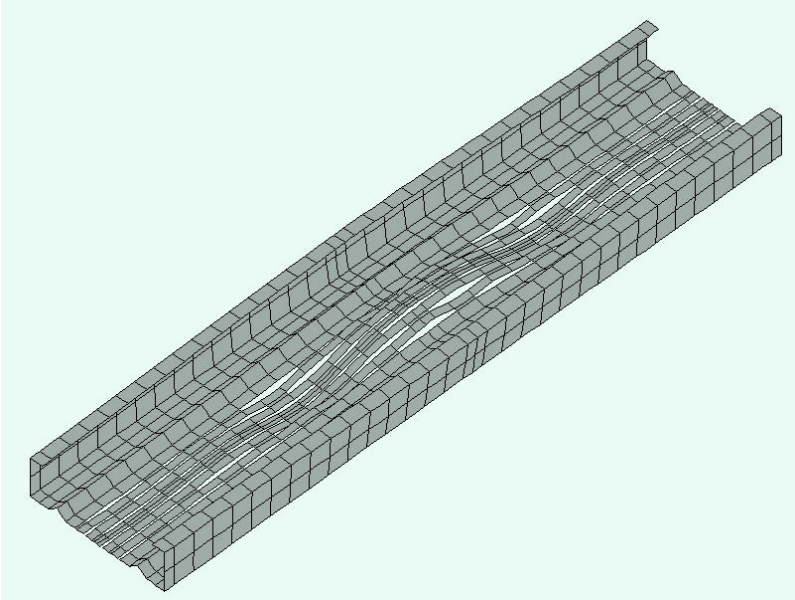

Fig. 6.15: Deformed shape of section CC-1.2 at the load level F=32 kN.

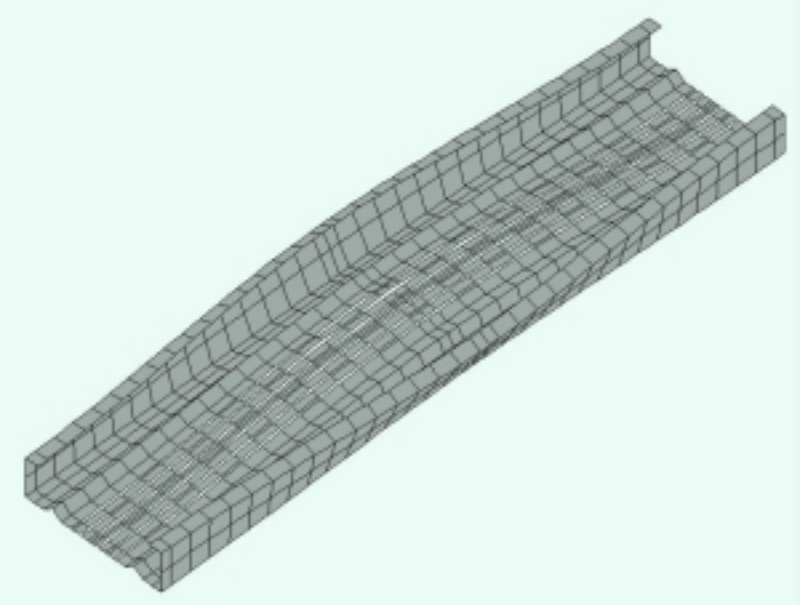

Fig. 6.16: Deformed shape of section CC-1.2 at the ultimate load level F=66.9 kN.

6.2.6 Comparison of Test Results and FE Results

The experimental results of the compression tests for perforated studs CC-1.2-W and CC-1.5-W were compared with the non-linear FE results achieved using perforated models. The results obtained from the pure flange part tests CC-1.2-F and CC-1.5-F were compared with the flange model FE results. It should be noted that some of the test results include only the initial part of the deformation (5…7mm) due to insufficient capacity of LVD-transducers. However, the maximum load level may be read from graphs.

The comparison of the test results and FE results for section CC-1.2-W is shown in Fig. 6.17. Figure 6.17 clearly shows two different cases when the section fails with the lips turning inwards or outwards. The higher test result is for the section that fails inwards and the lower for the section failing outwards. The FE analysis showed the same behaviour and the ultimate loads are in good agreement with test results. The test result of flange section CC-1.2-F is shown in Fig. 6.18 along with the FE –results, which correlate again quite well with test results, giving about 5% higher ultimate load values.

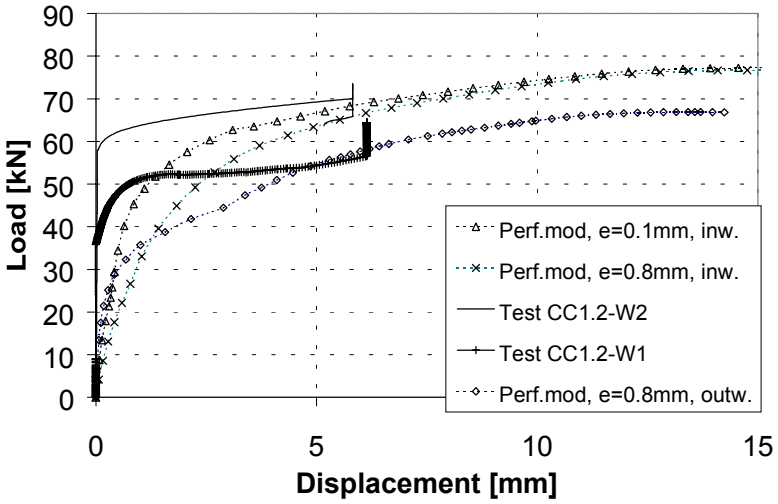

Fig. 6.17: Non-linear FE-results compared with test results for the whole CC-1.2-W section.

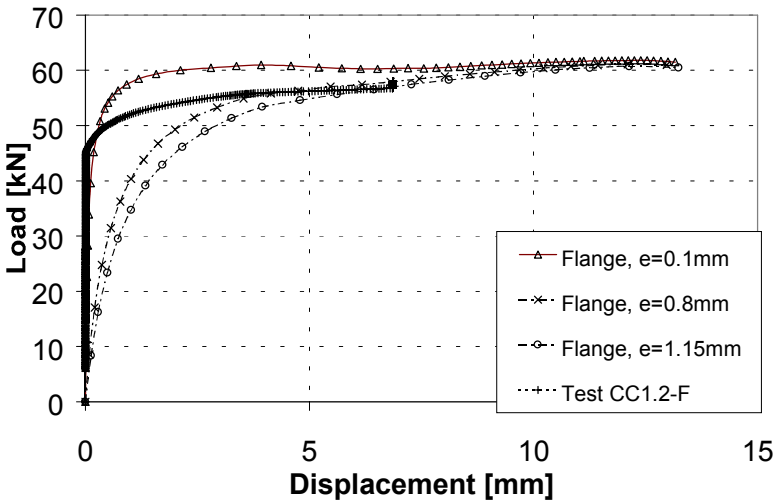

Fig. 6.18: Non-linear FE-results compared with test results for flange section CC-1.2-F.

Figure 6.19 shows a comparison for the CC-1.5-section. Three test results and the corresponding FE analysis result are presented. The highest result is for the case where the section lips failed inwards, the middle one for the case where the lips failed outwards, and the lowest result is for the pure flange part. The behaviour of the CC-1.5 sections is quite similar to that of the CC-1.2 sections.

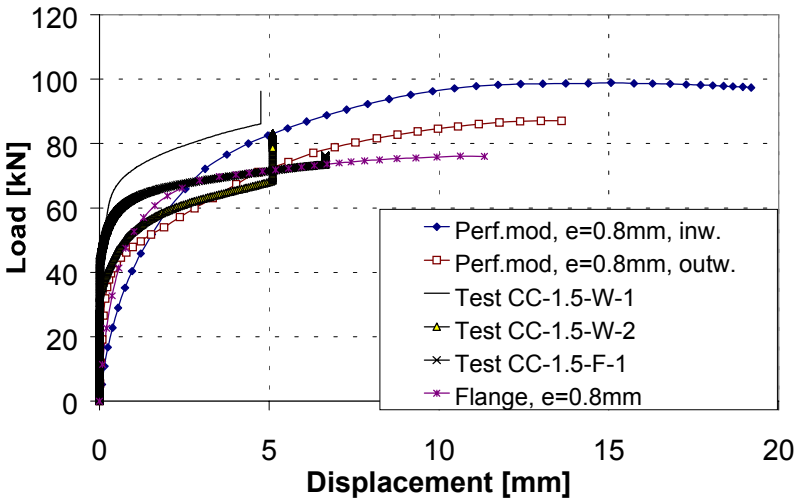

Fig. 6.19: Non-linear FEM-results compared with test results for section CC-1.5.

6.2.7 Conclusions from Non-Linear Analysis

The ultimate compression capacity of the web-stiffened C-section is only slightly dependent on the imperfection magnitude. Instead, the failure load level of the web-stiffened C-sections was found to be sensitive to the given initial imperfection direction. The failure loads were considerably lower if the imperfection mode was given such that the edge stiffeners failed outwards. Thus, if e.g. the eigenmode shape is used for the imperfection pattern, it is important to run the non-linear analysis by using both (+) and (-) signed eigenmodes respectively.

The use of the model where the perforated part of the web was replaced by plain plate elements with a reduced Young's modulus seems to give only slightly higher results than the model where the perforation was modelled perfectly. The lateral displacements of the stiffeners were smaller using the E-reduced model, but both models gave almost the same ultimate load level. This behaviour indicates that the reduced perpendicular bending stiffness of the web seems to be the most important factor to describe the behaviour of the perforated web and its influence on the distortional buckling strength of the section.

The non-linear FE analysis gives a good prediction of the compression capacity of the perforated stud sections. By using an initial imperfection magnitude of L/1000, the mean resistance ratio between the tested and predicted values for all of the tested sections is m = 0.96 and standard deviation is s = 0.02. This result encourages the use of FEM instead of testing at least for different parametric studies and for tentative predictions of perforated sections.

7 COMPARISON OF TEST RESULTS AND ANALYTICAL PREDICTIONS

7.1 Short Column Tests

7.1.1 "Flange Part" Tests

In the case of test specimens CC1.2-F and CC1.5-F, whose web parts were removed, the flange parts behaved independently and their buckling mode was torsional buckling. According to Eurocode 3, the strength should be determined in this case using column curve c (α = 0.49). Local buckling should be considered using the effective cross-section area. The effective widths were determined for each plane element using local buckling coefficient values of k = 4.0 for supported elements, and k = 0.43 for unstiffened elements. The failure load, elastic buckling stress given by GBT analysis, and the comparisons of test results and predicted values are given in Table 7.1. In order to compare different design methods, Table 7.1 also presents the comparison using all the other column curves and using design methods for distortional buckling as well (presented in Chapter 4). In later cases, the elastic global buckling stress was used as distortional buckling stress in design expressions. As Table 7.1 shows, the Eurocode 3 column curve c (α = 0.49) gives about 40% conservative values for specimens whose web part was removed.

TABLE 7.1

COMPARISON OF TEST RESULTS AND PREDICTED VALUES FOR "FLANGE" SPECIMENS.

Specimen	Failure load kN	Elastic buckling stress N/mm^2	N_{Test}/N_P EC3 c-curve	N_{Test}/N_P EC3 b-curve	N_{Test}/N_P EC3 a-curve	N_{Test}/N_P EC3 a_0-curve	N_{Test}/N_P AUS distort.	N_{Test}/N_P Schafer and Peköz distort.	N_{Test}/N_P EC3 distort.
CC-1.2-F	58.0	203	1.46	1.33	1.21	1.12	0.96	0.91	0.94
CC-1.5-F	76.2	225	1.39	1.27	1.15	1.07	0.95	0.92	0.85
		Mean	1.43	1.30	1.18	1.10	0.96	0.92	0.90
		St.dev.	0.05	0.04	0.04	0.04	0.01	0.01	0.06

7.1.2 Whole Section Tests

The whole test specimens failed in distortional buckling mode. Analytical predictions for column capacities according to the Australian Standard, Schafer and Peköz method and the modified EC3 were determined for all specimens. The elastic buckling stresses were determined using GBT combining all buckling modes, apart from the local buckling mode. The perforated part of

the web was replaced with a plain plate with equivalent thickness, as described in Section 2.7.6. The actual end boundary conditions, column length and dimensions as material properties were taken into account in the analysis. In the modified EC3 method, the actual distortional buckling stress was used in order to reduce the stiffener thickness. The effective widths of the plane elements were determined based on the measured yield stress. Local buckling coefficient values of k = 4.0 for supported elements and k = 0.43 for unstiffened elements were used. The plate between the web-stiffener and the perforation part was assumed as unstiffened. An example calculation for section CC-1.2-W-1 according to EC3 is presented in Appendix D.

The failure loads, elastic buckling stresses and comparison of the test values with predicted values are shown in Table 7.2. The table also gives a comparison of the test values and predicted values determined using EC3 column curves, i.e. the distortional buckling stress is assumed as global buckling stress and the strength of the column is reduced instead of reducing the stiffener thickness. As can be seen, all the predictions based on distortional buckling correlate quite well with the test results The EC3 method gives slightly higher capacities than other methods for CC-1.5 sections. By using Schafer and Peköz method, the mean resistance ratio N_{test}/N_{calc} for all four sections is 1.04, while the standard deviation is 0.08. The EC3 method gives m = 1.02 and s = 0.10 and the AUS method m = 1.06 and s = 0.07, correspondingly. Conversely, the strength reduction of the whole section according to the EC3 design curves seems to lead to too conservative values.

TABLE 7.2

COMPARISON OF TEST RESULTS AND PREDICTED VALUES FOR WHOLE SPECIMENS.

Specimen	Failure load kN	Elastic buckling stress N/mm^2	N_{Test}/N_P AUS distort.	N_{Test}/N_P Schafer and Peköz distort.	N_{Test}/N_P EC3 distort.	N_{Test}/N_P EC3 b-curve	N_{Test}/N_P EC3 a-curve	N_{Test}/N_P EC3 a_0-curve
CC-1.2-W-1	64.4	219	0.99	0.97	1.00	1.38	1.25	1.16
CC-1.2-W-2	73.5	219	1.13	1.10	1.14	1.58	1.43	1.33
CC-1.5-W-1	96.2	241	1.11	1.11	1.05	1.51	1.37	1.27
CC-1.5-W-2	83.1	241	0.96	0.96	0.90	1.31	1.18	1.09
		Mean	**1.06**	**1.04**	**1.02**	**1.45**	**1.31**	**1.21**
		St.dev.	**0.07**	**0.08**	**0.10**	**0.12**	**0.11**	**0.11**

7.1.3 Comparisons with Short Column Test Results of other Researchers

7.1.3.1 Description of Tests

Salmi (1998) performed a short column test series on web-perforated C-sections and web-stiffened C-sections. The purpose of these tests was to verify the calculation method for the effective cross-section area for web-perforated steel studs. The tests were conducted between rigid-end plates. Pieces of wood with a height of 50mm were fitted inside the specimen ends. A 10-mm gap was left between the piece of wood and the end plates. The perforation-type was similar to that used in sections CC-1.2 and CC-1.5, as shown in Fig. 7.1. The measured mid-line dimensions as the yield stresses of the sections are shown in Table 7.3 for web-stiffened C-sections, and in Table 7.4 for the C-sections. The nomenclature of the dimensions is shown in Fig. 7.1. Subscripts 1 and 2 indicate the upper and lower part of the cross-section.

TABLE 7.3

MEASURED SPECIMEN DIMENSIONS FOR WEB-STIFFENED C-SECTIONS

	L [mm]	h [mm]	b_1/b_2 [mm]	c_1/c_2 [mm]	e_1/e_2 [mm]	a_1/a_2 [mm]	f_1/f_2 [mm]	d [mm]	t [mm]	Area A [mm^2]	Yield Stress [N/mm^2]
TCJ1	797	149.5	45.3/46.2	16.7/15.5	22.1/25.3	5.1/5.3	18.0/17.8	4.2	1.16	256.1	387
TCJ2	700	149.1	46.7/48.4	19.9/15.5	12.7/16.3	5.3/5.1	17.0/17.2	14.0	1.45	329.6	363
TCJ3	798	174.6	43.2/44.4	14.9/16.8	33.6/37.9	5.3/5.3	17.8/17.8	4.8	1.17	282.8	395
TCJ4	700	198.9	39.2/40.0	16.9/17.0	33.9/37.8	5.3/5.2	16.8/17.8	17.4	1.45	376.9	366
TCJ5	700	224.3	46.6/46.3	17.0/16.8	35.3/38.0	5.3/5.3	17.4/18.0	28.8	1.16	346.6	395

TABLE 7.4

MEASURED SPECIMEN DIMENSIONS FOR C-SECTIONS

	L [mm]	h [mm]	b_1/b_2 [mm]	c_1/c_2 [mm]	e [mm]	t [mm]	Area A [mm^2]	Yield Stress [N/mm^2]
TCS1	800	149.0	49.7/48.2	16.8/15.9	45.5	1.16	257.1	388
TCS2	796	173.7	46.2/47.5	16.4/17.0	57.9	1.17	284.1	392
TCS3	796	173.8	49.1/49.6	16.4/13.4	57.9	1.95	476.6	356
TCS4	798	199.0	44.0/43.3	16.2/16.2	70.5	1.45	378.1	366
TCS5	897	223.8	49.0/49.2	18.9/15.7	82.9	1.16	346.6	395

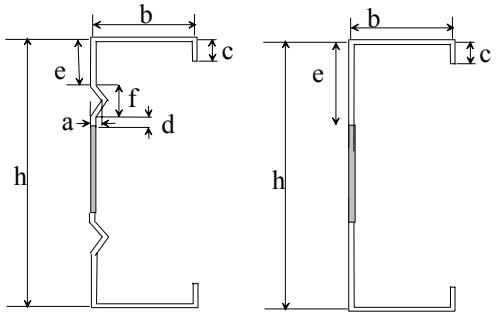

Fig. 7.1: Notations for section dimensions.

The failure mode for the TCJ sections was mainly distortional buckling. The TCJ1 and TCJ2 sections failed such that the edge stiffeners buckled inside and the rest of the TCJ sections such that the stiffeners buckled outwards. TCS1, TCS2 and TCS3 also failed in distortional buckling mode (TCS1 inwards, TCS2 and TCS3 outwards). The relatively slender TCS4 and TCS5 sections failed mainly in local buckling mode.

7.1.3.2 Comparisons for Web-Stiffened C-Sections (TCJ-sections)

A comparison of test and predicted values is shown in Table 7.5 for the TCJ specimens. The elastic buckling stress, given by GBT, is the lowest buckling stress in all the buckling modes apart from local. As can be seen, the results are slightly conservative, especially for high sections. The best correlation between test and predicted values is given by the EC3 method. The results also show that reducing the yield stress using EC3 buckling curves a_0 or a, leads to very conservative predictions of the compression strength of these kinds of sections.

TABLE 7.5

COMPARISON OF TEST AND PREDICTED VALUES FOR WEB-STIFFENED C-SECTIONS

	Failure load kN	Elastic buckling stress N/mm^2	N_{Test}/N_P EC3	N_{Test}/N_P AUS	N_{Test}/N_P Schafer and Peköz	N_{Test}/N_P EC3-α=0.21	N_{Test}/N_P EC3-α=0.13
TCJ1	59.9	182	1.11	1.24	1.15	1.57	1.47
TCJ2	84.1	272	1.00	1.05	1.07	1.26	1.16
TCJ3	63.3	128	1.17	1.34	1.31	2.02	1.92
TCJ4	76.6	135	1.06	1.24	1.20	1.75	1.66
TCJ5	67.3	102	1.28	1.28	1.28	2.18	2.08
		Mean	1.12	1.23	1.20	1.76	1.66
		St.dev.	0.11	0.11	0.10	0.36	0.36

As given in Table 7.4, the web stiffeners of the TCJ specimens are quite low and thus the lowest distortional buckling mode may consist mainly of distortional buckling of the web stiffeners. In the EC3 and Schafer and Peköz methods, it is possible to use different buckling stresses for the distortional modes of the web and the flange. Table 7.6 shows the comparison in the case where the lowest elastic buckling stress is used for the web part, and pure flange distortional buckling stress for the flange part of the section. Table 7.6 shows that both methods give quite good predictions. The predictions for the most slender TCJ5 section are still about 20% conservative.

TABLE 7.6

COMPARISON OF TEST AND PREDICTED VALUES FOR WEB-STIFFENED C-SECTIONS USING DIFFERENT DISTORTIONAL BUCKLING STRESS FOR WEB AND FLANGE

	Failure load kN	Elastic buckling stress N/mm^2	Distortional buckling stress (flange) N/mm^2	N_{Test}/N_P EC3	N_{Test}/N_P Schafer and Peköz
TCJ1	59.9	182	217	1.07	1.10
TCJ2	84.1	272	348	0.95	1.00
TCJ3	63.3	128	155	1.13	1.25
TCJ4	76.6	135	159	1.03	1.16
TCJ5	67.3	102	135	1.23	1.20
			Mean	1.08	1.14
			St.dev.	0.10	0.10

7.1.3.3 Comparisons for C-Sections (TCS-sections)

The web of the web-perforated C-section was similarly analyzed according to the EC3 method and the Schafer and Peköz method. Local buckling stress of the perforated web was achieved using a reduced thickness for the whole web and using the local buckling factor of $k = 4.0$. The reduction factor for thickness $k_{red} = 0.72$ was used for all the sections. The effective area was finally determined reducing the full web area ($h \cdot t$) with the reduction factor ρ. The flange and the edge stiffener were analyzed just as the web-stiffened sections were. Pure distortional buckling stress was used in the design. The predicted values according to the Australian Standard method were achieved based only on reduced distortional buckling strength using Eq. (3.1), i.e. the section capacity based on local buckling was not checked.

The comparison of the test results and predicted values in Table 7.7 shows that the predicted values are quite conservative for slender sections. It was shown in Section 2.7.2.1 that the local buckling factor based on a simply supported plate is quite conservative for sections with particularly slender webs. Local buckling stresses were therefore determined by FEM. Buckling analysis in the NISA application was used and the sections were modelled perfectly including perforations. Table 7.8 shows that the local buckling stresses are on average 93% higher when determined taking into account the whole section. This led to more accurate predictions for compression capacity, as can be seen from Table 7.8. The FE analysis indicates that the analytical local buckling stress of slender web-perforated sections should be determined assuming the web fixed rather than simply supported.

TABLE 7.7

COMPARISON OF TEST AND PREDICTED VALUES FOR C-SECTIONS

	Failure load kN	Distort. buckling stress N/mm^2	Local buckling stress N/mm^2	N_{Test}/N_P EC3	N_{Test}/N_P AUS	N_{Test}/N_P Schafer and Peköz
TCS1	52.5	218	23.8	1.09	0.95	1.06
TCS2	55.3	166	17.8	1.21	1.05	1.23
TCS3	108.3	205	49.5	1.05	1.13	1.16
TCS4	74.5	124	20.9	1.25	1.25	1.43
TCS5	57.3	92	10.5	1.40	1.15	1.50
			Mean	1.20	1.10	1.28
			St.dev.	0.14	0.11	0.18

TABLE 7.8

COMPARISON OF TEST AND PREDICTED VALUES FOR C-SECTIONS USING LOCAL BUCKLING STRESS GIVEN BY FEM

	Failure load kN	Distort. buckling stress N/mm^2	Local buckling stress (fem) N/mm^2	N_{Test}/N_P EC3	N_{Test}/N_P Schafer and Peköz
TCS1	52.5	218	40.8	1.00	0.98
TCS2	55.3	166	34.2	1.07	0.99
TCS3	108.3	205	92.0	0.94	1.02
TCS4	74.5	124	42.6	1.08	1.21
TCS5	57.3	92	22.4	1.20	1.27
			Mean	1.06	1.09
			St.dev.	0.10	0.14

7.1.4 Conclusion for Comparisons of Short Column Test Results

The above comparisons showed that the compression capacity of the short, web-perforated section may be predicted quite well using effective area approaches according to EC3, or Schafer and Peköz, or by using distortional buckling strength according to AUS/NZS4600. In each case, the elastic distortional buckling stress was determined by the generalized beam theory taking into account the actual column length and end boundary conditions. The comparison showed that the EC3 predictions are quite conservative if the compression capacity is determined using effective widths due to local buckling, and reducing the strength of the whole section due to distortional buckling using some of the design curves a_0, *a, b or c*.

It was shown that the assumption of simple support along the edges for the perforated web of the C-section is conservative and the contribution of the flanges to the local buckling behaviour of the web should be taken into account.

In the above comparisons, the local buckling stresses in the EC3 method were determined based on the actual yield stress of the section. In the original EC3 method, the effective width of the stiffener (including half of the adjacent element) may be optionally refined iteratively. In the first step, the effective width is determined based on yield stress. In the second step, the effective width of the stiffener is determined based on the reduced stiffener buckling strength. The iteration should be continued until the current value of the reduction factor, χ, is approximately equal, but not more than the previous value. The effective area of the studied sections was also determined using the above-mentioned procedure. Since the distortional buckling stress is determined by GBT, the actual iterative process is not used, but the local buckling of stiffener was based on reduced distortional strength.

Figure 7.2 shows the comparison of the test results and predicted values for all the sections studied. The predicted values were determined using the above-mentioned EC3 method and the Schafer and Peköz method as well. Different distortional buckling stress was used for the web and the flange part for the TCJ sections and local buckling stress was achieved by FEM for the TCS sections. Figure 7.2 shows that the EC3 method, where stiffener effective widths are based on distortional buckling strength (EC3, "iter."), gives slightly higher capacities than other methods. The mean resistance ratios N_{Test}/N_p and standard deviations are shown in Table 7.9.

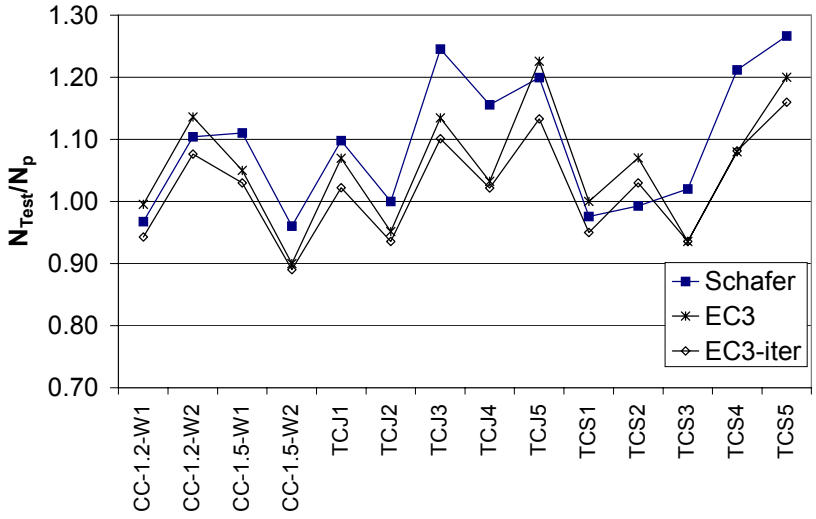

Fig. 7.2: Comparison of test results and predicted values using the Schafer and Peköz method and EC3 method.

TABLE 7.9
MEAN VALUE AND STANDARD DEVIATIONS FOR RESISTANCE RATIO N_{TEST}/N_P

	EC3	EC3,"iter."	Schafer and Peköz
Mean	1.06	1.02	1.09
St.dev.	1.10	0.08	0.11

7.2 Gypsum Board Braced Column Tests

Elastic distortional buckling stresses of the gypsum-sheathed sections were determined by FEM, as described in Section 6.1.3. A typical spring stiffness value of k_y = 350 N/mm (Kesti 1997, Miller 1994) was used in the analysis. The spring stiffness k_A was determined by penetration tests and a mean value of k_A = 3120 N/mm was used in the analysis. The rotational stiffness, $C_{D,C}$, corresponding to the flexural stiffness of the sheathing was determined by FEM using the model shown in Fig. 7.3 and using an elastic modulus value of E_G = 2500 N/mm^2 for the gypsum sheathing. The value for the rotational stiffness was found to be $C_{D,C}$ = 4950 Nmm/rad/mm. Finally, the value of perpendicular stiffness k_z was determined from:

$$k_z = \frac{1}{\frac{1}{k_A} + \frac{(b/2)^2}{C_{D,C}\, w_{eff}}} \tag{7.1}$$

A flange width of b = 50 mm was used in the analysis. For the effective board width w_{eff} was used for the value of screw pitch when the pitch was 200 mm or 300 mm, and in other cases w_{eff} = 300 mm. It should be noted that the perpendicular spring stiffness k_z is not necessarily the same along the stud. The value of the stiffness may be larger in some degree when the flange buckles outwards, and the screws are not necessarily in tension. Nevertheless, constant value was used along the stud as a conservative assumption.

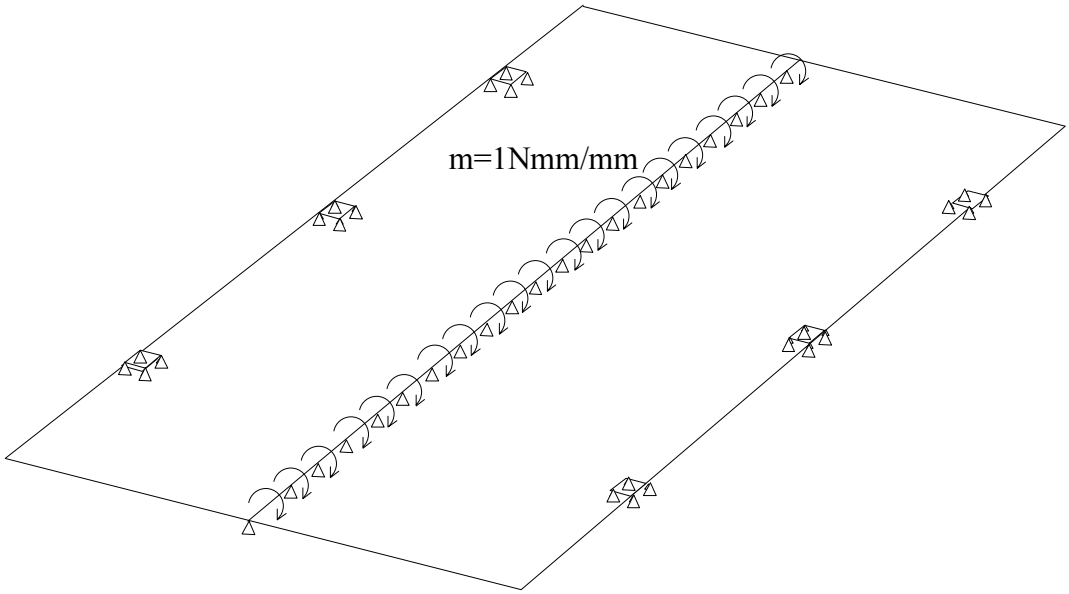

Fig. 7.3: Model for calculating $C_{D,C}$.

Comparisons of test results and predicted values according to Australian Standard, Schafer and Peköz and Eurocode 3 are presented in Table 7.10. Table 7.10 shows that predictions according to EC3 would seem to correlate best with the test results. All the methods predict the compression capacities of gypsum sheathed stud with an adequate accuracy. Australian Standard and Schafer and Peköz methods are conservative in some degree for unsupported stud CC-1.2-1800.

TABLE 7.10

COMPARISON OF TEST RESULTS AND PREDICTED VALUES FOR GYPSUM SHEATHED SPECIMENS.

Specimen	Failure load kN	Distortional buckling stress N/mm^2	N_{Test}/N_P AUS	N_{Test}/N_P Schafer and Peköz	N_{Test}/N_P EC3 ("iter")
CB-1.2-200	74.6	261	1.02	1.03	1.01
CB-1.2-300	69.3	220	1.07	1.04	1.01
CB-1.2-450	65.4	196	1.11	1.04	1.01
CB-1.2-600	62.2	168	1.13	1.07	1.04
CC-1.2-1800	48.7	78	1.34	1.36	1.14
CB-1.5-200	95.3	312	0.96	0.97	0.91
CB-1.5-300	92.5	264	1.01	1.02	0.95
CB-1.5-450	90.5	228	1.08	1.07	1.00
CB-1.5-600	85.4	197	1.15	1.08	1.01
CC-1.5-1800	71.6	139	1.12	1.08	0.99
		Mean	**1.10**	**1.08**	**1.01**
		St.dev.	**0.10**	**0.11**	**0.06**

Höglund (1998) has presented a design method for gypsum sheathed perforated wall studs. Two buckling modes are considered in the case of pure compression: 1) lateral buckling of the flanges when the gypsum boards are assumed to act as elastic supports and 2) buckling of the flange stiffeners between screws. Furthermore, the local buckling is taken into account using the effective width approach and buckling of the web stiffeners is taken into account by reducing the area of the web stiffeners. When calculating flange stiffener buckling (flexural buckling of stiffener plus half of the flange), an effective buckling length of 0.6 times the screw pitch was used. Due to flange stiffener buckling or lateral buckling, the strength of the whole section was reduced by a reduction factor of Swedish code StBK-N5 (1979) corresponding closely to European column curve a or curve b. Compression capacities according to both Höglund and EC3 methods and the test results are shown in Fig. 7.4 for sections with thickness of 1.2 mm and in Fig. 7.5 for sections with thickness of 1.5 mm. The critical failure modes in Höglund method are also shown in Figures 7.4 and 7.5. Shear spring stiffness values of 91 N/mm for 1.2 mm thickness and 114 N/mm for 1.5 mm thickness were used in the Höglund method.

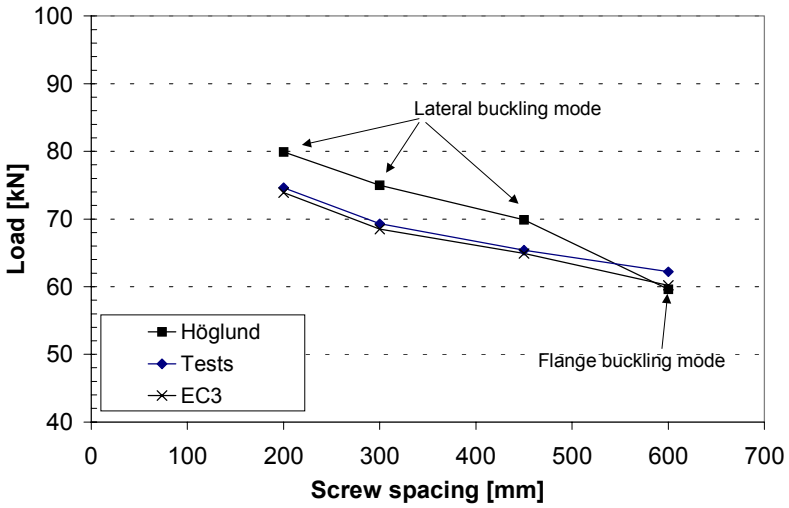

Fig. 7.4: Compression capacities according to Höglund method and EC3 method for gypsum board braced studs with thickness of 1.2 mm.

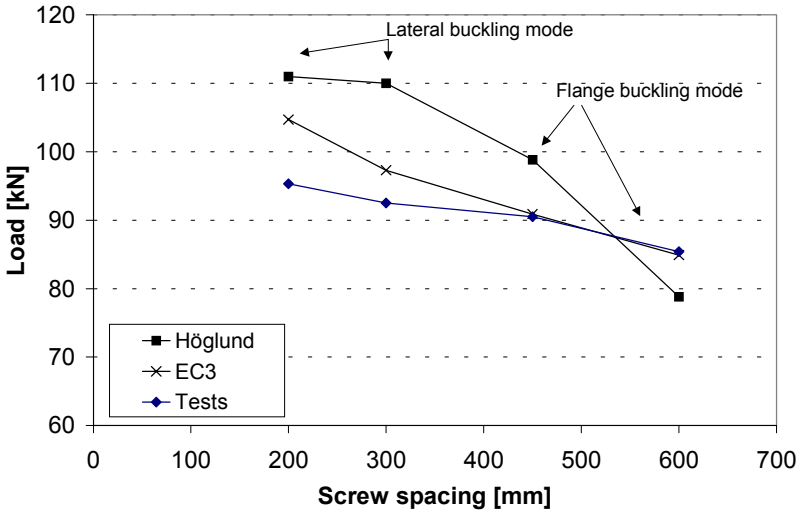

Fig. 7.5: Compression capacities according to Höglund method and EC3 method for gypsum board braced studs with thickness of 1.5 mm.

Fig. 7.4 and Fig. 7.5 show that the Höglund method seems to give slightly unconservative values when the screw pitch is between 200 mm and 450 mm. Figs 7.4 and 7.5 also show that the critical failure mode according to the Höglund is lateral buckling in small screw pitch values. It can be seen from Fig. 7.5 that in the Höglund method, the capacity in the flange buckling mode seems to be more dependent on the screw pitch than in the method proposed by the author. On the other hand, the practical screw pitch is usually 200 mm or 300 mm and thus the importance of this phenomena is not so significant.

8 CONCLUSIONS AND FURTHER STUDIES

8.1 Conclusions

The local and distortional buckling behaviour of flange and web-stiffened compression members was investigated. In particular, the behaviour of web-perforated sections was investigated both numerically and experimentally. Perforation reduces the perpendicular flexural stiffness of the web and thus particularly reduces the distortional buckling strength of the section. The main task of the research was to develop a design method for estimating the compression capacity of a perforated steel wall-stud under centric loading. The influence of the gypsum sheathing on the distortional buckling strength is also taken into account.

Several analytical methods for predicting the elastic distortional buckling stress of a simple C-section and intermediate stiffened steel plate were compared. It was shown that the method given in Eurocode 3 is quite rough and sometimes gives inaccurate results for both C-sections and intermediate stiffened plates. In the case of C-sections, the method developed by Lau and Hancock and the method developed by Schafer and Peköz correlate better with the results defined numerically. For the plates with intermediate stiffeners, the method presented by Schafer and Peköz also correlates better with numerically determined values than the Eurocode 3 method. The Finite Strip Method (FSM) and Generalized Beam Theory (GBT) provided particularly good tools with which to analyze local and distortional buckling modes.

The additional stiffeners in the web cause more distortional buckling modes in the section. The interaction of different distortional buckling modes was studied and it was noted that the interaction modes are particularly critical if the distortional buckling stresses and buckling half-waves of the different modes are of the same magnitude.

Local buckling stress of the web-perforated C-section was found to be conservative if the web was treated independently, and assuming it as simply supported. Better correlation with numerically determined values was achieved if the web was assumed as fixed along the longitudinal edges. In general, it is worthwhile to take into account the whole section in local buckling analyses. Distortional buckling stress of the web-perforated C-section with or without web stiffeners can be determined by replacing the perforated web part with an equivalent plain plate corresponding to the same perpendicular bending stiffness. Distortional buckling stress

may be determined by some numerical method such as FSM or GBT. For the web-perforated C-section, an analytical method for the distortional buckling is also presented.

A short description of the determination of the ultimate strength of compressed members is presented. Eurocode 3, the Australian Standard and the proposal by Schafer and Peköz are included in the review. Consideration of the interaction of local, distortional and global buckling is discussed and a comparisons between the different methods has been performed.

Gypsum sheathing connections give rotational restraint to the wall–stud, thus improving distortional buckling strength. Rotational stiffness mainly consists of flexural stiffness of the sheathing and rotational stiffness between the sheathing and the stud. Some practical guidelines are given for calculating the rotational restraint. Sheathing also provides lateral support to the stud and thus improves or eliminates flexural buckling of the stud in the plane of the wall.

Buckling analysis by FEM showed the influence of the rotational restraint given by the sheathing on the distortional buckling stress and on the length of the distortional buckling half-wave. Analysis showed that relatively small restraint may double the distortional buckling stress of the web-perforated section. It was also shown that the screw position does not form the nodal point for the buckling half-wave. Screw pitch also has a considerable effect on the distortional buckling stress. An example showed that, by making the screw pitch dense from 600 mm to 200 mm, the distortional buckling stress doubles in a typical web-perforated section.

Experimental research consisted of short column tests and gypsum board braced column tests. The short column tests were conducted for the web-perforated sections and for the sections whose perforated area was cut away. The results showed that the perforated web part gives some restraint with respect to distortional buckling. The test results of the short columns also indicated that the compression capacity depended on the direction of the distortional buckling mode. Gypsum board braced column tests showed that the screw connection prevented quite efficiently the displacement of the flange stiffener in distortional buckling mode until the screw penetrated the sheathing at the stage of failure. The failure loads of the gypsum-sheathed studs with a screw pitch of 200 mm were at least 30% higher than that of the plain section without gypsum boards. The screw pitch also had a considerable effect on the compression capacity.

Non-linear analysis for short columns showed that the failure load of web-stiffened C-sections is sensitive to the direction of the initial imperfection. If the imperfections are modelled using the

eigenmode of the section, non-linear analysis should be performed using both (+) and (-) signed eigenmodes, respectively. The non-linear analysis gave good prediction of the compression capacity of the web-perforated stud sections.

The short column test results and analytically determined ultimate load predictions according to the Australian Standard, Eurocode 3, and Schafer and Peköz were in good accordance. In each case, the elastic distortional buckling stresses were determined using the generalized beam theory taking into account the actual column length and the end boundary conditions. The best correlation between the test results and Eurocode 3 values were achieved using effective widths for plane elements due to local buckling, and using effective thickness for stiffeners due to distortional buckling. Reducing the strength of the whole section due to distortional buckling using the European column curves seems to give conservative values.

The compression capacity of the gypsum board braced stud is highly dependent on the restraint given by the gypsum sheathing. Using restraint values given by the connection tests, the predicted values for the gypsum board braced columns are in good accordance with the test results. In practical design, utilizing the gypsum board in the determination of the distortional buckling stress requires that the sheathing retains its capacity and stiffness for the expected service life of the structure. Furthermore, the connection characteristics should be carefully examined.

Based on the results of the experimental and theoretical studies, design proposals were made for the design of compressed web-perforated steel wall studs. Some practical guidelines were also given for taking into account the gypsum sheathing. These design proposals are also valid for solid steel wall studs, especially for slender sections, which are sensitive to distortional buckling.

8.2 Further Studies

This work is conducted within a well-defined field of study. Further research is needed on the following aspects:

The interaction of local and distortional buckling, especially for slender plain sections, should be investigated more precisely. The applicability of the present manual calculation methods given in Eurocode 3 for the design of web-stiffened C-sections should also be verified.

Gypsum board braced column tests should also be conducted for the web-perforated C-sections without web stiffeners. More tests should be performed to determine the rotational restraint offered by gypsum board sheathing. Different types and thickness of gypsum boards should be included in the test series.

The overall behaviour of the web-perforated steel wall-stud assemblies under lateral and axial loads should also be studied. Shear deformations of the perforated web influence the flexural buckling of the section as well as the bending behaviour. The interaction between local, distortional and global buckling modes should be studied.

REFERENCES

AISI. (1996). The Specification for The Design of Cold-Formed Steel Structural Members, American Iron and Steel Institute, Washington DC.

AS/NZS 4600. (1996). Australian / New Zealand Standard for Cold-formed Steel Structures, Standards Australia, Sydney.

Borglund, J. and Jonsson, J. (1997). Resistance of slotted steel studs (In Swedish). MSc Thesis 84, Department of Structural Engineering, Royal Institute of Technology, Stockholm.

Buhagiar, D., Chapman, J.C. and Dowling, P.J. (1992). Design of C-sections Against Deformational Lip Buckling, Proceedings of the 11th International Specialty Conference on Cold-formed Steel Structures, St.Louis, Missouri, U.S.A, pp. 75-94.

Engebrtsen, P.A. and Ramstad, T. (1978). Vegger med stålprofiler av tynnplater, Norges byggforskningsinstitutt, arbeidsrapport 15.

Eurocode 3. (1996). CEN ENV 1993-1-3, Design of Steel Structures - Supplementary Rules for Cold Formed Thin Gauge Members and Sheeting, Brussels.

Frederiksen, J.O. and Spange,H. (1992). Undersögelse af bäreevnen af lette ydervägge. Dansk Teknologisk Institut, Byggeteknisk Institut 13726.

Davies, J. M. and Leach P. (1994a). First-Order Generalised Beam Theory, *Journal of Constructional Steel Research*, **31:2-3**, 187-220.

Davies, J. M. and Leach P. (1994b). Second-Order Generalised Beam Theory, *Journal of Constructional Steel Research*, **31:2-3**, 221-241.

Davies, J.M. and Jiang, C. (1995). GBT- Computer program, public domain, University of Manchester.

Davies, J.M. and Jiang, C. (1996). Design of Thin-Walled Columns for Distortional Buckling, Proc. of the Second Int. Conference on Coupled Instability in Metal Structures CIMS'96, Liege, Belgium, p. 165-172.

Davies, J.M. and Jiang, C. (1996b). Non-Linear Buckling Analysis of Thin-Walled Metal Columns. Proceedings of the 13th International Conference on Cold-formed Steel Structures, St.Louis, Missouri, U.S.A, pp. 321-334.

Davies, J.M., Jiang, C. and Ungureanu, V. (1998). Buckling Mode Interaction in Cold-Formed Steel Columns and Beams. Proceedings of the 14th International Specialty Conference on Cold-formed Steel Design and Construction, St.Louis, Missouri, U.S.A, pp. 53-67.

Hancock, G.J., Kwon, Y.B. and Bernard, E.S. (1994). Strength Design Curves for Thin-Walled Sections Undergoing Distortional Buckling, *Journal of Constructional Steel Research*, **31:2-3,**169-186.

Höglund, T. (1998). Design of Slotted Light Gauge Studs, Report 54, Royal Institute of Technology, Department of Structural Engineering, Stockholm, Sweden.

Höglund, T. and Burstrand, H. (1998). Slotted Steel Studs to Reduce Thermal Bridges in Insulated Walls, *Thin-Walled Structures*, **32:1-3**, 81-109.

Ife, L.W. (1975). The Performance on Cold-Formed Steel Products in Housing. Proceedings of the 3th International Conference on Cold-formed Steel Design and Construction, St.Louis, Missouri, U.S.A, pp. 621-667.

von Kármán, T., Sechler, E.E., Donnell,L.H.(1932). The Strength of Thin Plates in Compression, *Transactions of ASME,* **54**, 53-57.

Kesti, J. (1997) Design of Web-Perforated Steel Wall Studs, Licentiate Thesis, 71p. + app. (in Finnish)

Kesti, J., Mäkeläinen, P. (1998). Design of Gypsum Sheathed Perforated Steel Wall Studs, *Journal of Constructional Steel Research*, **46:1-3**,116.

Kesti, J. and Davies, J.M. (1999a). Local and Distortional Buckling of Thin-Walled Short Columns, *Thin-Walled Structures*, **34:2**, 115-134.

Kesti, J. and Davies, J.M. (1999b). The Applicability of Eurocode 3 to the Design of Thin-Walled Columns Undergoing Distortional Buckling, Stability and Ductility of Steel Structures - Proceedings of the 6th International Colloquium SDSS'99, Timişoara, Romania, pp. 517-524.

Key, P.W. and Hancock, G.J. (1993). A Finite Strip Method for the Elastic-Plastic Large Displacement Analysis of Thin-Walled and Cold-Formed Steel Sections, *Thin-Walled Structures*, 16,3-29.

Kwon, Y. B. and Hancock, G. J. (1991). Tests of Cold-Formed Channels with Local and Distortional Buckling, *Journal of Structural Engineering*, ASCE, **117:7**, 1786-1803.

Kwon, Y.B. and Hancock, G.J. (1991b). A Nonlinear Elastic Spline Finite Strip Analysis for Thin-Walled Sections, *Thin-Walled Structures*, **12**, 295-319.

Lau, S.C.W. and Hancock, G.J. (1987). Distortional Buckling Formulas for Channel Columns, *Journal of Structural Engineering*, ASCE, **113:5**, 1063-1078.

Lau, S.C.W. and Hancock, G. J. (1988). Strength Tests and Design Methods for Cold-Formed Channel Columns Undergoing Distortional Buckling, Research Report No. R579, The University of Sydney, School of Civil and Mining Engineering.

Lau, S.C.W. and Hancock, G.J. (1989). Inelastic Buckling Analyses of beams, Columns and Plates Using the Spline Finite Strip Method, *Thin-Walled Structures*, **7**, 213-238.

Lindner, J. and Guo, Y.L. (1994). Buckling Behaviour of Cold-Formed Thin-Walled Members by Spline Finite Strip Analysis, Proceedings of the 12th International Specialty Conference on Cold-formed Steel Structures, St.Louis, Missouri, U.S.A, pp. 229-249.

Marques da Costa, M. (1999). Support Strength of Walls with Slotted Studs, Master Thesis 127, KTH, Royal Institute of Technology, Department of Structural Engineering, Sweden.

Miller, T.H. and Peköz, T. (1994). Behaviour of Gypsum-Sheathed Cold-Formed Steel Wall Studs, *Journal of Structural Engineering*, **120:5**, 1644-1650.

NISA, Version 6.0. (1996). Users manual, Engineering Mechanics Corporation (EMRC), Michigan, U.S.A.

Rasmussen, K.J.R. (1997). Bifurcation of Locally Buckled Members, Thin-Walled Structures, **28:2**, 117-154.

Salmi, P. (1998). Design of web-perforated steel wall studs (In Finnish), 4th Finnish Steel Structures R&D Days, 1998, Lappeenranta, Finland.

Schafer, B. and Peköz, T. (1996). Design of Cold-Formed Steel Stiffened Elements with Multiple Longitudinal Intermediate Stiffeners, Proceedings of the 13th Specialty International Conference on Cold-formed Steel Structures, St.Louis, Missouri, U.S.A, pp. 47-63.

Schafer, B. and Peköz, T. (1998). Computational Modeling of Cold-Formed Steel: Characterizing Geometric Imperfections and Residual Stresses, *Journal of Constructional Steel Research*, **47:3**, 193-210.

Schafer, B. and Peköz, T. (1999). Laterally Braced Cold-Formed Steel Flexural Members with Edge Stiffened Flanges, *Journal of Structural Engineering*, **125:2**, 118-127.

Schafer, B. and Peköz, T. (1999b). Local and Distortional Buckling of Cold-Formed Steel Members with Edge-Stiffened Flanges, Light-Weight Steel and Aluminium Structures - Proceeding of the 4th International Conference on Steel and Aluminium Structures, ICSAS'99, Espoo, Finland, pp. 89-97.

Schardt, R. (1989). Verallgemeinerte Technische Biegetheorie (Generalized Beam Theory), Springler Verlag, Berlin, Heidelberg.

Simaan, A. and Peköz, T. (1976). Diaphragm Braced Members and Design of Wall Studs, *Journal of Structural Division, ASCE*, **102:1**, 77-92.

StBK-N5 (1979). Swedish Code for Light Gauge Metal Structures 79, Svensk Byggtjänst.

Telue, Y. and Mahendran, M. (1999). Buckling Behaviour of Cold-Formed Steel Wall Frames Lined with Plasterboard, Light-Weight Steel and Aluminium Structures - Proceedings of the 4th International Conference on Steel and Aluminium Structures, ICSAS'99, Espoo, Finland, pp. 37-44.

Teo, K.Y. and Chou, S.M. (1998). Design Procedures for Stub Columns, Proc. of the Second International Conference on Thin-walled Structures, Singapore, pp.401-408.

THIN-WALL (1996). Cross-Section Analysis and Finite Strip Buckling Analysis of Thin-Walled Structures, Centre for Advanced Structural Engineering, University of Sydney.

Timoshenko, S.P. and Gere, J.M. (1961). Theory of Elastic Stability, 2nd ed., McGraw-Hill, New York.

Winter, G. (1947). Strength of Thin Steel Compression Flanges, *Transactions of ASCE*, **112**, Paper No. 2305:1-50.

Young, B. and Rasmussen, K.J.R. (1997). Bifurcation of SINGLY Symmetric Columns, *Thin-Walled Structures*, **28:2**, 155-177.

Young, B and Rasmussen, K.J.R. (1998). Design of Lipped Channel Columns, *Journal of Structural Engineering*, ASCE, **124:2**,140-148.

Young, B. and Rasmussen, K.J.R. (1999). Local, Distortional, Flexural and Flexural-Torsional Buckling of Thin-Walled Columns, Light-Weight Steel and Aluminium Structures - Proceedings of the 4th International Conference on Steel and Aluminium Structures, ICSAS'99, Espoo, Finland, pp. 27-34.

Schafer and Peköz Model for Distortional Buckling Prediction of C-section

Critical elastic buckling stress:

$$f_{od} = \frac{k_{\phi fe} + k_{\phi we}}{\tilde{k}_{\phi fg} + \tilde{k}_{\phi wg}}$$

$$L = min(L_{cr}, L_m)$$

Flange rotational stiffness:

$$k_{\phi fe} = \left(\frac{\pi}{L}\right)^4 \left(E I_{xf} \left(x_{0f} - h_{xf}\right)^2 + E I_{wf} - E\frac{I_{xyf}^2}{I_{yf}} \left(x_{0f} - h_{xf}\right)^2 \right) + \left(\frac{\pi}{L}\right)^2 GI_{tf}$$

$$\tilde{k}_{\phi fg} = \left(\frac{\pi}{L}\right)^2 \left[A_f \left(\left(x_{0f} - h_{xf}\right)^2 \left(\frac{I_{xyf}}{I_{yf}}\right)^2 - 2 y_o \left(x_{0f} - h_x f\right) \left(\frac{I_{xyf}}{I_{yf}}\right) + h_{xf}^2 + y_{0f}^2 \right) + I_{xf} + I_{yf} \right]$$

Web rotational stiffness:

$$k_{\phi we} = \frac{Et^3}{6h_w(1-\upsilon^2)}$$

$$\tilde{k}_{\phi wg} = \left(\frac{\pi}{L}\right)^2 \frac{th_w^3}{60}$$

Critical length:

$$L_{cr} = \left[\frac{6\pi^4 h_w (1-\upsilon^2)}{t^3} \left[I_{xf} \left(x_{0f} - h_{xf}\right)^2 + I_{wf} - \frac{I_{xyf}^2}{I_{yf}} \left(x_{0f} - h_{xf}\right)^2 \right] \right]^{0.25}$$

where
E = Modulus of Elasticity
G = Shear Modulus
ν = Poisson's ratio
t = plate thickness
h_w = web depth
L_m = Distance between restraints which limit rotation of the flange/web junction
A_f, I_{xf}, I_{yf}, I_{wf} = Section properties of the compression flange
x_{0f} = x-distance from the flange/web junction to the centroid of the flange.
h_x = x-distance from the centroid of the flange to the shear center of the flsnge

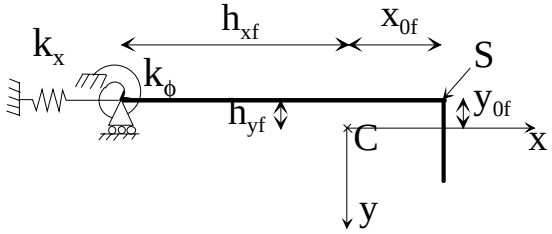

APPENDIX B

Load-displacement curves for short columns and gypsum board braced columns

Load-displacement curves for short columns and gypsum board braced columns are shown in Figs B2-B17. Locations of transducers are shown in Fig. B1. Transducers were installed in the middle of the section length. The transducers d1-d4 were measured the lateral displacements of the section parallel to y-axis and the transducers dz5 and dz6 were measured the lateral displacements of the section parallel to z-axis. One displacement transducer dx7 measured the axial shortening of the section.

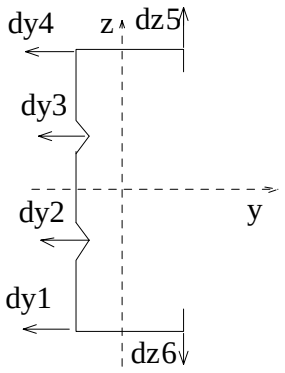

Fig B1: Locations of transducers around section.

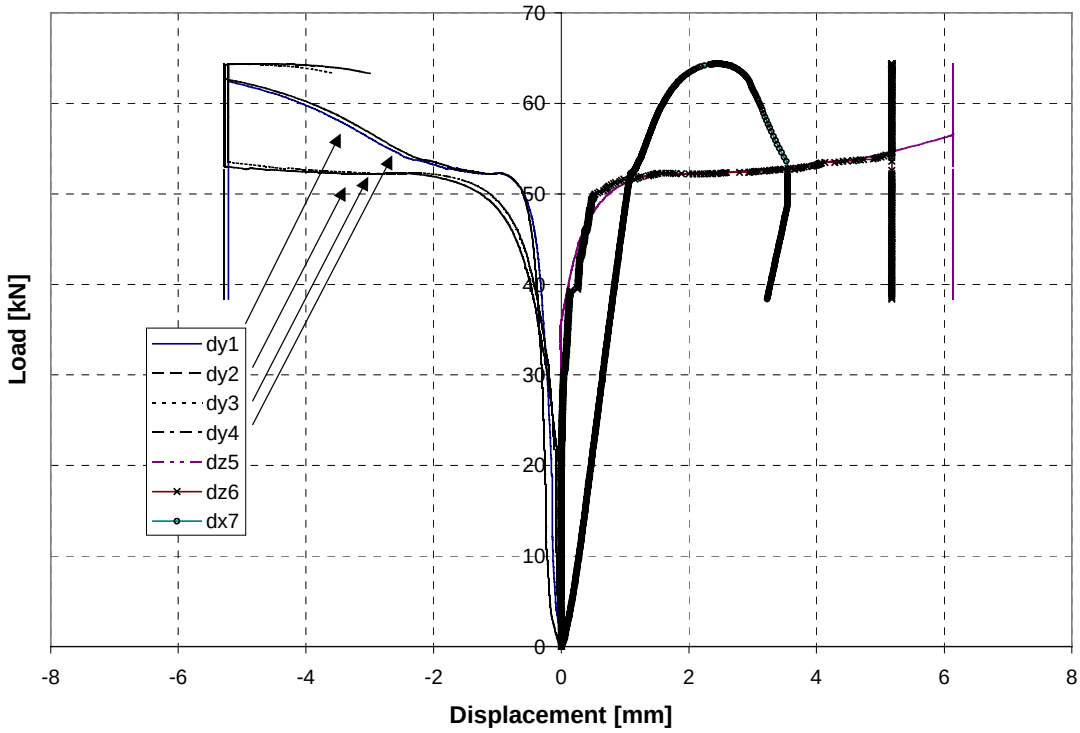

Fig B2: Load-displacement curves for the test specimen CC-1.2-W-1

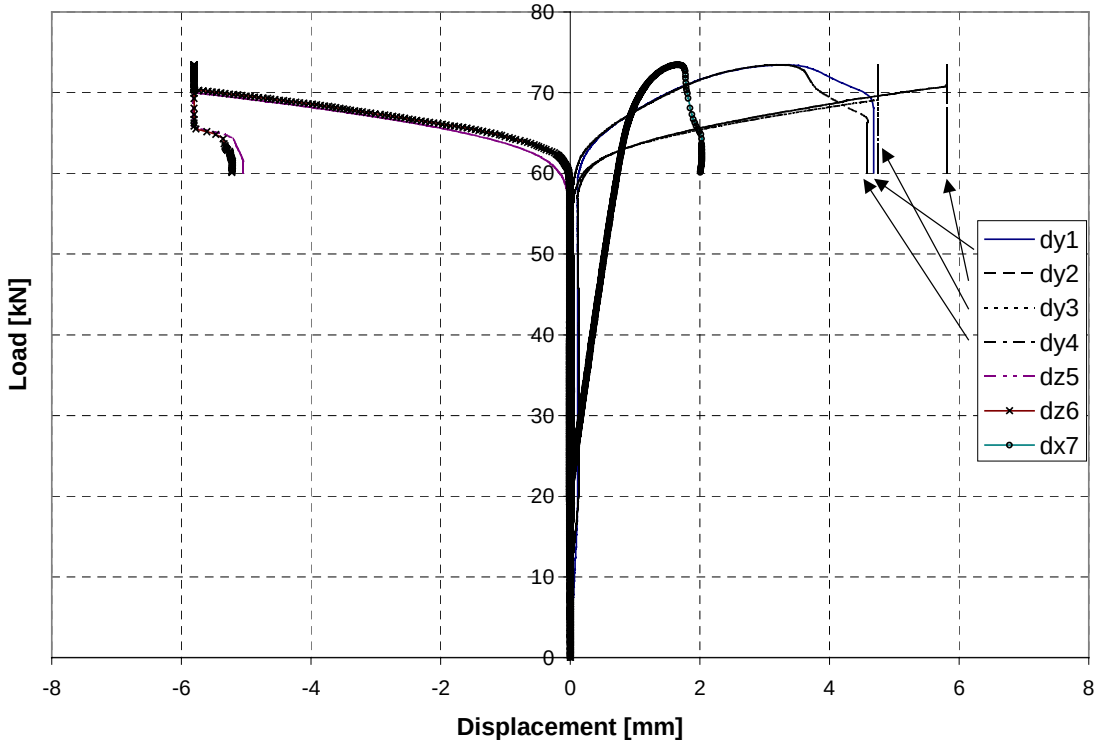

Fig B3: Load-displacement curves for the test specimen CC-1.2-W-2

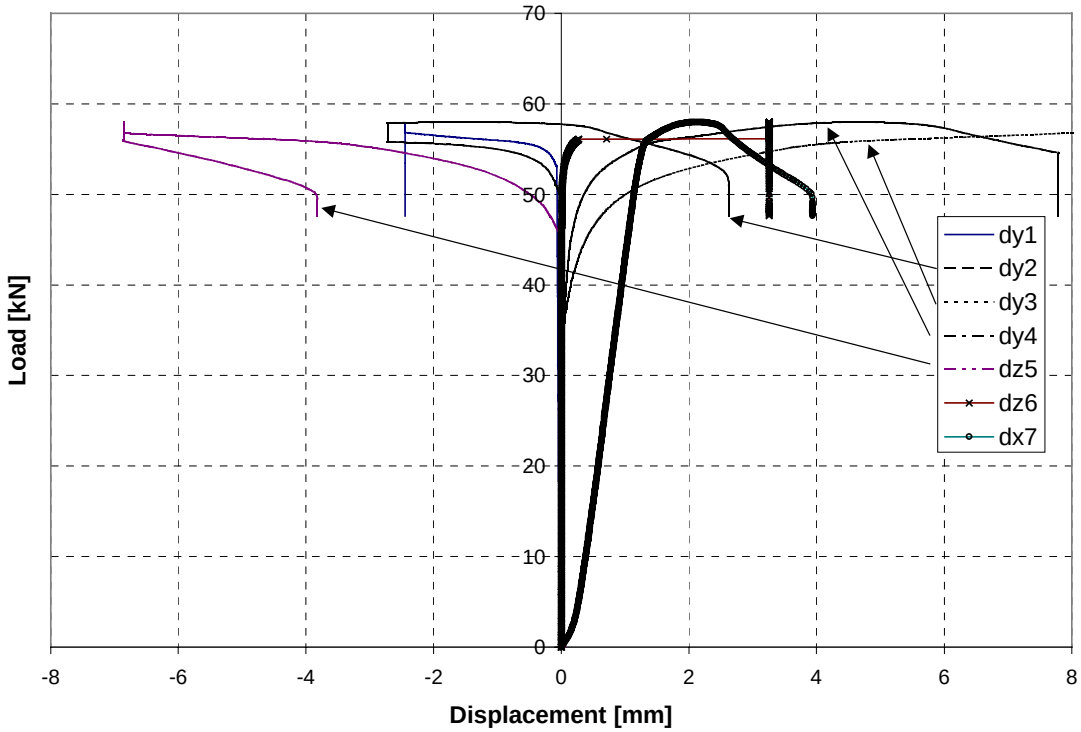

Fig B4: Load-displacement curves for the test specimen CC-1.2-F-1.

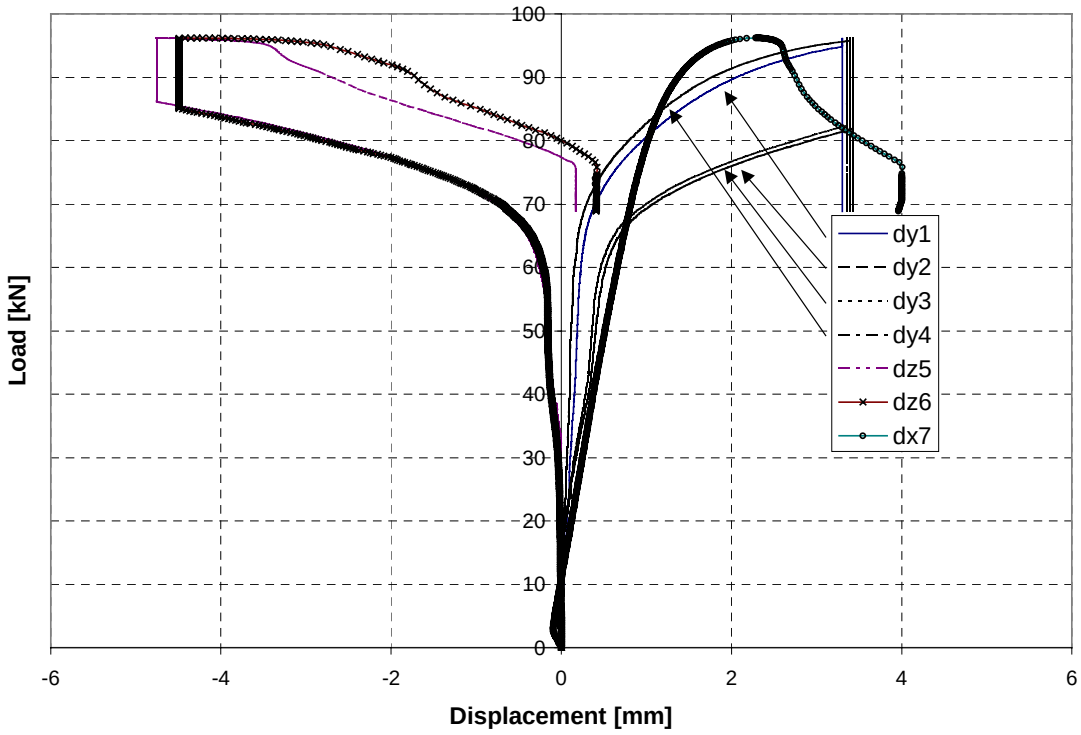

Fig B5: Load-displacement curves for the test specimen CC-1.5-W-1.

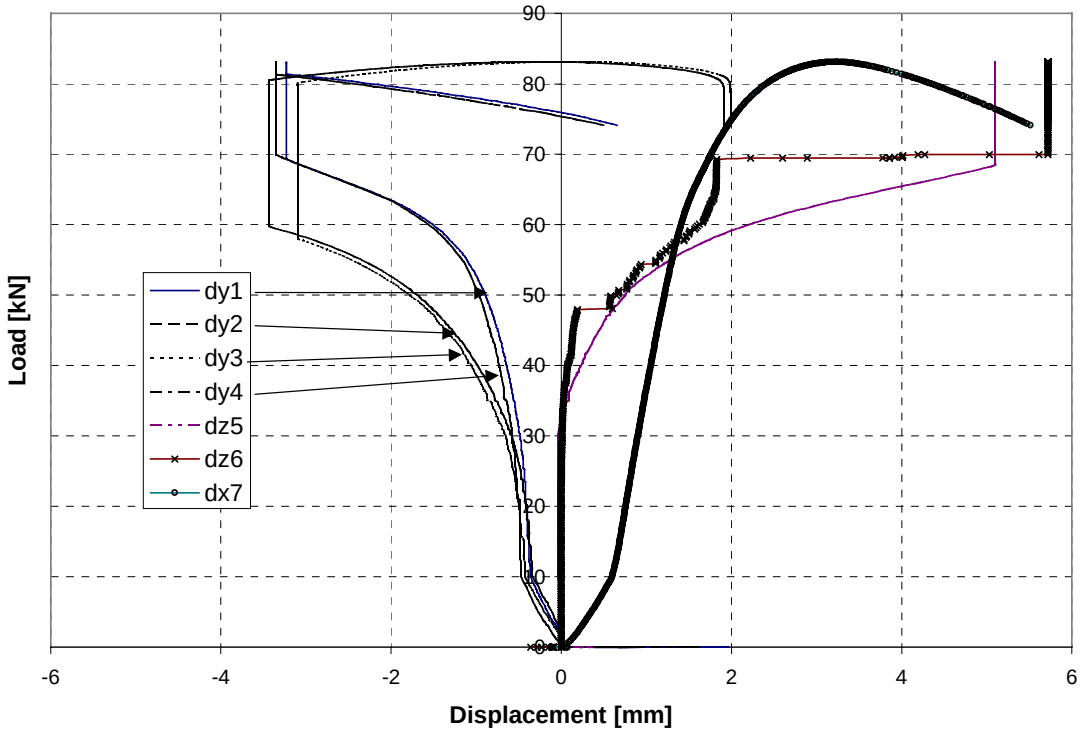

Fig B6: Load-displacement curves for the test specimen CC-1.5-W-2.

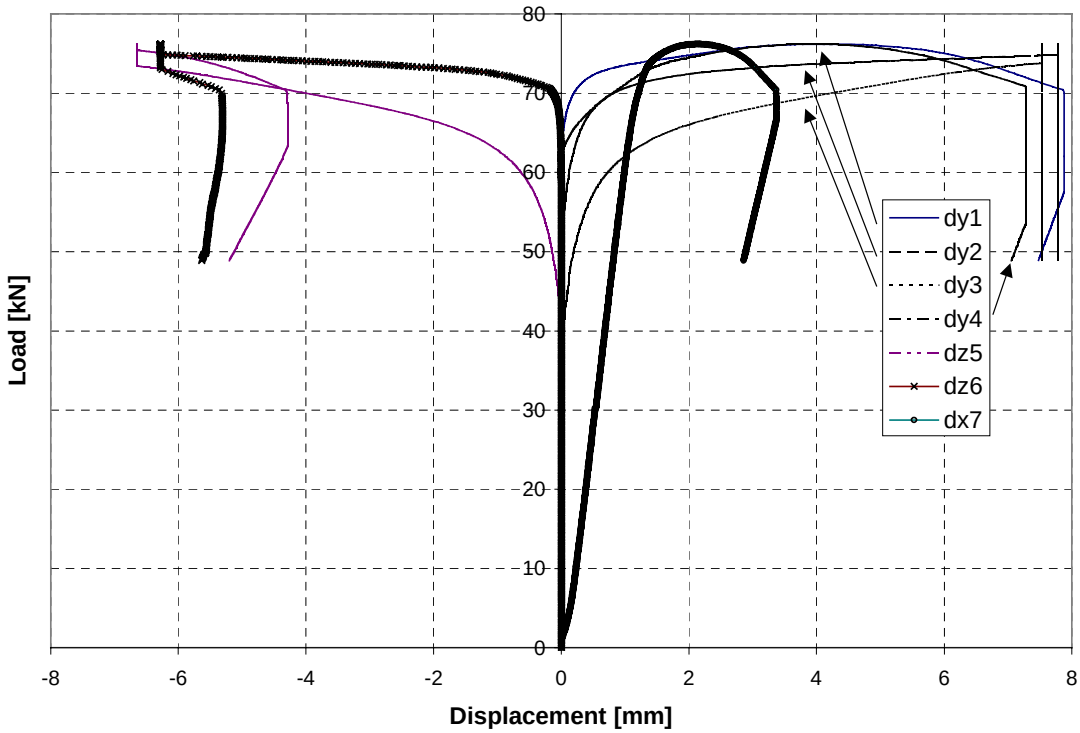

Fig B7: Load-displacement curves for the test specimen CC-1.5-F-1.

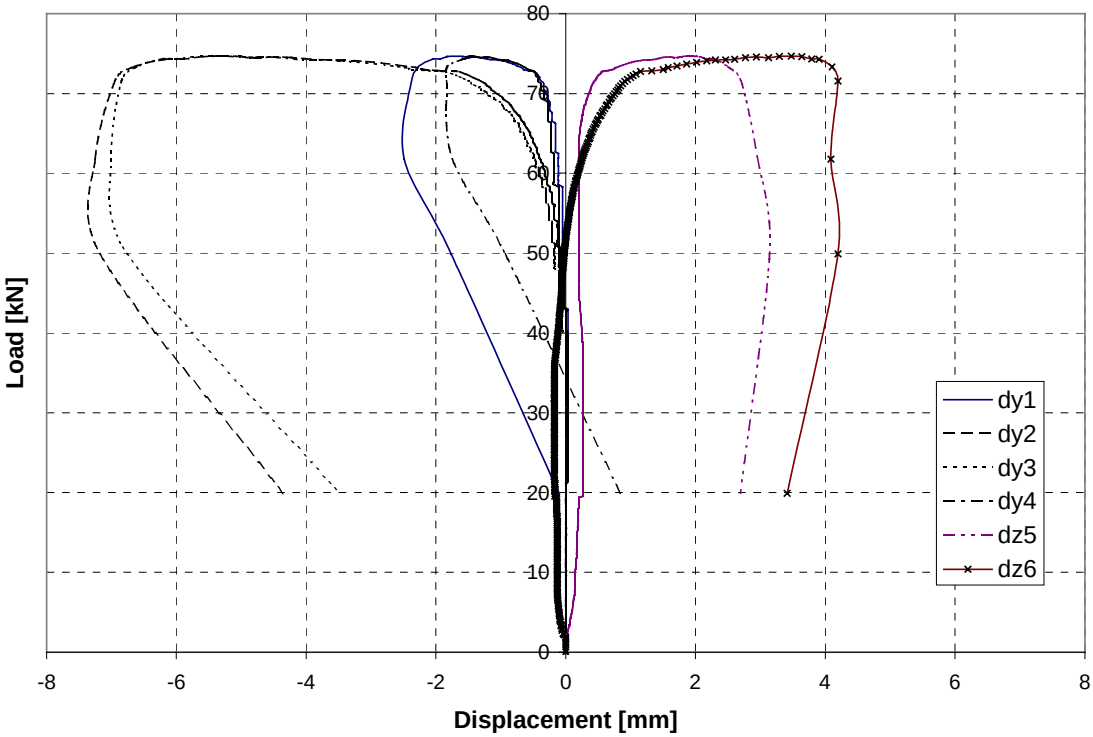

Fig B8: Load-displacement curves for the test specimen CB-1.2-200.

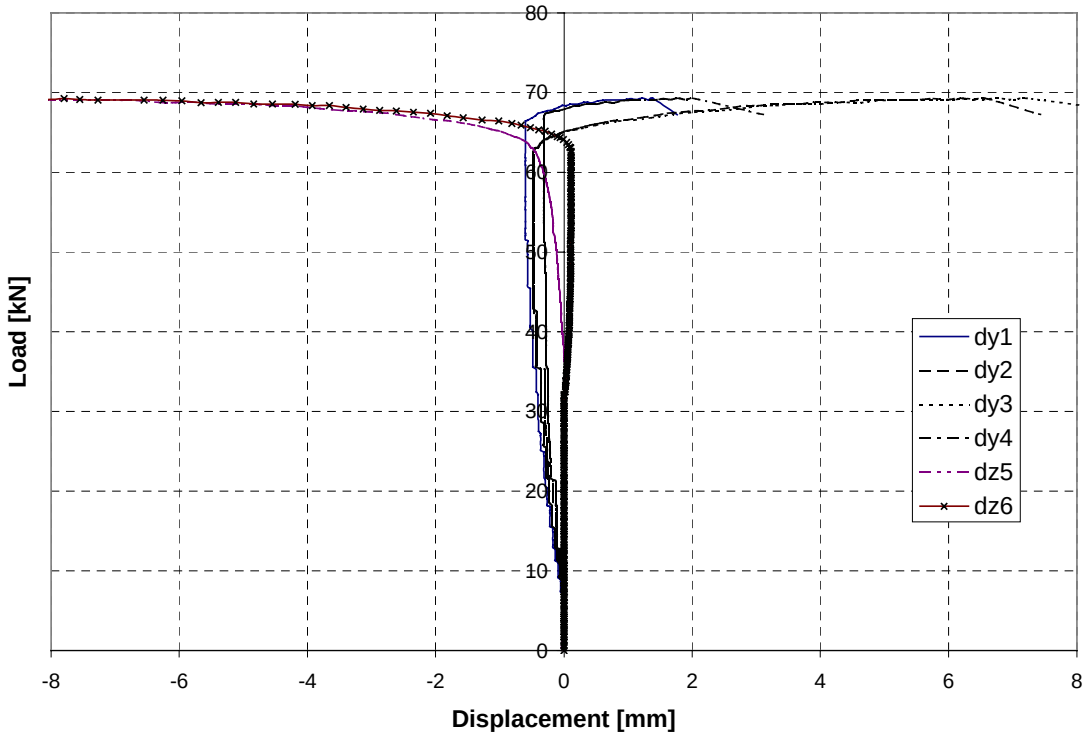

Fig B9: Load-displacement curves for the test specimen CB-1.2-300.

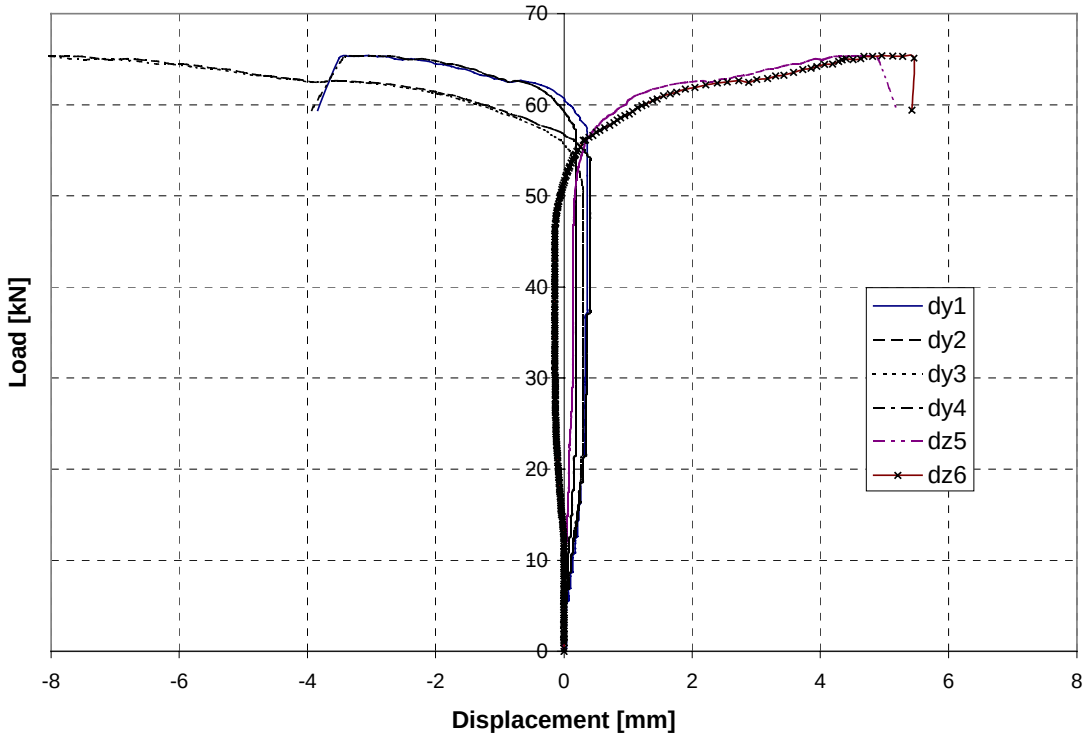

Fig B10: Load-displacement curves for the test specimen CB-1.2-450.

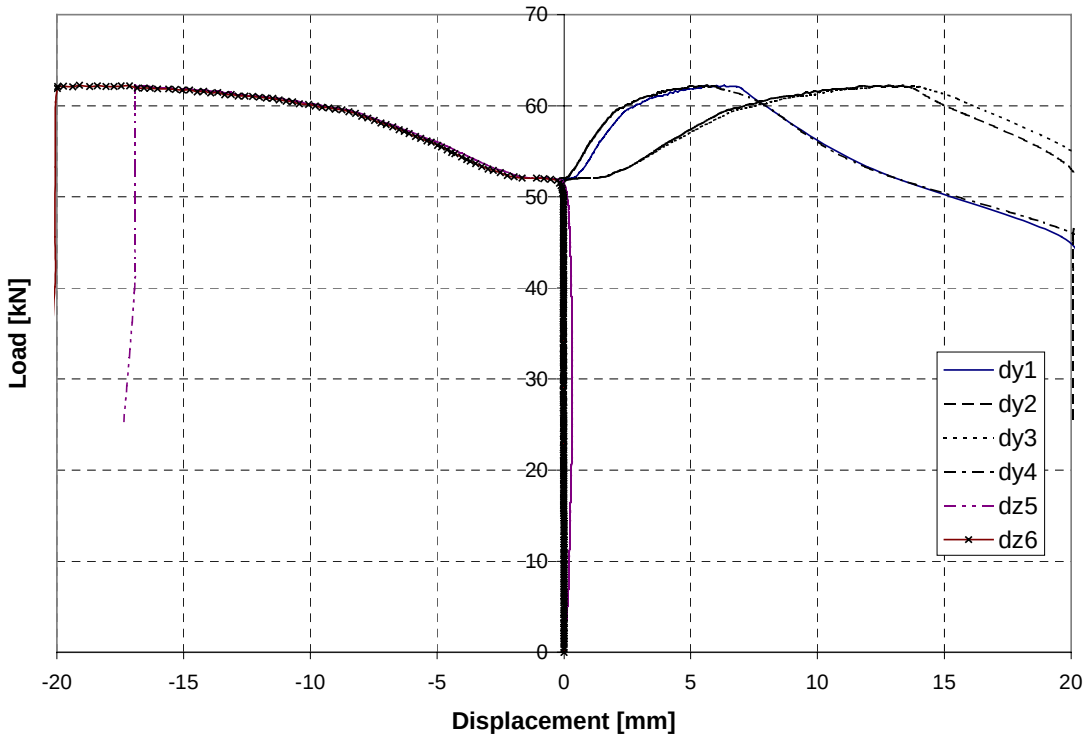

Fig B11: Load-displacement curves for the test specimen CB-1.2-600.

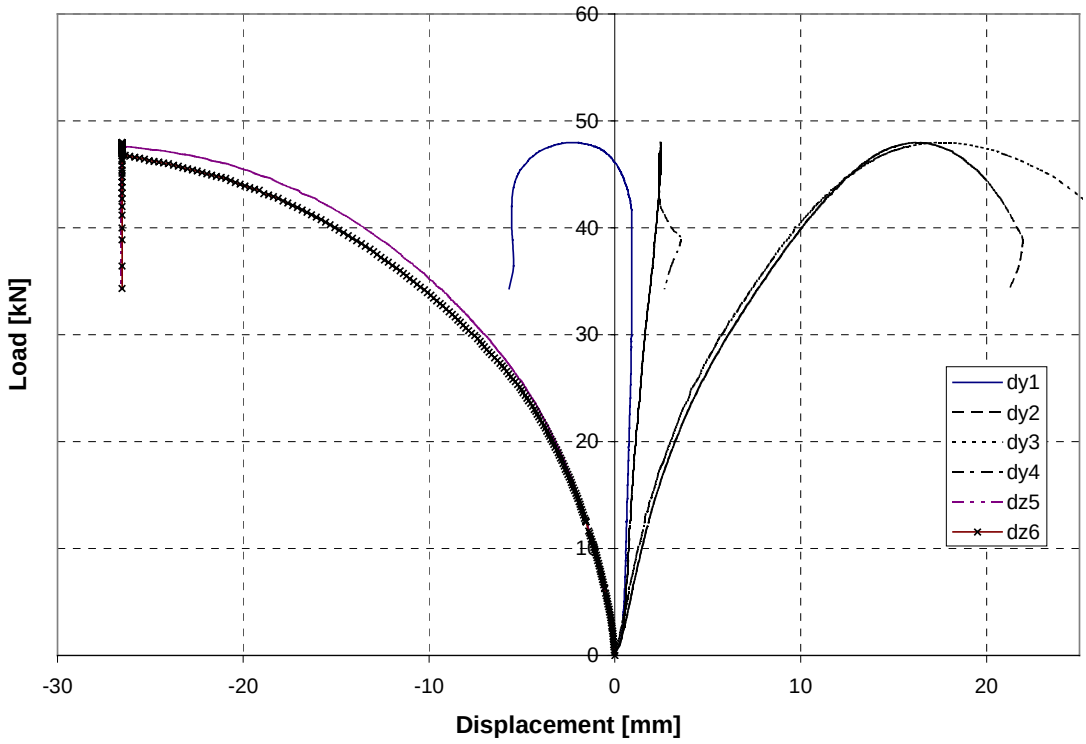

Fig B12: Load-displacement curves for the test specimen CC-1.2-1800.

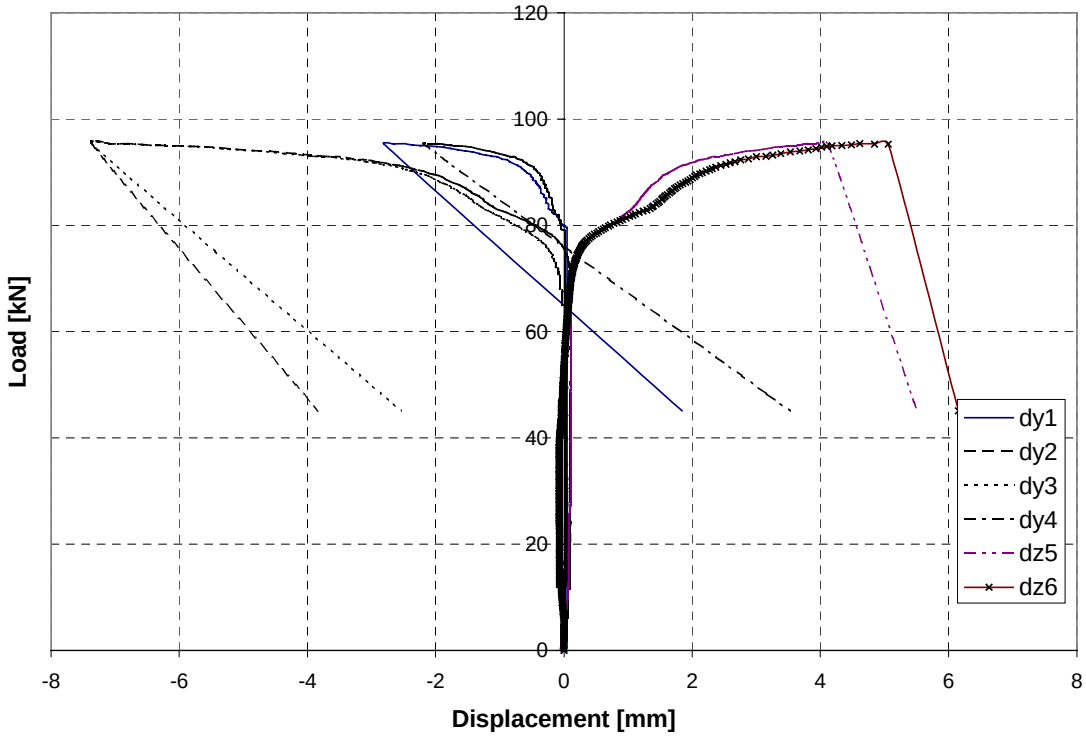

Fig B13: Load-displacement curves for the test specimen CB-1.5-200.

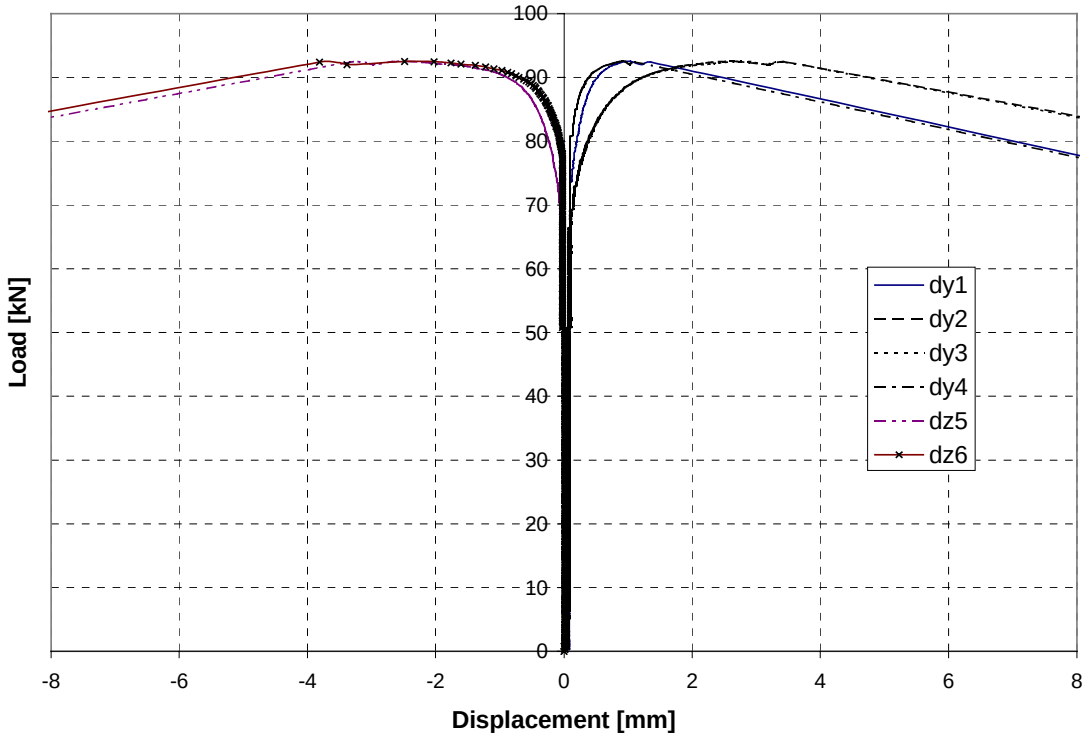

Fig B14: Load-displacement curves for the test specimen CB-1.5-300.

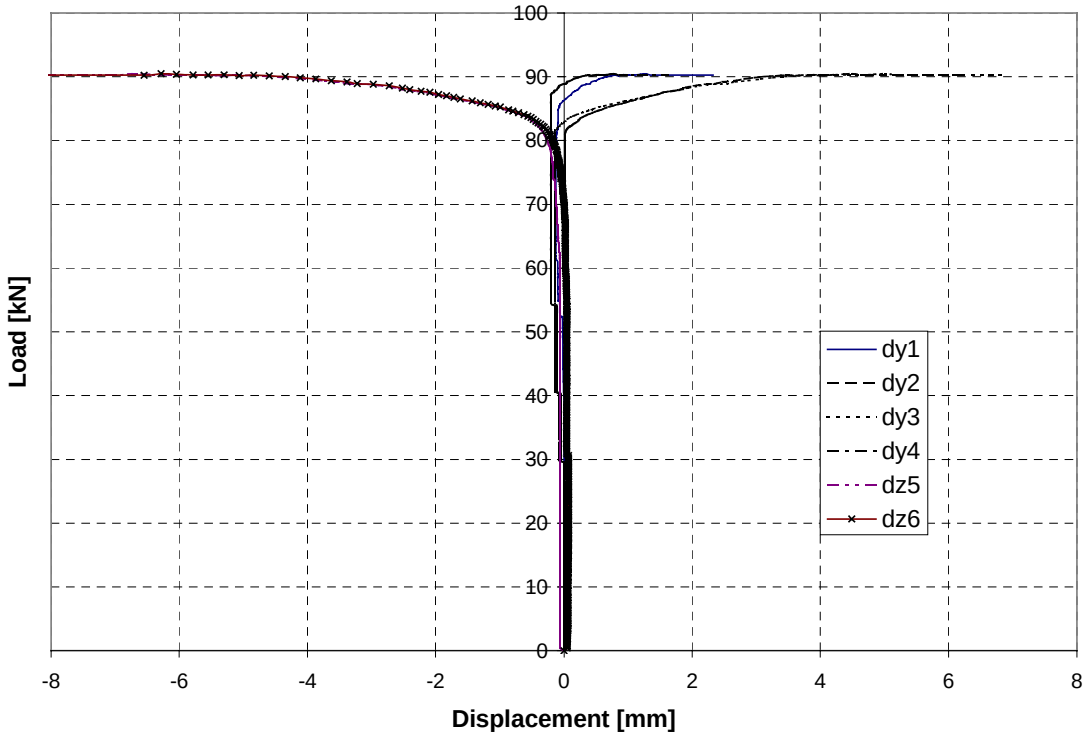

Fig B15: Load-displacement curves for the test specimen CB-1.5-450.

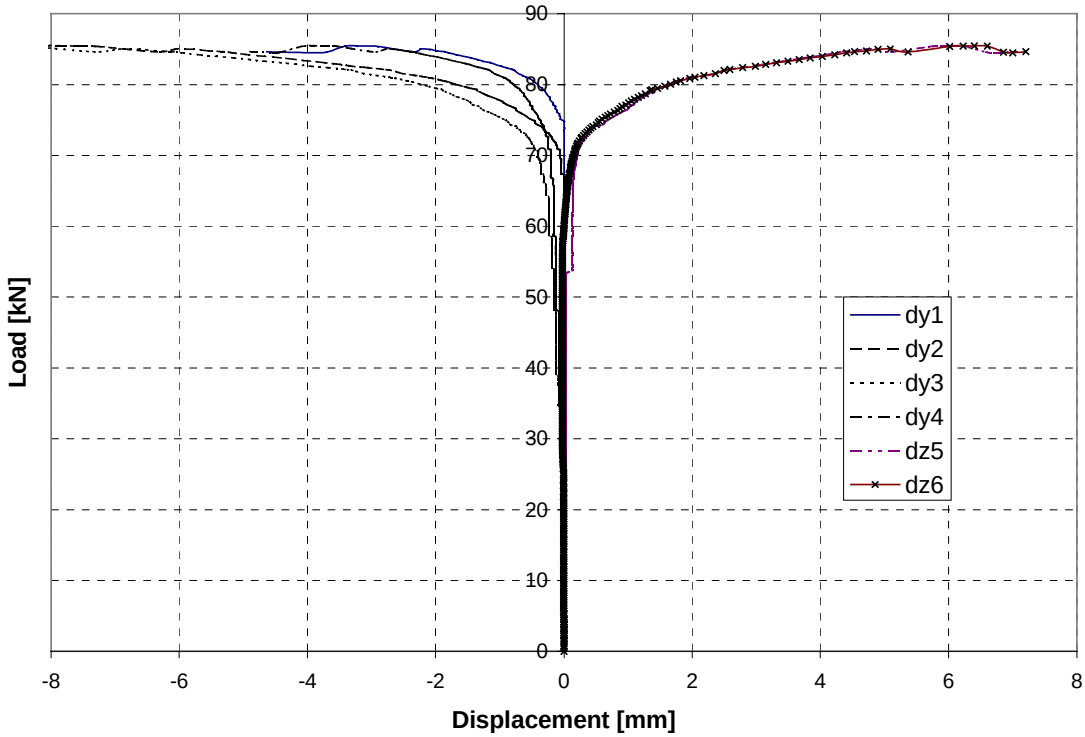

Fig B16: Load-displacement curves for the test specimen CB-1.5-600.

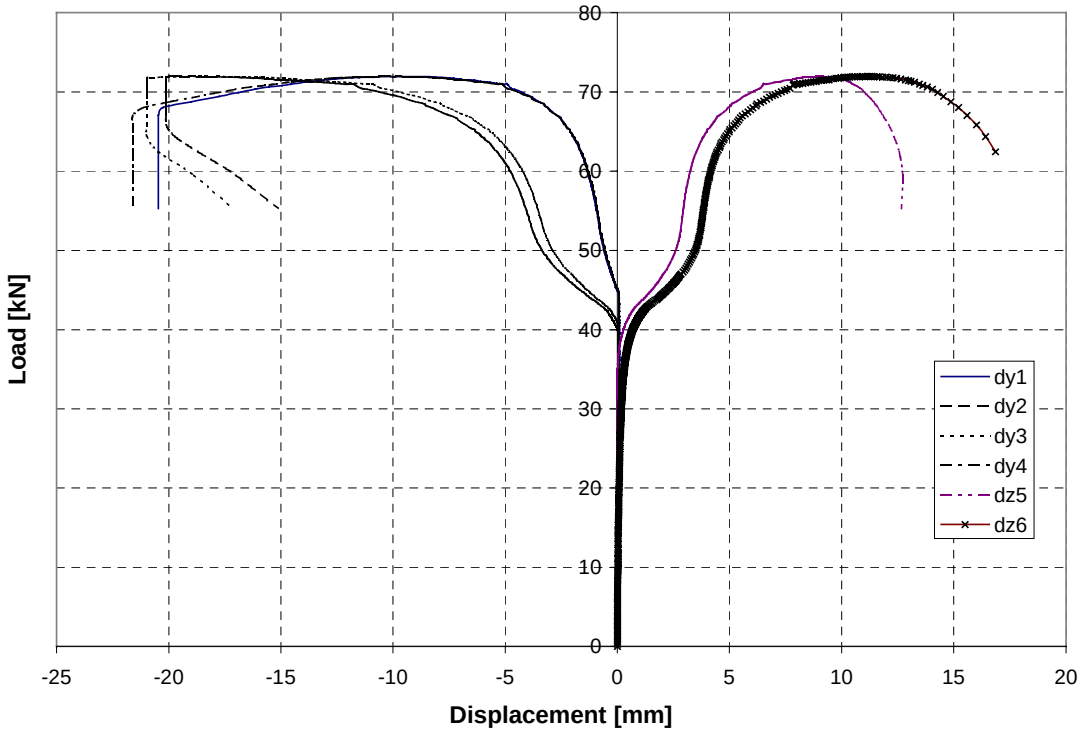

Fig B17: Load-displacement curves for the test specimen CC-1.5-1800.

APPENDIX C
1(5)

Failure modes of compression test specimens

Failure modes of short columns and gypsum board braced columns are shown in Figs C1-C5.

Fig. C1: Failure modes of web stiffened C-section short columns with thickness of 1.2 mm and length of 800 mm.

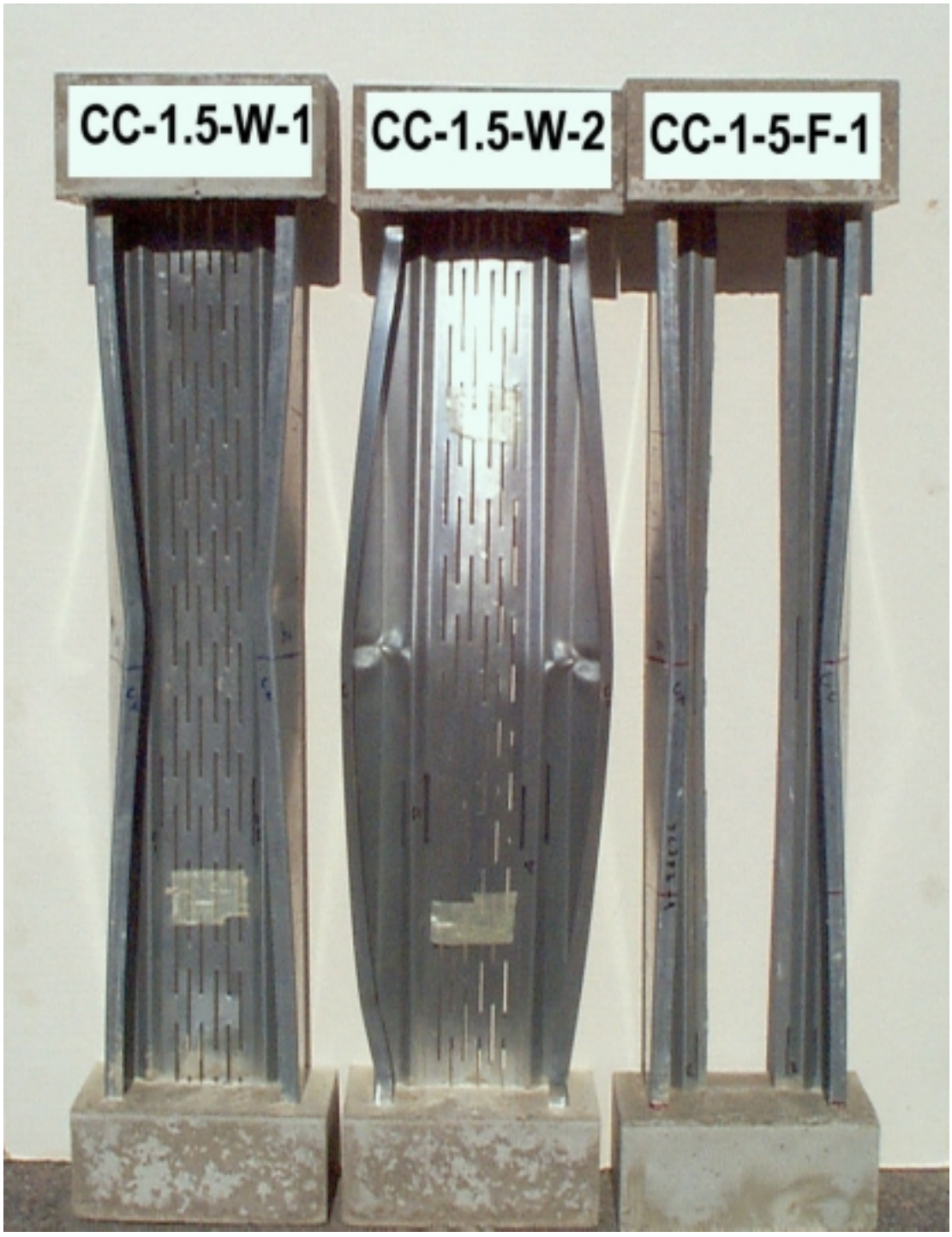

Fig. C2: Failure modes of web stiffened C-section short columns with thickness of 1.5 mm and length of 800 mm.

Fig C3: Failure modes of gypsum board braced web stiffened C-section short columns with thickness of 1.2 mm and length of 1800 mm.

Fig C4: Failure modes of gypsum board braced web stiffened C-section short columns with thickness of 1.2 mm and length of 1800 mm.

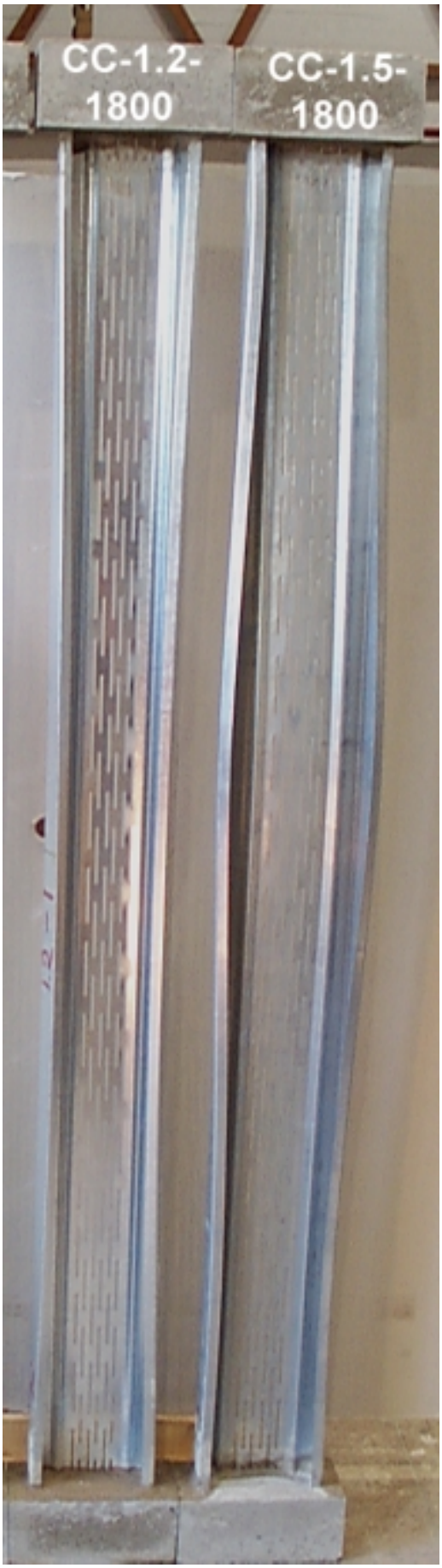

Fig C5: Failure modes of web stiffened C-section columns with thickness of 1.2 mm and 1.5 mm and length of 1800 mm.

Compression capacity of the web-stiffened web-perforated C-section without global buckling

Basic Data

[N,mm]

Material data:

$f_y := 387$

$E := 200000$

$\nu := 0.3$

Distortional buckling stress from buckling analysis:

$\sigma_{cr} := 219$

Cross-sectional dimensions:

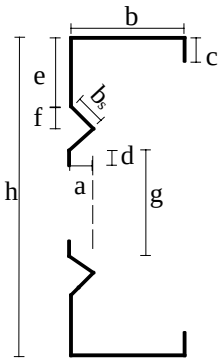

$h := 173.6$

$f := 11.2$

$d := 11.9$

$b := 49.5$

$a := 9.3$

$t := 1.15$

$c := 16.2$

$g := 58$

$e := 23.8$

$b_s := \sqrt{a^2 + f^2}$

Effective cross-section area under compression

Effective flange width

$k_\sigma := 4.0$

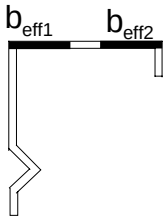

$\lambda_p := 1.052 \cdot \frac{b}{t} \cdot \sqrt{\frac{f_y}{E \cdot k_\sigma}}$

$\lambda_p = 0.996$

$\rho := \frac{1 - \frac{0.22}{\lambda_p}}{\lambda_p}$

$\rho := \text{if}\left(\lambda_p < 0.673, 1, \rho\right)$

$\rho = 0.782$

$b_{eff} := \rho \cdot b$

$b_{eff} = 38.723$

$b_{eff1} := 0.5 \cdot b_{eff}$

$b_{eff2} := 0.5 \cdot b_{eff}$

Effective flange stiffener width

$k_\sigma := 0.5$

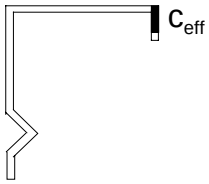

$\lambda_p := 1.052 \cdot \frac{c}{t} \cdot \sqrt{\frac{f_y}{E \cdot k_\sigma}}$

$\lambda_p = 0.922$

$\rho := \frac{1 - \frac{0.22}{\lambda_p}}{\lambda_p}$

$\rho := \text{if}\left(\lambda_p < 0.673, 1, \rho\right)$

$\rho = 0.826$

$c_{eff} := \rho \cdot c$

$c_{eff} = 13.379$

Effective flange stiffener thickness

$\sigma_{cr.r} := \sigma_{cr}$ Given by buckling analysis

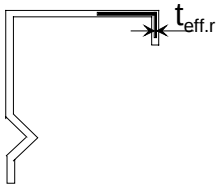

$\lambda_r := \sqrt{\frac{f_y}{\sigma_{cr.r}}}$

$\lambda_r = 1.329$

$\phi := 0.5 \cdot \left[1 + 0.13 \cdot \left(\lambda_r - 0.2\right) + \lambda_r^{\,2}\right]$

$\phi = 1.457$

$\chi_r := \frac{1}{\phi + \sqrt{\phi^2 - \lambda_r^{\,2}}}$

$\chi_r = 0.487$

$t_{eff.r} := \chi_r \cdot t$

$t_{eff.r} = 0.56$

Effective flange stiffener area

$A_{eff.r} := t_{eff.r} \cdot \left(c_{eff} + b_{eff2}\right)$

$A_{eff.r} = 18.337$

Effective area for web part e

$k_\sigma := 4.0$

$\lambda_p := 1.052 \cdot \frac{e}{t} \cdot \sqrt{\frac{f_y}{E \cdot k_\sigma}}$

$\lambda_p = 0.479$

$\rho := \frac{1 - \frac{0.22}{\lambda_p}}{\lambda_p}$

$\rho := \text{if}(\lambda_p < 0.673, 1, \rho)$

$\rho = 1$

$e_{eff} := \rho \cdot e$

$e_{eff} = 23.8$

$e_{eff1} := 0.5 \cdot e_{eff}$

$e_{eff2} := 0.5 \cdot e_{eff}$

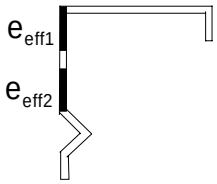

Effective width for web stiffener part b_S

$k_\sigma := 4$

$\lambda_p := 1.052 \cdot \frac{b_s}{t} \cdot \sqrt{\frac{f_y}{E \cdot k_\sigma}}$

$\lambda_p = 0.293$

$\rho := \frac{1 - \frac{0.22}{\lambda_p}}{\lambda_p}$

$\rho := \text{if}(\lambda_p < 0.673, 1, \rho)$

$\rho = 1$

$b_{s.eff} := \rho \cdot b_s$

$b_{s.eff} = 14.558$

Effective width for web stiffener part d

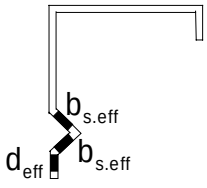

$k_\sigma := 0.43$

$\lambda_p := 1.052 \cdot \frac{d}{t} \cdot \sqrt{\frac{f_y}{E \cdot k_\sigma}}$

$\lambda_p = 0.73$

$\rho := \frac{1 - \frac{0.22}{\lambda_p}}{\lambda_p}$

$\rho := \text{if}(\lambda_p < 0.673, 1, \rho)$

$\rho = 0.957$

$d_{eff} := \rho \cdot d$

$d_{eff} = 11.386$

Effective web stiffener thickness

$\sigma_{cr.s} := \sigma_{cr}$ Given by buckling analysis

$$\lambda_s := \sqrt{\frac{f_y}{\sigma_{cr.s}}}$$

$\lambda_s = 1.329$

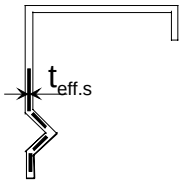

$$\phi := 0.5\cdot\left[1 + 0.13\cdot\left(\lambda_s - 0.2\right) + \lambda_s^{\,2}\right]$$

$\phi = 1.457$

$$\chi_s := \frac{1}{\phi + \sqrt{\phi^2 - \lambda_s^{\,2}}}$$

$\chi_s = 0.487$

$t_{eff.s} := \chi_s \cdot t$

$t_{eff.s} = 0.56$

Effective web stiffener area

$A_{eff.s} := t_{eff.s}\cdot\left(e_{eff2} + 2\cdot b_{s.eff} + d_{eff}\right)$

$A_{eff.s} = 29.349$

2 x

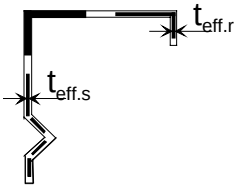

Effective area of the whole section

$A_{eff} := 2\cdot t\cdot\left(b_{eff1} + e_{eff1}\right) + 2\cdot\left(A_{eff.r} + A_{eff.s}\right)$

$A_{eff} = 167.272$

Compression capacity of the section

$N_s := A_{eff}\cdot f_y$

$N_s = 6.473\times 10^4$